BEHAVIOR AND DESIGN OF
ALUMINUM MEMBERS IN BENDING

by

Yongwook Kim [1]

Teoman Peköz [2], Project Director

August 2003   Report 03-04

1. Postdoctoral Associate (formerly Graduate Research Assistant) – School of Civil and Environmental Engineering, Cornell University

2. Professor - School of Civil and Environmental Engineering, Cornell University

PREFACE

This report is based on a thesis presented to the Faculty of the Graduate School of Cornell University for the Degree of Doctor of Philosophy.

TABLE OF CONTENTS

LIST OF TABLES

LIST OF FIGURES

1. INTRODUCTION

One of the advantages of aluminum alloys as structural materials is that they can be extruded. Through extrusion, structural members made of aluminum alloys have a wide variety of cross-sectional shapes, from a simple shape composed of just flat flanges and webs to a complex one that may include edge-stiffeners and intermediate stiffeners. In addition, aluminum alloys have a wide range of material properties through chemical composition and tempering. However, the current specification approaches do not take into account these defining characteristics of aluminum extrusions.

Complex aluminum extrusions may contain additional component elements besides the flanges and webs. The additional component elements are usually intended for non-structural functions such as screw chases and grooves. However, these elements usually contribute to the member strength. In Aluminum Association *Specifications for Aluminum Structures* (2000a), hereafter referred to as the AA *Specification*, boundaries between component elements are idealized as simply-supported, for which plate buckling coefficients are generally known. However, the boundary idealization may not be applicable or appropriate for all complex extrusions. For this reason, the specification covers only a limited range of geometric shapes.

Extrusion is presently an economical way to produce aluminum members. However, due to practical limitations in the extrusion process, extruded sections usually are composed of relatively thicker elements, as opposed to slender cold-formed sections. For this reason, a significant proportion of extruded sections have capacities beyond the yield strength. From the first edition of the AA *Specification* published in 1967, the possibility of using a capacity beyond the yield strength has been overlooked regardless of material properties or geometric shapes: a uniform factor of safety on yield strength is maintained in the specification. There are more

than a thousand materials listed in the Aluminum Standards and Data by the Aluminum Association (2000c) according to types of alloys, tempers, dimensions, orientations, and products. The ratios of the ultimate to yield stresses of these materials range approximately from 1.07 to over 3.6. For example, stress-strain curves of two alloy-temper combinations are compared in Figure 1.1. It would seem not to be reasonable to apply a uniform factor of safety on yield strength regardless of the wide variety of the margins between the ultimate and yield stresses.
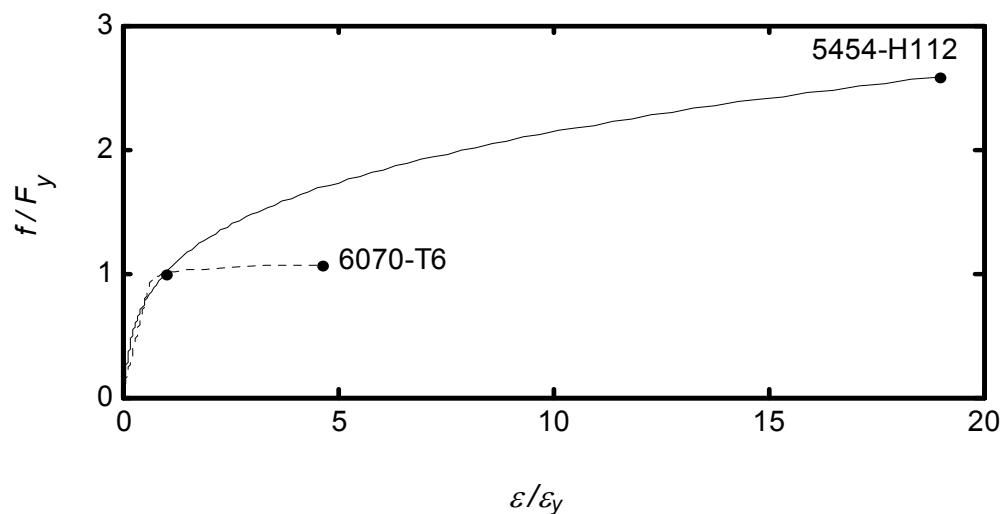
Note: The material properties used in this figure are obtained from AA (2000a and 2000b) with an assumption that the strain at the ultimate stress is approximately half of the minimum percent elongation. The points corresponding to the yield and ultimate stresses are shown with solid circles. F_y denotes the yield stress and ε_y denotes the strain corresponding to the yield stress.

Figure 1.1 Normalized uniaxial tensile stress-strain curves of extruded aluminum alloys generated by Ramberg-Osgood equation

One type of the standard extruded shapes available in the Aluminum Design Manual by the Aluminum Association (2000b) is cross-sections with tapered thickness, which were to facilitate the rolling process when the extrusion process was not common or available. This type of section is also common in steel. The buckling behavior of tapered thickness component elements is quite different from that of

uniform thickness elements. However, neither the Steel *Specification* by the American Institute of Steel Construction (AISC, 1998) nor the AA *Specification* (2000a) provides a way to account for the slope of tapered thickness elements. Instead, treatment of a tapered component element as a uniform element using an averaged thickness is implied.

The study presented in this report is aimed at improving the current AA *Specification* (2000a) so that the aforementioned problems can be properly resolved. All the investigations in this study are based on laterally supported members or members that do not buckle laterally under flexural loading.

In Chapter 2, the ultimate-plastic capacity is studied. To begin with, important terminologies used in this study are defined. An analytical closed-form equation of the ultimate shape factor is derived for rectangular web elements. Using this equation, the ultimate shape factor implicit in the AA *Specification* (2000a) is examined for almost a thousand available alloy-temper combinations. In addition, a parametric study is conducted to account for the inelastic buckling behavior of component elements in compression. Additional studies are conducted on the approaches in the AA *Specification* (2000a) that cover the limit state stresses for all component elements to compute the member moment capacity. These will be referred to as the "moment capacity evaluation approaches". In addition, a more general approach than those in the present specification is developed. Parametric studies using finite element analyses as well as physical tests are conducted to validate the proposed approaches in this chapter. Finally, to maintain a certain factor of safety on yield strength, the use of a specified percentage of the ultimate strength of a member with two safeguards is suggested.

In Chapter 3, the behavior of sections with tapered thickness is investigated. To understand the buckling behavior of a tapered thickness plate, stiffness matrices are derived for use in an available finite strip program. Using the program, the

buckling coefficients for tapered plates are computed. Based on the plate buckling coefficients, the current specification equations are modified for the tapered thickness component element. To validate the modified equations, a parametric study of I-sections with tapered flanges with a wide variety of slenderness is performed and physical flexural tests are conducted.

In Chapter 4, a general design approach is developed for complex extrusions, for which simply-supported boundary idealization is not applicable or appropriate. This approach relies on a numerical buckling analysis tool. In addition, the rigorous analytic expression of the ultimate shape factor developed for symmetric sections in Chapter 2 is extended to the ultimate shape factor for unsymmetric sections. Additional moment capacity evaluation approaches are developed for cross-sections with a neutral axis that is not at mid-depth. Parametric studies of five different kinds of cross-sections are conducted using finite element analysis to validate the approaches developed in this chapter. Some additional physical tests are also conducted for further validation.

In Chapter 5, major conclusions of the study are provided. In the Appendix, step-by-step design examples are provided. In addition, detailed cross-sectional dimensions and numerical results of most of the parametric studies are tabulated for future reference. Moreover, uniaxial tension test results and initial geometric imperfection measurements conducted in this study are summarized.

The studies in this report refer to valuable studies by a number of researchers. First, for understanding the behavior of aluminum structures, textbooks by Kissell and Ferry (1995), Sharp (1993), Mazzolani (1985) and Mazzolani (1995) have been very useful. The first two are based on the AA *Specification* (2000a); the others are related to the European specifications, such as Eurocode 9 (1997). Templin et al. (1938), Stowell (1948), Stowell (1950), Bleich (1952), Hill and Clark (1955), Anderson and Anderson (1956), Alcoa (1958), Clark and Rolf (1966), Sharp (1966), Jombock and

Clark (1968) and Sooi and Peköz (1993) have provided a significant portion of bases for the AA *Specification* (2000a) with respect to the compressive strength of component elements. Plecher (2000) has concentrated on evaluating existing aluminum bridges in the United States.

The ultimate-plastic capacity of aluminum structures studied in Chapter 2 has also been studied by Sharp (in Gaylord and Gaylord, 1979), Mazzolani (1985), Mazzolani and Piluso (1997), Faella et al. (2000), De Matteis et al. (2001), and a number of other researchers. For the development of the stiffness matrices for the tapered thickness plate element in Chapter 3, the studies by Kobayashi et al. (1990), Mizusawa (1993), Ohga et al. (1995), Cheung (1976), McGuire et al. (2000), Schafer (1997), and Huebner et al. (1995) have been investigated. Attempts to incorporate numerical buckling analyses into the specification approaches, as is done in Chapter 4, have also been made by Schafer and Peköz (1998), and Mennink (2002).

2. SYMMETRIC CROSS-SECTIONS WITH UNIFORM THICKNESS COMPONENT ELEMENTS

Most standard cross-sections listed in AA (2000b) are symmetric with respect to at least one principal bending axis without any edge or intermediate stiffeners. The cross-sectional shapes that fall into this category are exemplified in Figure 2.1. The shapes are composed of equal flanges at the extreme fibers and of one or more web elements.
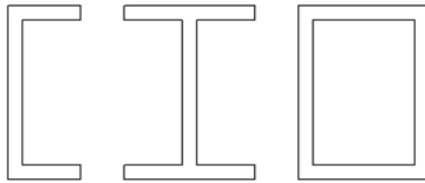
Figure 2.1 Examples of standard simple extrusions

Once such a member is supported against lateral movement, the moment capacity of the member mainly depends on the component elements. Specifications customarily assume junctions between the component elements as simply supported hinges, e.g., the American Institute of Steel Construction (AISC, 1998), American Iron and Steel Institute (AISI, 1996), and Aluminum Association (AA, 2000a). As such, each component element can be treated as an independent plate element under corresponding boundary and loading conditions, of which the buckling behavior has been shown, e.g., see Gerard and Becker (1957). Such cross-sections are referred to as "simple extrusions" hereafter. Although extensive studies have been performed to evaluate the precise flexural capacity of aluminum simple extrusions, there is still room for improvement as shown in this study.

2.1   Introduction to Shape Factor and Limit State

For a steel member, the ratio of the plastic moment capacity (M_p, Figure 2.2d) to the yield moment capacity ($M_y = F_yS$, Figure 2.2b) is generally called "the shape factor." The computation of the shape factor is straightforward, since the stress distribution is assumed to be rigid-plastic for the plastic moment capacity and linear-elastic for the yield moment capacity. Since the stress distributions are linear, the shape factor is dependent on the geometric shape and not the material properties. For example, the shape factor for a solid rectangular cross-section is 1.5, regardless of the material properties.

On the other hand, the shape factor of an aluminum member is more complicated: the stress distribution cannot be assumed to be rigid-plastic because the stress-strain curve for aluminum does not have a constant yielding range, and strain hardening occurs without a clearly defined yield point. So for aluminum, when the stresses at both extreme fibers are at the ultimate stress, as shown in Figure 2.2e, this stress distribution is defined as the limit state of the ultimate stress, and hereafter will be referred to as the ultimate limit state.
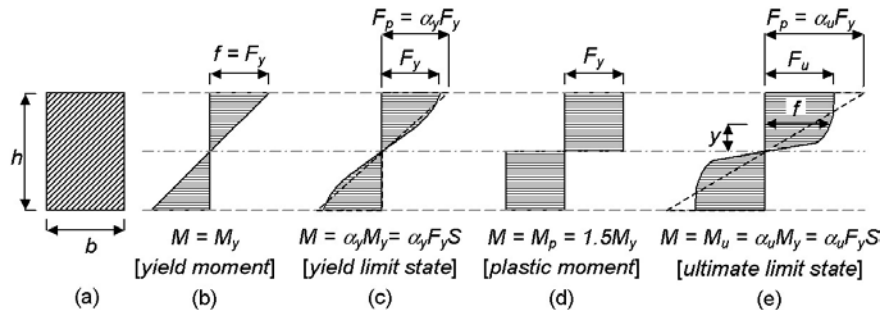
Figure 2.2 Stress distributions of a rectangular aluminum section

The corresponding moment capacity is obtained through the integration of the non-linear stress distribution, which is defined as the moment capacity at the ultimate limit state and hereafter will be referred to as the ultimate moment capacity (M_u):

$$M_u = b \int_{-h/2}^{h/2} f \, y \, dy \qquad (1)$$

The ratio of the ultimate moment capacity (M_u) to the yield moment (M_y) is defined as the shape factor for the ultimate limit state and will be referred to as the ultimate shape factor (α_u). This ultimate shape factor is dependent on the geometric shape and material properties including strain hardening.

In addition to the ultimate shape factor, another shape factor is used for aluminum members. When the stresses at both extreme fibers are at the yield stress as shown in Figure 2.2c, the moment capacity calculated through integration of the stress distribution is defined as the moment capacity at the yield limit state. The moment capacity at this state is significantly larger than the yield moment capacity (M_y), because the proportional limit of the stress-strain curve is appreciably smaller than the yield stress based on the 0.2% offset method. The ratio of the moment capacity at the yield limit state to the yield moment capacity (M_y) is defined as the shape factor for the yield limit state and will be referred to as the yield shape factor (α_y).

The shape factors for both the ultimate and yield limit states can be simplified into Equation (2):

$$\alpha = \frac{M}{M_y} \qquad (2)$$

where M is the moment capacity obtained from integrating the stress distribution at either the yield or ultimate limit state. The shape factors can also be expressed in terms of the stresses: the combination of Equation (2) and $F_p \equiv M/S$ results in

$$\alpha = \frac{F_p}{F_y} \qquad (3)$$

where F_p denotes the limit state stress. The limit state stress is a convenient measure of the capacity of a component element, since the corresponding moment capacity is simply obtained from the multiplication of the limit state stress by the elastic section modulus. As a result of this process, the non-linear stress distribution of an aluminum alloy is linearized as shown by the dashed lines in Figure 2.2c and Figure 2.2e. For a

component element under compression, the limit state stress varies according to the width-to-thickness ratio of the cross-section. However, for a component element under tension, the limit state stress is constant for each limit state. Details regarding the limit state stress can be found in Section 2.2.

The results of numerical analysis and experimental studies shown in Table 2.1 present a value of 1.3 for the yield shape factor (α_y) of solid rectangular aluminum flexural members. However, it is noted that the ultimate shape factor (α_u) proposed by Sharp (1993) is considerably larger than the yield shape factor because the ultimate stress, F_u, is always larger than the yield stress, F_y.

Table 2.1 Shape factors for solid rectangular aluminum flexural members

yield shape factor by Clark and Rolf (1966) and Sharp (1993)	ultimate shape factor by Sharp (1993)
$\alpha_y = 1.3$	$\alpha_u = 1.4\dfrac{F_u}{F_y}$

Note: The ultimate shape factor shown here is modified from its original form to correspond with Equation (3).

symmetric cross sections
(a)

[yield limit state]
(b)

[ultimate limit state]
(c)
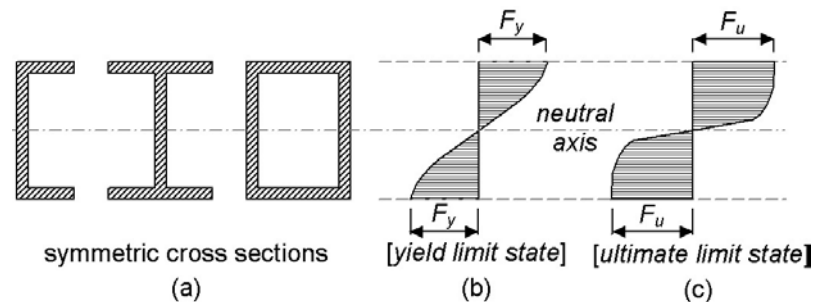
Figure 2.3 Limit states for fully compact symmetric cross-sections

The web elements of symmetric cross-sections such as those seen in Figure 2.3a can be simplified into a solid rectangular element under bending as shown in Figure 2.2a with simply-supported boundary conditions at web-flange junctions. Since the stress magnitude at the web-flange junction is not significantly different from that

at the extreme fiber, the former is assumed to be the same as the latter. This is based on the assumption that the element thickness is sufficient to prevent buckling.

The shape factor defined in Equation (2) is the ultimate load carrying capacity divided by the idealized yield capacity ($M_y = F_y S$). Hence, the term "shape factor" can also be used for members under other types of loading such as uniform compression. Examples include the flange elements of sections such as those shown in Figure 2.3a under bending with respect to the strong axis, assuming buckling is not a problem. Disregarding the stress variation on flanges, the ratio of the ultimate stress to the yield stress is the ultimate shape factor for the flange,

$$\alpha_u = \frac{F_u}{F_y} \qquad (4)$$

while the yield shape factor for the flange is obviously unity.

2.2 Limit State Stresses of Component Elements in the AA Specification

Limit state stress is defined as the estimated actual strength of a component element based on selection of governing limit state, either yielding, fracture (ultimate), or buckling, obtained from theoretical and/or experimental studies. As mentioned in Section 2.1, by simply multiplying the limit state stress with a fixed section property, either the section modulus or area of the cross-section, the moment capacity or axial load capacity can be calculated.

Due to uncertainties such as over-loading, construction flaws, and variations of material properties, in Allowable Stress Design the limit state stress is divided by a safety factor to obtain the Allowable Stress. In Load and Resistance Factor Design (LRFD), the limit state stress is multiplied by a resistance factor (ϕ) to obtain the Factored Limit State Stress. The resistance factor ϕ accounts for the uncertainties related to strength. Although this study is based on the Allowable Stress Design, the

term "allowable stress" can be replaced with the "factored limit state stress" for the Load and Resistance Factor Design.

As summarized in Table 2.2 for the Allowable Stress Design, the AA *Specification* (2000a) provides two different limit state stress expressions for tensile stresses in component elements depending on the limit state that may be yield or ultimate. The minimum of the two allowable stresses is used in design. In Load and Resistance Factor Design, the minimum of the two factored limit state stresses is used.

The allowable stresses shown in Table 2.2 incorporate the shape factors for component elements discussed in Section 2.1. The safety factors on yield and ultimate strength are denoted by n_y and n_u, respectively, while the coefficient k_t is an additional safety factor on ultimate strength due to the notch sensitivity of some alloy-temper combinations, e.g., 2014-T6, 6066-T6, and 6070-T6. Details of the notch sensitivity are given in the AA *Specification* (2000a). As seen in Table 2.2, allowable tensile stress for each component element is constant for a given limit state.

Table 2.2 Options to compute tension allowable stresses of a flexural member by AA *Specification*

component element	allowable stress based on yield limit state	allowable stress based on ultimate limit state
tension flange of structural shapes	F_{ty}/n_y	$F_{tu}/k_t n_u$
tension web of structural shapes	$1.30 F_{ty}/n_y$	$1.42 F_{tu}/k_t n_u$

Note: F_{ty} = tensile yield stress
F_{tu} = tensile ultimate stress

Allowable compressive stress or factored limit state compressive stress varies according to the equivalent slenderness ratio (λ_p), which falls into one of three ranges, the yielding, inelastic buckling, and post buckling ranges, as shown in Figure 2.4.
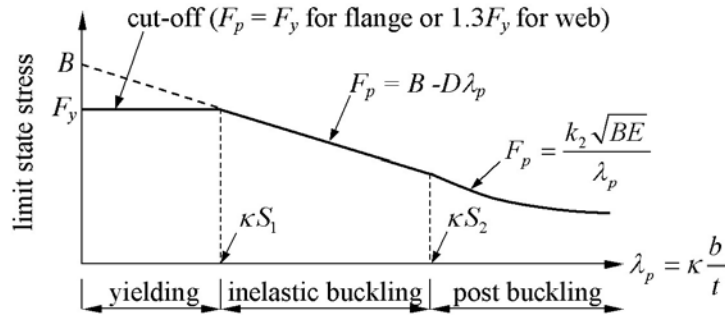
Figure 2.4 Limit state stress for a component element from the AA *Specification*

The equivalent slenderness ratio is defined in Equation (5), which is derived from Equation (6):

$$\lambda_p = \kappa\left(\frac{b}{t}\right), \text{ where } \kappa = \sqrt{\frac{12\left(1-\nu^2\right)}{k_p}} \tag{5}$$

$$F_{cr} = k_p \frac{\pi^2 E}{12(1-\nu^2)(b/t)^2} \equiv \frac{\pi^2 E}{\lambda_p^2} \tag{6}$$

where k_p = the plate buckling coefficient depending on the edge conditions and aspect ratio of the plate, ν = Poisson's ratio, E = Young's modulus, b = plate width, t = plate thickness, and F_{cr} = buckling stress. For flange and web component elements with simply-supported boundary conditions at the web-flange junctions, examples of the equivalent slenderness ratios are shown in Table 2.3.

Table 2.3 Equivalent slenderness ratios in the AA *Specification* (2000a)

boundary and loading conditions [b]	equivalent slenderness ratio	plate buckling coefficient (k_p)
S.S / S.S / S.S / S.S	$\lambda_p = 1.6\left(\frac{b}{t}\right)$	4.00
S.S / S.S / FREE	$\lambda_p = 5.1\left(\frac{b}{t}\right)$	0.405 [a]
S.S / S.S / S.S	$\lambda_p = 0.67\left(\frac{b}{t}\right)$	23.9

Note: a. 0.405 is back calculated from the equivalent slenderness ratio listed in Alcoa (1958): $\lambda_p = 5.13(b/t)$
b. *S.S* denotes a simply-supported boundary condition.

The post-buckling range equation illustrated in Figure 2.4 proposed by Jombock and Clark (1968) takes into account the non-linear stress distribution of a buckled plate. The inelastic buckling range equation proposed by Clark and Rolf (1966) is a linear equation composed of *B* and *D* factors, which is a simplification of the original inelastic plate buckling equation based on experimental studies by Stowell (1948). Further details are summarized in Kim (2000). The cut-off in the yielding range is equal to the yield shape factor multiplied by the yield stress, which is based on the yield limit state. However, experimental studies, such as DOD (1994), show that the uniaxial stress-strain relationship of aluminum alloys under compression is very similar to that of tension up to the tension fracture point. Because the uniaxial stress-strain relationship under compression progresses beyond the equivalent tension fracture point, it is generally conservative to assume that the ultimate stress and strain for compression are the same for tension. For these reasons, this study suggests including the use of a cut-off that is calculated according to the ultimate limit state, in addition to the yield limit state. In other words, the cut-off should increase to a level similar to the ultimate limit state of tension elements as shown in Table 2.2. Before applying the implied tension shape factors in this table to compression, the ultimate shape factor for web elements will be examined in the following section.

2.3   *Rigorous Equation of Ultimate Shape Factor for Rectangular Web Elements*

Numerical integration of the non-linear stress distribution when the stresses at both extreme fibers are at the ultimate stress, as shown in Figure 2.2e, is the most common approach to obtaining the ultimate shape factor. In this approach, the stress-strain relationship is approximated by the modified Ramberg-Osgood equation, as shown in Equation (7):

$$\varepsilon = \frac{f}{E} + 0.002 \left(\frac{f}{F_y} \right)^n \qquad (7)$$

where E = Young's modulus, F_y = yield stress, ε = variable strain, f = variable stress and n = exponent. The original equation is given in Ramberg and Osgood (1943). In order to use Equation (7), the exponent, n, must be determined. However, although the AA *Specification* gives the yield stress, Young's modulus, and the ultimate stress, the strain at the ultimate stress (will be referred to as the ultimate strain hereafter, ε_u) is still needed to determine the exponent, n:

$$n = \log\left[500\left(\varepsilon_u - \tfrac{F_u}{E}\right)\right]\Big/ \log\left(\tfrac{F_u}{F_y}\right) \qquad (8)$$

Although statistical data for the ultimate strain is not available, the minimum percent elongation is available in the Aluminum Standards and Data (AA, 2000c). Since generally the percent elongation is somewhat larger than the ultimate strain, the ultimate strain may be estimated from the percent elongation, and hence the exponent, n, can be determined.

It is a cumbersome task to compute the shape factor using the numerical integration method due to the iterative nature of the method itself and the high non-linearity of the modified Ramberg-Osgood equation. For this reason, an analytical integration is used to derive the closed-form shape factor equation in this study. As shown by Eberwien and Valtinat (2001), the moment capacity for a rectangular solid member with a non-linear stress distribution expressed by the modified Ramberg-Osgood equation can be obtained through the Bernoulli hypothesis.
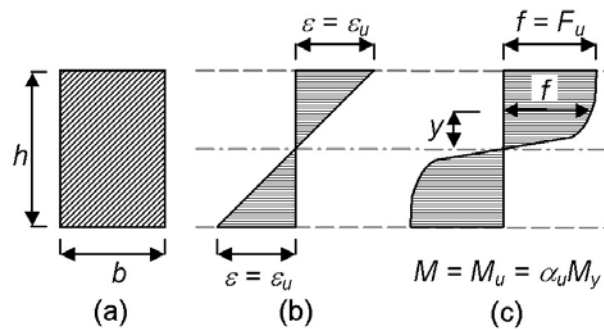
Figure 2.5 Strain and stress distributions for a rectangular aluminum section

With the hypothesis, a linear strain distribution can be assumed, as shown in Figure 2.5b. Using the stress-strain relationship given in Equation (7),

$$y = \frac{h/2}{\varepsilon_u}\varepsilon = \frac{h/2}{\varepsilon_u}\left\{\frac{f}{E} + 0.002\left(\frac{f}{F_y}\right)^n\right\} \qquad (9)$$

and the derivative of Equation (9) is

$$dy = \frac{h/2}{\varepsilon_u}d\varepsilon = \frac{h/2}{\varepsilon_u}\left\{\frac{1}{E} + \frac{nf^{n-1}}{500F_y^n}\right\}df \qquad (10)$$

The ultimate moment capacity expression is derived by introducing Equations (9) and (10) into the following integral expression using notations from Figure 2.5. Since a typical stress-strain relationship from uniaxial tension tests is quite similar to that from compression tests as shown in DOD (1994), the integral for the upper region is doubled to obtain the complete ultimate moment capacity:

$$M_u = 2b\int_0^{h/2} f\, y\, dy \qquad (11)$$

In this integral, the *h/2* limit is replaced with F_u due to a change in variable from *y* to *f*. The final closed-form ultimate moment capacity is shown in Equation (12).

$$M_u = \frac{bh^2 F_u}{2\varepsilon_u^2}\left[\frac{1}{3}\left(\frac{F_u}{E}\right)^2 + \frac{1}{500^2}\left(\frac{n}{2n+1}\right)\left(\frac{F_u}{F_y}\right)^{2n} + \frac{1}{500}\left(\frac{n+1}{n+2}\right)\left(\frac{F_u}{F_y}\right)^n\left(\frac{F_u}{E}\right)\right] \qquad (12)$$

$$M_y = \frac{bh^2 F_y}{6} \qquad (13)$$

The closed-form ultimate shape factor for a rectangular aluminum solid section is obtained by normalizing the ultimate moment capacity of Equation (12) using the yield moment capacity of Equation (13):

$$\alpha_u = \alpha_{wo} = \frac{M_u}{M_y} = \frac{3}{\varepsilon_u^2}\left(\frac{F_u}{F_y}\right)\left[\frac{1}{3}\left(\frac{F_u}{E}\right)^2 + \frac{1}{500^2}\left(\frac{n}{2n+1}\right)\left(\frac{F_u}{F_y}\right)^{2n} + \frac{1}{500}\left(\frac{n+1}{n+2}\right)\left(\frac{F_u}{F_y}\right)^n\left(\frac{F_u}{E}\right)\right] \qquad (14)$$

where α_{wo} is an alternative denotation for emphasizing that the shape factor is limited to a symmetric section. For an unsymmetric section, another denotation is used, α_w, as shown in Equation (50).

As seen in DOD (1994) and uniaxial tension tests performed in this study, the typical values of the ultimate strain (ε_u) for 6061-T6 are between approximately 6 and 8%. For the same material, the typical value of percent elongation is 12% as tabulated in AA (2000b). Similarly, since the minimum value of the percent elongation is 8% for 6061-T6 as shown in AA (2000c), it is reasonable to predict that the minimum value of the ultimate strain be in the range of 4 to 6%. To evaluate the effect of a variation in the ultimate strain, shape factors are computed based on various ultimate strain values using Equation (14), with results shown in Figure 2.6. The shape factor variation is less than 1% for ultimate strain values that are within 50% larger or smaller than the minimum percent elongation.
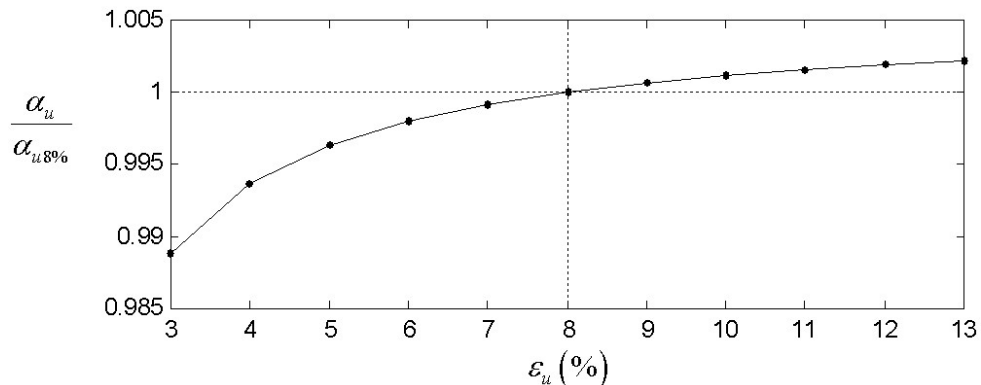
Note: $\alpha_{u8\%}$ is α_u when $\varepsilon_u = 8\%$.

Figure 2.6 Variation of the ultimate shape factor for a rectangular web element with respect to the ultimate strain (6061-T6)

Thus, the aforementioned assumption that the ultimate strain may be estimated from the percent elongation is reasonable. In this study, the recommended value for the ultimate strain is between half and equal to the minimum percent elongation. The ultimate shape factors are computed using Equation (14) for some 6000 series alloys

in Table 2.4, which are more frequently used for building construction than any other alloys.

Table 2.4 Material properties and ultimate shape factors for solid rectangular sections for some 6000 series alloys (extrusions)

Alloy-temper	F_y (MPa) [a]	E (MPa) [b]	F_u (MPa) [a]	ε_u [c]	n [d]	$\alpha_u = \alpha_{wo}$ [e]	$\dfrac{\alpha_u}{1.42 F_{tu}/F_{ty}}$ [f]
6005-T5, 6105-T5, 6351-T5 & 6061-T6, -T6510, -T6511	241.15	68900	261.82	0.04	35.214	1.5975	1.0362
6063-T5 [g]	110.24	68900	151.58	0.04	9.2295	1.9467	0.9970
6063-T5 [h]	103.35	68900	144.69	0.04	8.7431	1.9766	0.9943
6063-T6, T62 & 6463-T6	172.25	68900	206.70	0.04	16.003	1.7361	1.0188
6066-T6, -T6510, -T6511	310.05	68900	344.50	0.04	27.166	1.6224	1.0283
6070-T6, -T62	310.05	68900	330.72	0.03	39.259	1.5617	1.0311

Note: a. Minimum values from AA (2000c).
    b. These are average values, which are 689 MPa (100 ksi) lower than compression.
    c. ε_u is assumed to be half of the minimum percent elongation listed in AA (2000c).
    d. See Equation (8).
    e. See Equation (14).
    f. $1.42 F_{tu}/F_y$ = Equation (15).
    g. Test coupon diameter or thickness up through 12.7mm.
    h. Test coupon diameter or thickness between 12.7 and 25.4mm.

The yield stress times the obtained shape factors (α_u) in Table 2.4 can be directly used as the cut-off at the ultimate limit state. Since the compressive stress distribution is approximately the same as that for tension, the shape factors (α_u) in this study are also compared to that implied in Table 2.2 for the tension web, which is available in the AA *Specification* (2000a). For the comparison, the ultimate limit state stress expression for the web without safety factors shown in Table 2.2 is multiplied by the section modulus and then introduced into Equation (2):

$$\alpha_u = \alpha_{wo} = 1.42 \frac{F_{tu}}{F_{ty}} \qquad (15)$$

The last column of Table 2.4 is the ratio of the shape factor obtained from the rigorous equation proposed in this study, Equation (14) to the shape factor in the specification,

Equation (15). From the small variation in these values, it can be concluded that for 6000 series alloys, the two give quite similar results.

2.4 Simplified Ultimate Shape Factor for Rectangular Web Elements

The rigorous analytic expression for the ultimate shape factor of a rectangular web element in Equation (14) is too complicated for practical design purposes. Thus, a simplified expression is necessary, such as the one used for tension component elements in the AA *Specification* (2000a): Equation (15).

Although the performance of Equation (15) is found to be satisfactory for the 6000 series alloys in Table 2.4, it has never been investigated for a wide variety of alloy-temper combinations. In AA (2000c), more than a thousand materials are listed according to alloy type, temper type, the dimensions of the tested coupons, the orientation of the tested coupons, and the type of product from which the tested coupons are obtained, such as plate, pipe, or extruded shape. From this data, 986 alloy-temper combinations have been chosen for this investigation. The basis for choosing the data is as follows. First, the minimum values of the material properties required for Equation (14) should be available. Second, the ultimate strain should exceed 1.5% when it is assumed to be half of the minimum percent elongation. Third, the orientation of the tested coupons should not be in the transverse direction.

For the selected alloy-temper combinations, the shape factors have been computed using Equation (14) and plotted with respect to the F_{tu}/F_{ty} ratio in Figure 2.7. It is clear that Equation (15) becomes more unconservative as the F_{tu}/F_{ty} ratio increases. Thus, a more precise curve-fit can be proposed for the ultimate shape factor:

$$\alpha_u = \alpha_{wo} = 1.25\frac{F_{tu}}{F_{ty}} + 0.2 \qquad (16)$$

For practical design purposes, Equation (16) could be used instead of Equation (14) for the ultimate shape factor of rectangular web elements under bending.
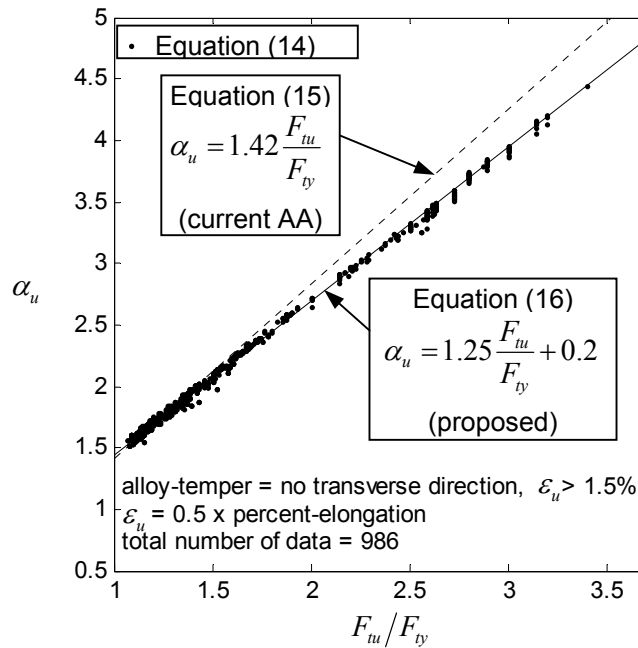
Figure 2.7 Comparison of the ultimate shape factor approximations using Equations (15) and (16) for rectangular web elements under bending

2.5 Parametric Study for Component Elements and Proposed Limit State Stress Equations for Ultimate Limit State

From the results in the previous sections, it can be seen that the cut-off can be raised to the yield stress times the ultimate shape factor for component elements. However, the raised cut-off should be limited to component elements with very low width-to-thickness ratios to eliminate possible buckling. A parametric study for component elements of doubly symmetric I-shaped sections was conducted in Kim (2000) using the finite element method to investigate the following: (1) the maximum possible width-to-thickness ratio for the raised cut-off that buckling will not occur and (2) the transition range resulting from the difference in the raised (ultimate limit state) and current (yield limit state) cut-off values. The following is a summary of this study.

The finite element program, ABAQUS developed by Hibbitt, Karlsson and Sorensen, Inc. (1998), was used for the analyses. Four-noded general-purpose shell

elements with 4 integration points are used to take into account a large variation of thickness. The alloy-temper is assumed to be extruded 6061-T6 with the minimum material properties given in Table 2.4 except for the ultimate strain. The two recommended ultimate strain values, 4% and 8%, which are half and equal to the percent elongation, respectively, are used to observe their effect on the limit state stress. As previously stated, the ultimate strain variation affects the Ramberg-Osgood exponent (n), which in turn affects the ultimate shape factor for the web (α_u).

Since this study deals with monotonic loading, the isotropic hardening model is used. In this case, once a stress reaches the ultimate stress, the stress remains constant as the plastic strain exceeds the ultimate strain. Due to uncertainty after this stage, it is assumed that a whole member reaches failure when the Von Mises stress at a single point of the member reaches the ultimate stress. This occurs when a member is too compact to buckle.

On the other hand, the failure of a member can also be initiated by buckling when the member is less compact. In this case, the peak load of the member is obtained before any point of the member reaches the ultimate stress. In this study, these two possibilities of failure are considered simultaneously so as to find an ultimate load factor.

The boundary conditions for component elements of doubly symmetric I-shaped sections are idealized as shown in Figure 2.8. To avoid singularity of the stiffness matrix, one longitudinal degree of freedom is restrained at the span center. Equal and opposite loadings are applied at the loaded edges, where rigid beam elements are attached. Elastic eigen-value analyses to generate initial geometric imperfections precede the non-linear analyses. The maximum imperfection amplitude is determined based on the standard flatness tolerance provided by AA (2000c).
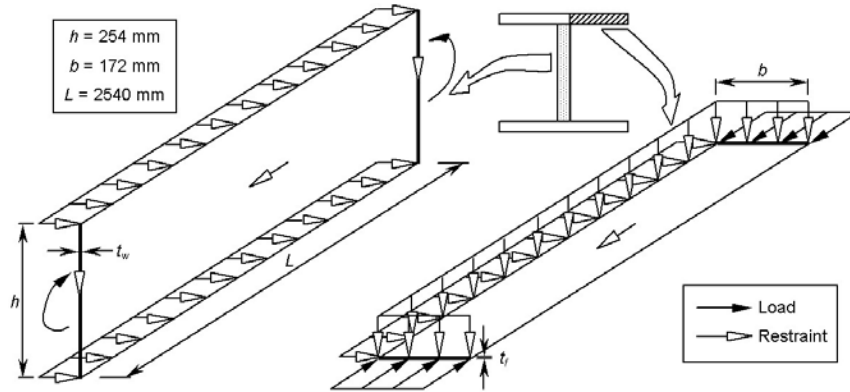
Figure 2.8 Boundary and loading conditions for finite element analyses
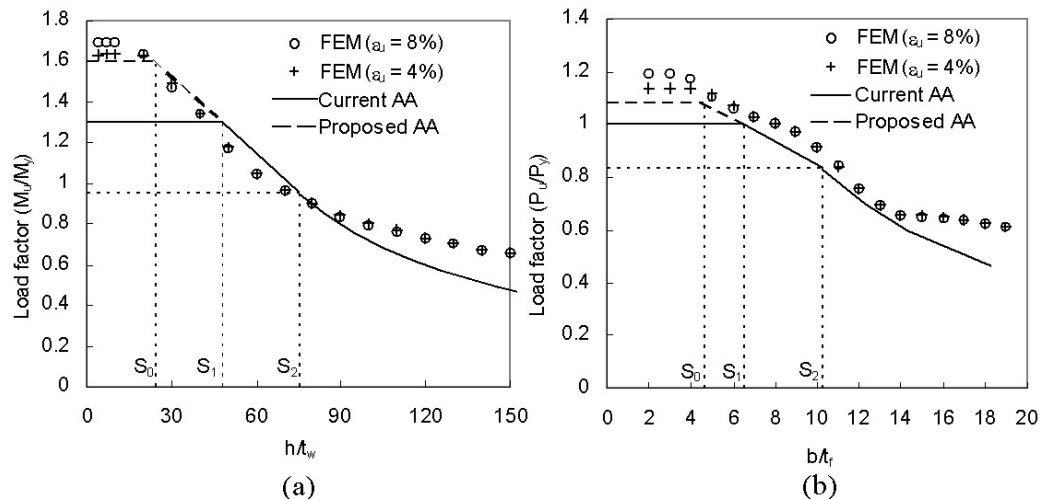
Figure 2.9 Parametric study results for component elements (a) web (b) flange

From the results of the parametric study for component elements shown in Figure 2.9, the following modifications of the limit state stress equations are made for the ultimate limit state. For a very low width-to-thickness range, the yield stress times the ultimate shape factor is employed for the raised cut-off. For the transition range between the raised and current cut-off values, the equation line of the inelastic buckling range ($S_1 \leq$ width/thickness $\leq S_2$) is extended to the raised cut-off value with the same slope.

For the material used in this parametric study, the ultimate shape factor is 1.598 for the web element using Equation (14) ($\varepsilon_u = 4\%$) and 1.086 for the flange

element using Equation (4). These modifications work well with both series of finite element analyses based on the two ultimate strain values, 4% and 8%. This parametric study confirms that the ultimate limit state can be considered for compressive component elements. The results of Kim (2000) are reevaluated in the present work and the equations of Kim (2000) are modified to what is shown in Table 2.5.

Table 2.5 (a) Limit state stress equations and limits and (b) shape factors

(a)

limit state stress $\dfrac{b}{t} \leq S_1$	limit S_1	limit state stress $S_1 \leq \dfrac{b}{t} \leq S_2$	limit S_2	limit state stress $S_2 \leq \dfrac{b}{t}$
$F_p = \alpha F_{cy}$	$\dfrac{B - \alpha F_{cy}}{\kappa D}$	$F_p = B - D\kappa \dfrac{b}{t}$	$\dfrac{k_1 B}{\kappa D}$	$F_p = \dfrac{k_2 \sqrt{BE}}{\kappa \dfrac{b}{t}}$

(b)

component element	yield limit state ($\alpha = \alpha_y$)	ultimate limit state ($\alpha = \alpha_u$)
Flange	1.0	F_{tu}/F_{cy}
Web	1.3	$1.25\,F_{tu}/F_{cy} + 0.2$

Note. a. F_p = flange limit state stress (F_f) or web limit state stress (F_w).
   b. B, D, k_1 and k_2 are factors provided in the AA *Specification* (2000a). The factors for a flange differ from those for a web.
   c. See Equation (5) for κ (Table 2.3).
   d. α_u = Equation (4) for flange and Equation (16) for web
   e. F_{cy} = compressive yield stress

2.6 *Moment Capacity Evaluation Approaches*

2.6.1 Minimum Moment Capacity Approach (MMCA)

In AA (2000b), to compute the allowable moment capacity of a member, the allowable stress (or factored limit state stress) of each component element is first computed. Then from the calculated allowable stresses (or factored limit state stresses), the minimum is selected and multiplied by the elastic section modulus of the entire cross-section (*S*). For the section given in Figure 2.10,

$$M_u = \min(F_f, F_w)\, S \qquad (17)$$

where F_f and F_w = allowable stress (or factored limit state stress) for the flange and web, respectively. However, instead of the use of the allowable stresses (or factored limit state stresses) for F_f and F_w, limit state stress values have been employed in the parametric study that follows in Section 2.7. This approach is demonstrated by AA (2000b) through the Illustrative Examples of Design (Part VIII, Example 21) for symmetric sections with respect to the bending axis.

This approach is denoted by the Minimum Moment Capacity Approach or MMCA hereafter. Since possible interactions and stress redistributions between component elements are disregarded, this approach is expected to be rather conservative.

2.6.2 Weighted Average Stress Approach (WASA and WASA2)

Another method is given in the AA *Specification* (2000a), where the limit state stresses obtained from all component elements in each of the compression and tension sides can be averaged according to contributory area. The averaged stress is multiplied by the section modulus to compute the moment capacity. This is called the Weighted Average Stress Approach or WASA in this study. The weighted average stress equation was first introduced by Jombock and Clark (1968) to compute the crippling strength of aluminum trapezoidal formed sheet members:

$$F_{WT} = \frac{F_f A_f + F_w \frac{1}{3} A_w}{A_f + \frac{1}{3} A_w} \qquad (18)$$

where A_f and A_w = flange and web area for either compression or tension (indicated in Figure 2.10). Sooi and Peköz (1993) extended the WASA to sections with edge-stiffened and intermediately-stiffened elements by adding further terms for stiffeners to Equation (18). See Table 4.3 for details. Although the WASA was verified through experiments in the aforementioned studies, a theoretical basis for the approach has

never been investigated. Thus, the accuracy of this method is questionable for geometric shapes other than tested.
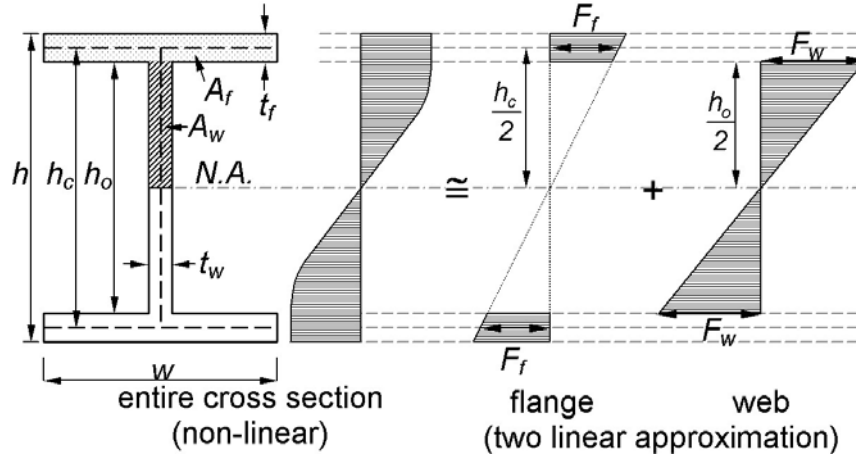
Figure 2.10 Contributions of element groups to the entire moment capacity

The theoretical basis of the WASA is investigated in this study for a doubly symmetric I-section shown in Figure 2.10. Multiplication of both the denominator and numerator of Equation (18) by $h_c^2/2$ and subsequent simplification of this equation through an assumption that the flange thickness is relatively small result in Equation (19):

$$F_{WT} \cong \frac{M_f + M_w}{I_f + I_w}\left(\frac{h_c}{2}\right) = \frac{M_u}{I}\left(\frac{h_c}{2}\right)$$

(19)

where M_f, M_w, M_u = moment capacity of the (top and bottom) flanges, web, and entire cross-section respectively, I_f, I_w, I = moment of inertia with respect to the neutral axis of the entire cross-section of the (top and bottom) flanges, web, and entire cross-section, respectively. For the section in Figure 2.10, $I_w = t_w h_o^3/12$ and $I_f = I - I_w$. Equation (19) implies that the weighted average stress is an approximately linearized bending stress measured at the mid-thickness of the flange. Therefore, to obtain an accurate total moment capacity, the correction shown in Table 2.6 should be made:

Table 2.6 Correction in the current WASA

current WASA (WASA)	proposed WASA (WASA2)
$M_u = (F_{WT})(S)$	$M_u = (F_{WT})\left(\dfrac{h}{h_c}\right)(S)$

Note: S = section modulus = $I/(h/2)$

The correction in Table 2.6 is insignificant when the flange thickness is relatively small, such as those of the thin-walled cold-formed sheet members used by Jombock and Clark (1968) and Sooi and Peköz (1993). Sections consisting of component elements with large width-to-thickness ratios are not suitable for extrusion due to production limits (for details, see Kissell and Ferry, 1995). For this reason, most standard sections listed in AA (2000b) are made of relatively thick component elements, falling into the yielding or, at least, inelastic buckling ranges. Thus, the modifications shown in Table 2.5 as well as Table 2.6 are significant for common aluminum extrusions.

2.6.3 Total Moment Capacity Approach (TMCA)

As an alternative to the WASA2, the Total Moment Capacity Approach (TMCA) is also proposed in this study. In this approach, the actual non-linear stress distribution is artificially divided into two linear stress distributions, as shown in Figure 2.10. Such approximation is consistent with the current AA *Specification* (2000a), which is implicit in the WASA. In this figure, the web area and the flange area are assigned separate linear stress distributions so that no overlap can occur. For more complicated cross-sections, the cross-sectional area is divided into a web group and a flange group (for details, see Section 4.4.3). The section modulus of each group is computed with respect to the neutral axis of the entire cross-section, which is at mid-depth for the example I-section. The limit state stress computed for each group is multiplied by the corresponding section modulus to compute the moment capacity.

Afterwards, the moment capacities from all groups are added to obtain a member moment capacity.

For example, the moment capacity of the example I-shaped section can be expressed as Equation (20) based on the TMCA.

$$M_u = M_f + M_w = F_f S_f + F_w S_w = \frac{F_f I_f}{h_c/2} + \frac{F_w I_w}{h_o/2} \qquad (20)$$

where S_f, S_w = the elastic section modulus with respect to the neutral axis of the entire cross-section of the flange and web groups, respectively. For purposes of comparison with the weighted average stress equation of Equation (18), another weighted average stress equation can be defined using the TMCA:

$$F_{TM} = \frac{F_f S_f + F_w S_w}{S} \qquad (21)$$

where F_{TM} denotes the weighted average stress based on the contributory section moduli according to the TMCA. Since all of the component elements contribute to the moment capacity in both the WASA2 and TMCA, these two methods are expected to be more accurate than the MMCA. In addition, the expression for the TMCA resembles that for the WASA, which implies that the WASA is a special case of the TMCA.

Table 2.7 Member allowable stress (or factored member limit state stress) for simple sections

approach	member allowable (or factored member limit state) stress	moment capacity
MMCA	$F_{MIN} = \min\left(F_f, F_w\right)$	$M = F_{MIN} S$
WASA	$F_{WT} = \dfrac{F_f A_f + F_w \frac{1}{3} A_w}{A_f + \frac{1}{3} A_w}$	$M = F_{WT} S$
WASA2	$F_{WT2} = \dfrac{F_f A_f + F_w \frac{1}{3} A_w}{A_f + \frac{1}{3} A_w}\left(\dfrac{h}{h_c}\right)$	$M = F_{WT2} S$
TMCA	$F_{TM} = \dfrac{F_f S_f + F_w S_w}{S}$	$M = F_{TM} S$

The member allowable (or factored member limit state) stress is defined as the combination of each component element allowable (or factored limit state) stress, and is expressed based on the approaches described in this section, which is summarized in Table 2.7. Based on the selected member allowable stress (or factored member limit state stress) expression, the moment capacities are computed for both the compression and tension sides. The minimum of the two moment capacities of the two sides is determined as the moment capacity of the member. When compressive component elements are in the yielding range, the WASA2 and TMCA can result in both of the extreme fiber flange stresses being larger than the maximum limit state stress, for the limit state stress is assumed to occur at mid-thickness of the flange and not the extreme fiber. Though this assumption does not concede to the initial assumptions made concerning the yield and ultimate limit states shown in Figure 2.3, this should not be a problem for simple symmetric sections such as those in Figure 2.1. This is because the actual non-linear stress distribution on the flange is almost uniform as seen in Figure 2.10.

Instead of the use of the allowable stresses (or factored limit state stresses) in Table 2.7, limit state stress values have been employed in the parametric study that follows in Section 2.7.

2.7 *Parametric Study of I-Shaped Sections*

To validate the improvements made in Sections 2.3 to 2.6, a parametric study is conducted for doubly symmetric I-shaped sections, which includes the results of the finite element analyses conducted in Kim (2000). The width of the entire flange ("w" in Figure 2.10) and the depth between the center-lines of flanges ("h_c" in Figure 2.10) are both held constant at 254 mm (10 in.), while the uniform component element thicknesses are varied to allow a wide range of width-to-thickness ratios, so that most of the standard sections listed in AA (2000b) can be covered. The length of the

from the finite element analysis divided by the moment capacity obtained with each approach specified in the graph. As seen in this figure, an approximately 7% difference in the member capacity is observed due to consideration of the ultimate limit state. The data variation also decreases when the ultimate limit state is considered.
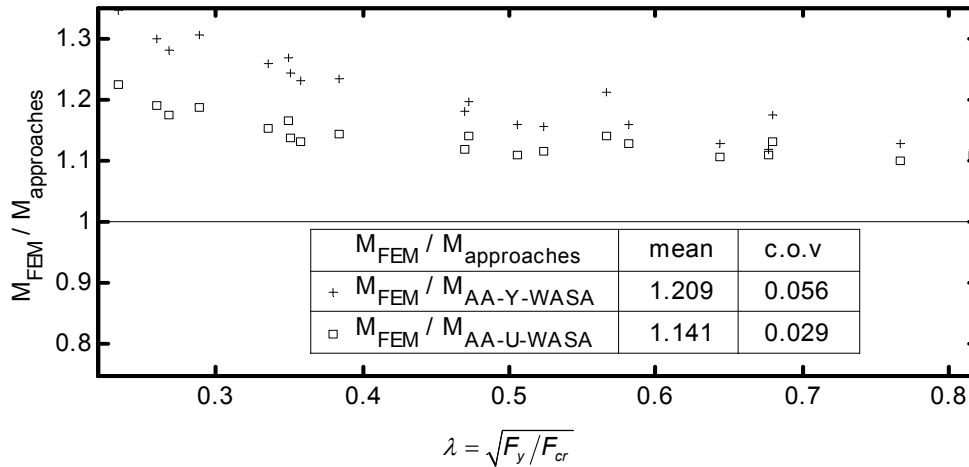
Figure 2.12 Effect of the use of the ultimate limit state ($\varepsilon_u = 4\%$)
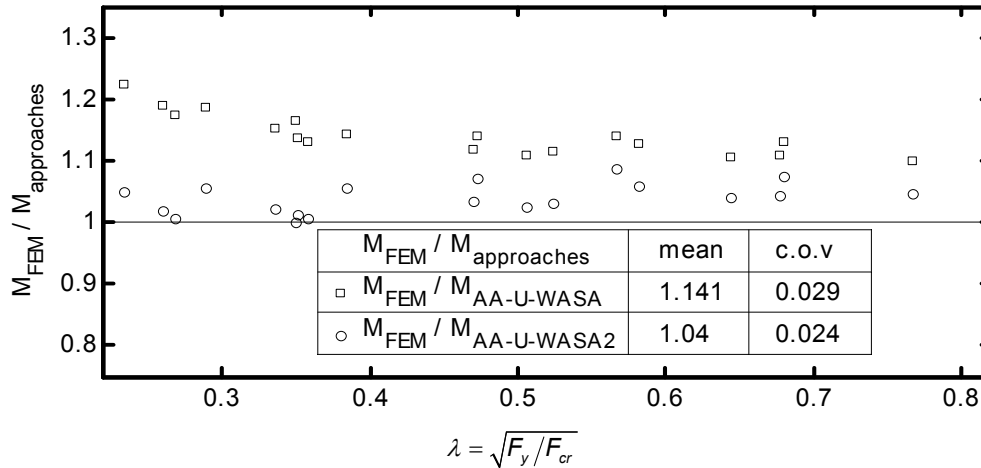
Figure 2.13 Effect of the modification of WASA ($\varepsilon_u = 4\%$)

The second step investigates the effect of the modification of WASA in the AA *Specification* (2000a), as shown in Figure 2.13. The difference from the finite

element analysis is significantly decreased by approximately 10% due to the modification in WASA.

The third and final step compares the two currently available approaches ($M_{AA-Y-MMCA}$ and $M_{AA-Y-WASA}$) in the AA *Specification* (2000a) and those developed in this study ($M_{AA-U-WASA2}$ and $M_{AA-U-TMCA}$). As seen in Figure 2.14, the approaches developed in this study predict the ultimate-plastic capacity more precisely than the current approaches in the AA *Specification* (2000a) for varied slenderness.

Since the difference between the WASA2 and TMCA is insignificant, either approach can be employed for the type of cross-sections considered in this chapter. The moment capacities obtained from all four approaches, as well as from the finite element analyses are listed in Table 2.8. All of the finite element computations shown in Figure 2.12 to Figure 2.14 are made at an ultimate strain (ε_u) of 4%. The percentages indicated in the subscripts of the FEM analyses in Table 2.8, 4% and 8%, represent the ultimate strain values used. When the ultimate strain is 8%, results do not change significantly from that of 4% as seen in this table. This is consistent with the conclusion made from Figure 2.6.

M_{FEM} / $M_{approaches}$	mean	c.o.v
△ M_{FEM} / $M_{AA-Y-MMCA}$	1.248	0.055
+ M_{FEM} / $M_{AA-Y-WASA}$	1.209	0.056
○ M_{FEM} / $M_{AA-U-WASA2}$	1.04	0.024
• M_{FEM} / $M_{AA-U-TMCA}$	1.037	0.023
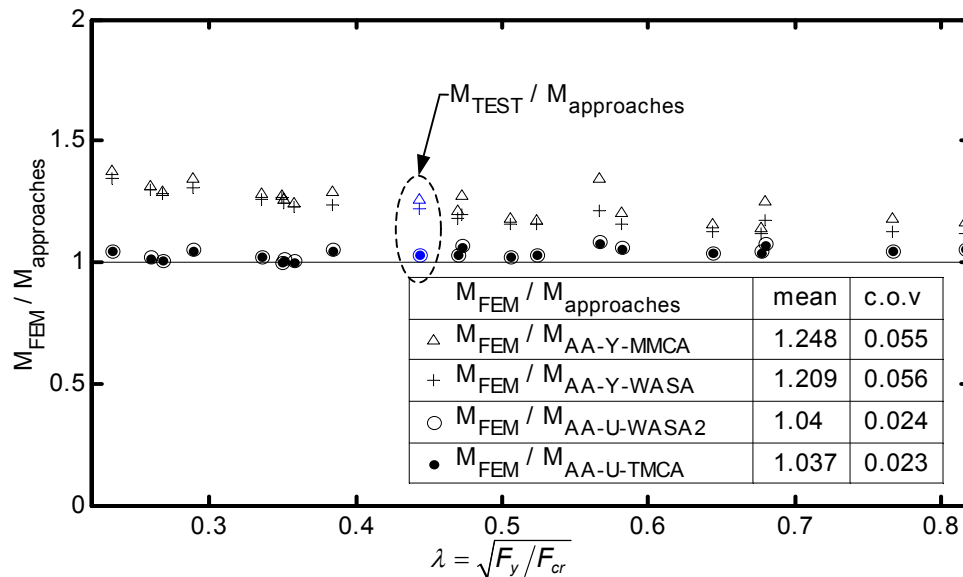
Figure 2.14 Comparison between the current and proposed approaches ($\varepsilon_u = 4\%$)

Table 2.8 Parametric study results

t_w (mm)	t_f (mm)	$\dfrac{M_{AA\text{-}Y\text{-}MMCA}}{M_y}$	$\dfrac{M_{AA\text{-}Y\text{-}WASA}}{M_y}$	$\dfrac{M_{AA\text{-}U\text{-}WASA2}}{M_y}$	$\dfrac{M_{AA\text{-}U\text{-}TMCA}}{M_y}$	$\dfrac{M_{FEM\text{-}4\%}}{M_y}$	$\dfrac{M_{FEM\text{-}8\%}}{M_y}$	$\lambda = \sqrt{\dfrac{F_y}{F_{cr}}}$
25.4	42.3	1.000	1.023	1.309	1.316	1.375	1.378	0.233
25.4	31.8	1.000	1.031	1.277	1.285	1.347	1.340	0.289
25.4	21.2	1.000	1.047	1.223	1.231	1.290	1.280	0.384
25.4	15.9	0.971	1.037	1.157	1.164	1.240	1.230	0.473
25.4	12.7	0.892	0.990	1.105	1.111	1.200	1.190	0.566
12.7	42.3	1.000	1.012	1.289	1.292	1.314	1.305	0.259
12.7	31.8	1.000	1.017	1.251	1.255	1.280	1.270	0.335
12.7	21.2	1.000	1.025	1.171	1.175	1.210	1.200	0.469
12.7	15.9	0.954	0.992	1.085	1.088	1.150	1.140	0.581
12.7	12.7	0.871	0.929	1.013	1.015	1.090	1.090	0.679
8.46	42.3	1.000	1.008	1.282	1.284	1.290	1.275	0.268
8.46	31.8	1.000	1.011	1.241	1.244	1.256	1.240	0.351
8.46	21.2	1.000	1.017	1.151	1.154	1.180	1.170	0.506
8.46	15.9	0.948	0.975	1.056	1.058	1.100	1.100	0.644
8.46	12.7	0.863	0.905	0.975	0.976	1.020	1.030	0.767
6.35	42.3	1.000	1.006	1.276	1.278	1.276	1.260	0.349
6.35	31.8	1.000	1.009	1.233	1.236	1.240	1.220	0.358
6.35	21.2	1.000	1.013	1.136	1.138	1.170	1.150	0.524
6.35	15.9	0.945	0.966	1.034	1.036	1.080	1.080	0.677
6.35	12.7	0.860	0.892	0.946	0.947	0.998	1.000	0.817

2.8   *Experiments and FEM Simulation*

To support the approaches developed in this study, physical tests have been conducted for three doubly symmetric Aluminum Association Standard I-Beams in AA (2000b): I-3x1.64. The alloy-temper of the specimens is 6063-T6, of which the minimum material properties are listed in Table 2.4. Since the study is based on the strength of component elements, continuous lateral supports are required. However, such supports are practically impossible to construct in physical tests.
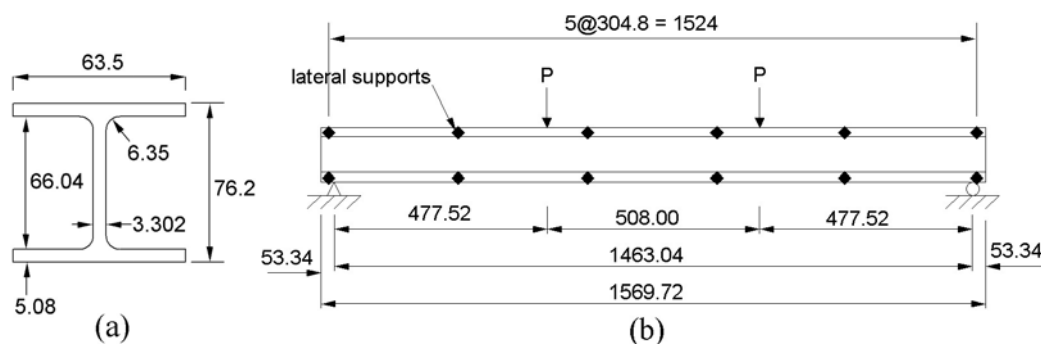
Note: All dimensions are in mm and not to scale

Figure 2.15 (a) Dimensions of section I-3x1.64 (b) schematic test setup
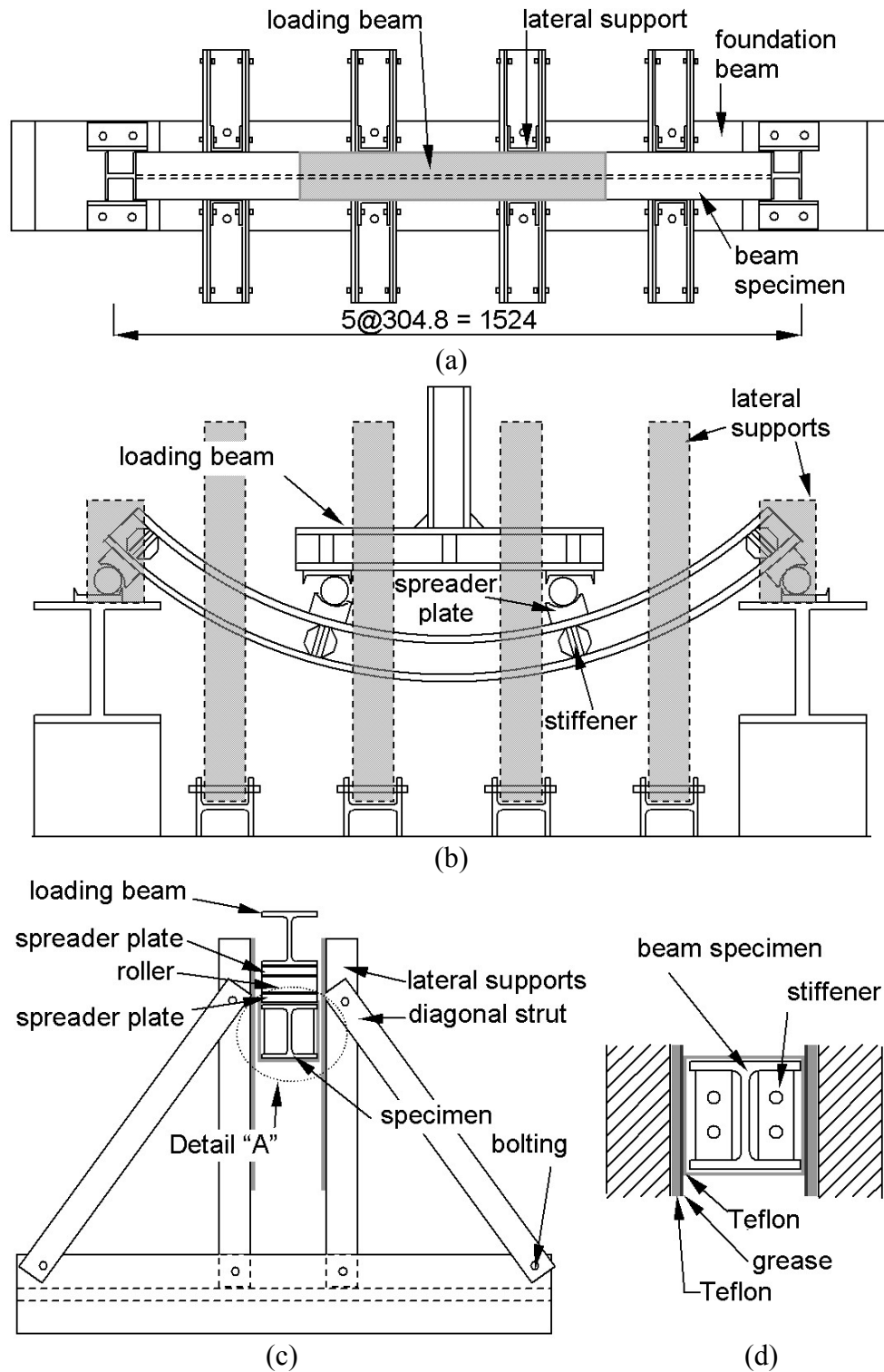
Note: all dimensions are in mm and not to scale

Figure 2.16 Test setup (a) plan view (b) longitudinal section (c) cross-section (d) Detail "A"

For this reason, a parametric study has been conducted using the finite element method to find appropriate lateral support spacing so that the ultimate load factor and the corresponding displacement can be similar to those of the continuous lateral support case. The study results show 304.8 mm (12 in.) is adequate for the lateral support spacing. The test setup is determined as shown in Figure 2.15, including dimensions for the tested specimens. Details of the test setup are shown in Figure 2.16.

All finite element modeling issues covered are similar to those for the parametric study in Section 2.7 except for the following. First, applied load is not pure bending but two-point bending as shown in Figure 2.15b. Second, the lateral support spacing is not continuous. Third, bi-linear spring elements are attached between the spreader plates and the specimen, so that only compression can be transferred. This is to simulate the contact behavior of the actual test setup, in which the spreaders were simply placed on the specimen without any moment connections such as welding or bolting. Fourth, the median of five uniaxial tension test results (Table 6.27a in the Appendix) obtained from one of the specimens is introduced into the finite element analyses. Fifth, different finite element models are used. The model using four-noded linear shell elements with reduced integration is denoted by SHELL; and the model using twenty-noded quadratic hexahedral solid elements with reduced integration is denoted by SOLID. The SOLID model uses two layers of solid elements in the thickness direction. Sixth, initial geometric imperfections are generated using elastic eigen-value analyses with a maximum amplitude based on either the maximum value from the actual measurements in this study (0.048 mm, model FEM 1) or the standard flatness tolerance (0.127 mm, model FEM 2 to 3) according to AA (2000c). The actual measurements for geometric imperfections are shown in Figure 6.6 in the Appendix.

When specimens are removed from the test frame, residual deformation remains, as shown in Figure 2.17. A single wave is formed near the span center in each specimen. The deformed shape near failure from one of the finite element simulations, as shown in Figure 2.18, is similar to those from the physical tests in Figure 2.17.
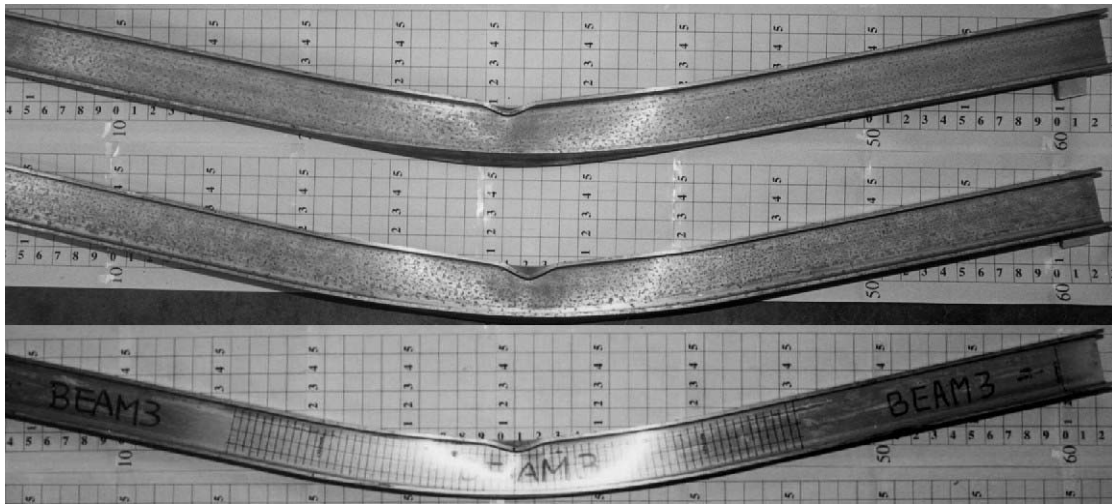
(a)

(b)

Figure 2.17 Residual deformation of tested specimens (I-3x1.64) (a) side (b) plan
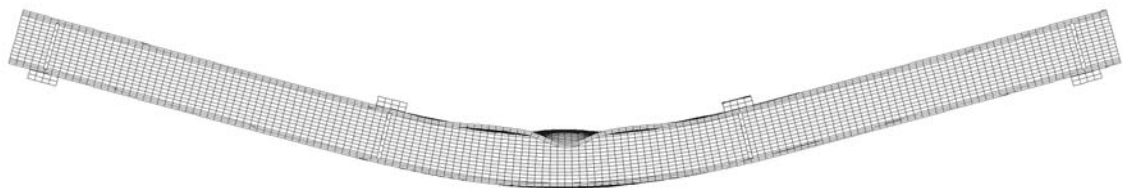
Figure 2.18 Deformed shape near failure using finite element method (SOLID)

As plotted in Figure 2.19, the load factor-displacement curves obtained from both the physical tests and the finite element simulations show close agreement with each other. The variation in the test results are most likely due to the variations in the material properties, as shown in Table 6.27a and Table 6.27b in the Appendix. The average of the maximum load factors from the physical tests is compared to the current specification approaches and those developed in this study within the dashed-line oval of Figure 2.14. The test results follow the trend of the parametric study, which further validates the two proposed approaches in this study. The proposed approaches are based on the ultimate limit state using the WASA2 or TMCA to integrate the moment capacities from individual component elements.
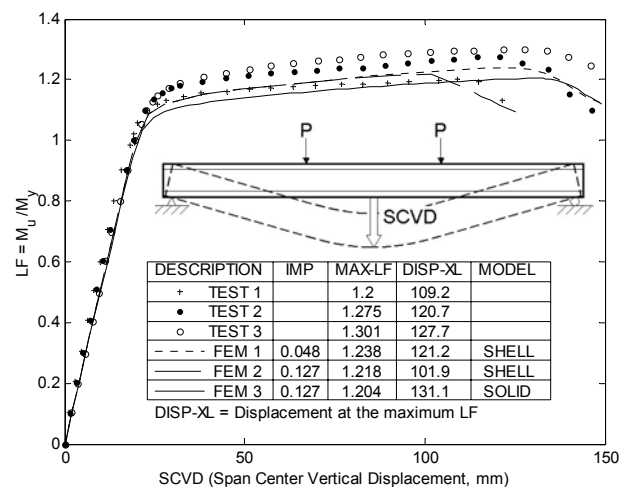
Figure 2.19 Comparison of load factor-displacement results for I-3x1.64 sections

2.9   *Application to the AA* Specification

This study shows that the proposed approaches based on the ultimate limit state are in good agreement with both the finite element simulations and physical tests. However, it is desirable to maintain a certain factor of safety on yield strength in actual designs. As summarized in Table 2.9, the AA *Specification* (2000a) requires choosing the minimum for the allowable stresses (or factored limit state stresses) based on the yield and ultimate limit states for each tension component element.

However, there is only one allowable stress (or factored limit state stress), which is based on the yield limit state, for compression component elements.

Procedure I, which is one of the proposed approaches shown in Table 2.9, is almost the same as the current AA *Specification*, except that allowable stresses (or factored limit state stresses) for both limit states are given not only for the tension but also for the compression component elements as a result of the development in this study. The allowable stress (or factored limit state stress) based on the yield limit state is referred to as the yield allowable stress (or yield factored limit state stress) (F_{ay}), and the allowable stress (or factored limit state stress) based on the ultimate limit state is referred to as the ultimate allowable stress (or ultimate factored limit state stress) (F_{au}) hereafter. In this approach, the same factor of safety on yield strength (n_y) is maintained as in the AA *Specification* (2000a), with a value of 1.65 for building and similar type structures.

Although Table 2.9 and Table 2.10 are based on the Allowable Stress Design, these tables can also be applied to the Load and Resistance Factor Design by replacing the reciprocal of each safety factor with the corresponding resistance factor.

However, it does not seem reasonable to employ a uniform safety factor on yield strength regardless of the margin between the yield and ultimate stresses for a wide variety of alloy-temper combinations. As seen in Figure 2.7, the ratio of the ultimate to yield stress varies from 1.07 to 3.67. The materials with larger margins should be safer than those with smaller margins, e.g., see Figure 1.1. Thus, an alternative approach to computing the allowable stress is proposed in Table 2.9, and is named Procedure II. In this approach, 25% of the margin between the yield and ultimate allowable stresses is added to the yield allowable stress. Thus, the allowable stress increases as the ratio of the ultimate to yield stress increases, which results in a varying safety factor on yield strength.

Table 2.9 Governing allowable stresses

approaches	governing allowable stress for tension	governing allowable stress for compression
current AA Specification	$F_a = \min\left(F_{ay}, F_{au}\right)$	$F_a = F_{ay}$
proposed approaches	Procedure I $$F_a = \min\left(F_{ay}, F_{au}\right) \qquad (23)$$ Procedure II $$F_a = F_{ay} + 0.25\left(F_{au} - F_{ay}\right) \le \min\left(1.25 F_{ay}, F_{au}\right) \qquad (24)$$	

Note: F_a = the governing allowable stress

F_{ay} = the member allowable stress based on the yield limit state. See Table 2.7.

F_{au} = the member allowable stress based on the ultimate limit state. See Table 2.7.

Table 2.10 Allowable stress equations for (a) tension component element, (b) compression component element, and (c) shape factors

(a)

AA Section	allowable stresses
3.4.2	$F_{ay} = \alpha_y F_{ty}/n_y$
3.4.4	$F_{au} = \alpha_u F_{ty}/\left(k_t n_u\right)$

(b)

AA Section	allowable stresses in yielding range $b/t \le S_1$	limit S_1	allowable stresses in inelastic buckling range $S_1 \le b/t \le S_2$	limit S_2	allowable stresses in post buckling range $S_2 \le b/t$
3.4.15 3.4.16 3.4.18	$F_{ay} = \dfrac{\alpha_y F_{cy}}{n_y}$ $F_{au} = \dfrac{\alpha_u F_{cy}}{n_u}$	$\dfrac{B - \alpha_y F_{cy}}{\kappa D}$ $\dfrac{B - \frac{n_y}{n_u}\alpha_u F_{cy}}{\kappa D}$	$F_{ay} = F_{au} = $ $\dfrac{1}{n_y}\left(B - D\kappa \dfrac{b}{t}\right)$	$\dfrac{k_1 B}{\kappa D}$	$F_{ay} = F_{au} = \dfrac{k_2\sqrt{BE}}{n_y \kappa \dfrac{b}{t}}$

(c)

AA Section	yield shape factor	ultimate shape factor
3.4.2	$\alpha_y = 1.0$	$\alpha_u = F_{tu}/F_{ty}$
3.4.4	$\alpha_y = 1.3$	$\alpha_u = 1.25 F_{tu}/F_{ty} + 0.2$ [a]
3.4.15, 3.4.16	$\alpha_y = 1.0$	$\alpha_u = F_{tu}/F_{cy}$ [b]
3.4.18	$\alpha_y = 1.3$	$\alpha_u = 1.25 F_{tu}/F_{cy} + 0.2$ [c]

Note: a, c. This is for a symmetric section. See Table 4.8c for an unsymmetric section.

a. In the AA *Specification*, $\alpha_u = 1.42 F_{tu}/F_{ty}$.

b, c. Not available in the AA *Specification*.

For other coefficients, see the AA *Specification*. Each allowable stress in this table is introduced into equations in Table 2.7 to compute the member allowable stress.

The safety factor on ultimate strength (n_u = 1.95 for building and similar type structures) given in the AA *Specification* (2000a) is maintained, since only the specified percentage of the ultimate allowable stress is used. Since the safety factor on yield strength is defined as the ratio of the yield limit state stress to the allowable stress, the following expression characterizes the varying safety factor on yield strength for a tension side component element:

$$\tilde{n}_y = \alpha_y F_y / F_a \qquad (25)$$
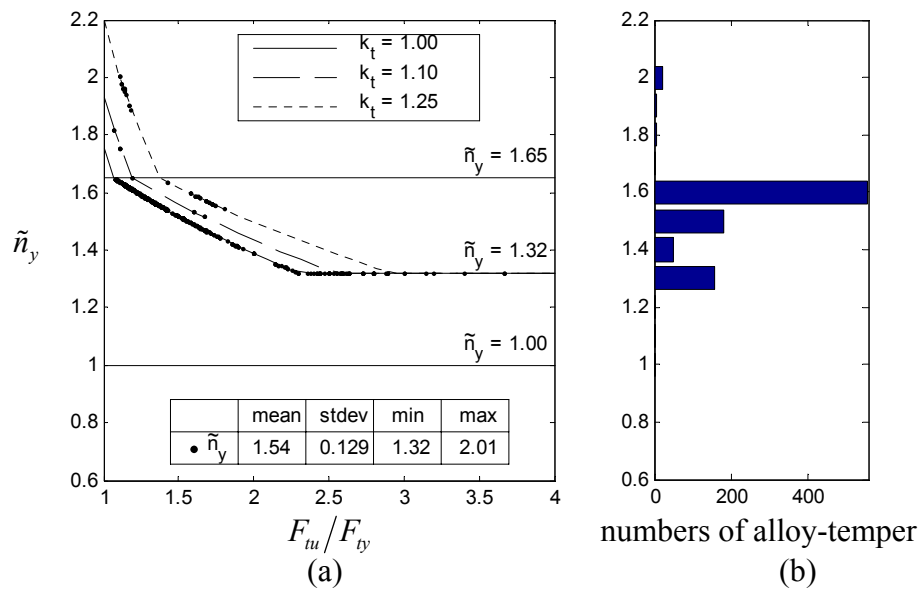
Figure 2.20 Safety factor on yield strength of the tensile allowable stress (AA Section 3.4.4) for a plate under bending based on Procedure II

In Figure 2.20a, using Equation (25) based on Procedure II, the varying safety factors on yield strength of a rectangular web element under bending are plotted with solid circles for the 986 alloy-temper combinations selected in Section 2.4. It is seen that the average of the varying safety factor on yield strength (1.54) is only 6.7% smaller than the current fixed safety factor on yield strength (1.65). The solid and dashed curves represent the analytic expressions of the varying safety factors for the materials with different notch sensitivities (k_t). Note that the majority of the alloy-temper combinations are concentrated near the average, as shown in Figure 2.20b. In

addition, the minimum of the varying safety factor on yield strength is set to 1.32 due to the first safeguard in Equation (24). The second safeguard in this equation is for the case that the yield allowable stress is larger than the ultimate allowable stress.

Similarly, varying safety factors on yield strength are computed for I-shaped sections used in Section 2.7, as seen in Figure 2.21. The varying safety factor on yield strength for an entire cross-section is defined as follows:

$$\tilde{n}_y = \frac{\text{moment capacity based on yield limit state stresses and TMCA}}{\text{moment capacity based on allowable stresses and given approaches}} \qquad (26)$$

This definition of the varying safety factor for a cross-section composed of web and flange elements is consistent with that for a rectangular web element in Equation (25). The only difference is that the moment capacity evaluation approaches in Section 2.6 are incorporated to combine limit state stresses for all component elements. The numerator is the moment capacity computed by the TMCA when each component element reaches the yield limit state stress implied in Table 2.2 for the tension side and defined in Table 2.5 for the compression side. The moment capacity in the denominator of Equation (26) is calculated as follows; the member allowable stress is calculated from Table 2.7, which is then used to calculate the governing allowable stress in Table 2.9, and this is then multiplied by the section modulus. The abbreviations used in Figure 2.21 are based on the approach combinations used in the denominator. SF_{AA}, SF_{P1} and SF_{P2} are the varying safety factor on yield strength computed when the allowable moment capacity is based on the current AA *Specification* (2000a) and Procedures I and II in Table 2.9, respectively. The last category in these abbreviations represents one of the moment capacity evaluation approaches in Table 2.7. In Figure 2.21, WASA2 is not shown because it is almost identical to TMCA.
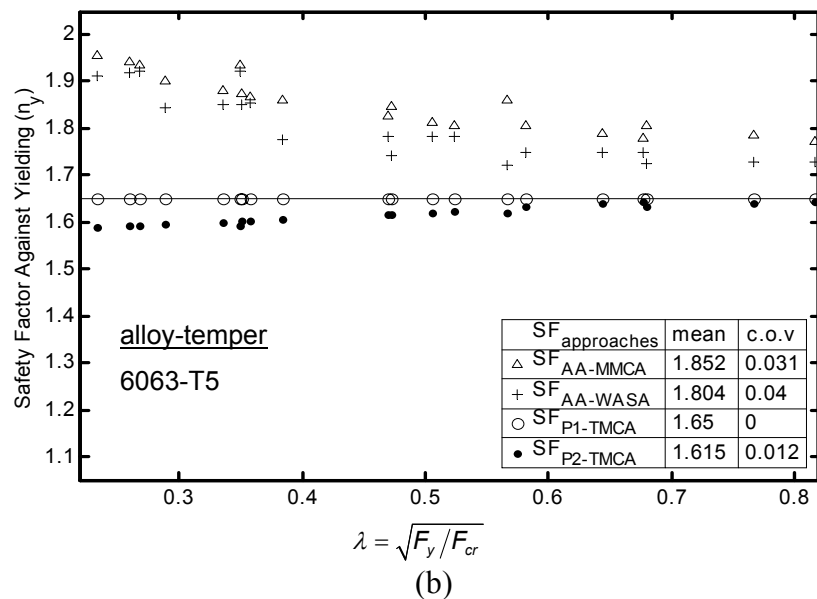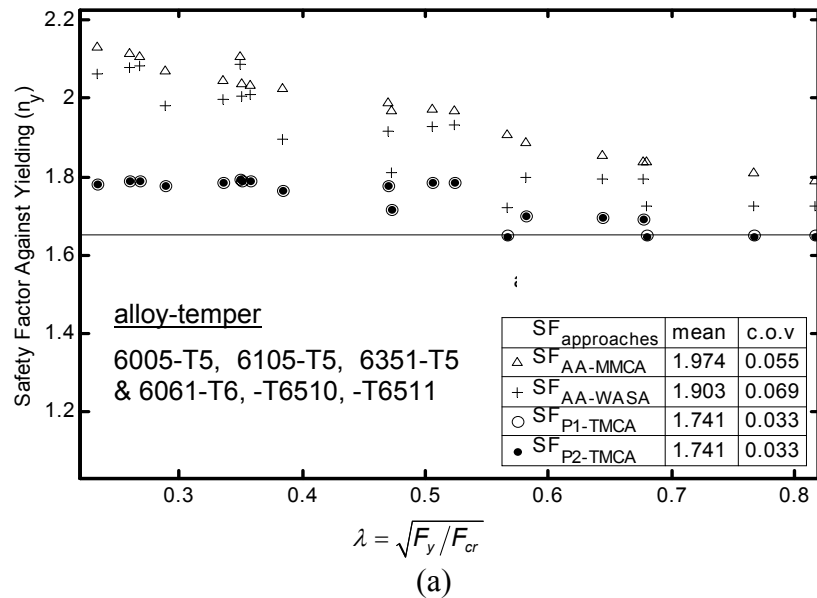
Figure 2.21 Comparison of safety factor on yield strength between current and proposed approaches for I-sections of Section 2.7

Two types of materials are used in Figure 2.21. In Figure 2.21a, the first group (6005-T5, 6105-T5, 6351-T5, 6061-T6, 6061-T6510, and 6061-T6511) from among the 6000 series alloy-temper combinations in Table 2.4 is used. When the width-to-thickness ratio (b/t) of a compression flange falls into the yielding range as specified

in Table 2.10b, the ultimate limit state will govern for this material, since the ultimate to yield stress ratio of this material group (F_{tu}/F_{cy} = 1.086) is smaller than the ratio of the safety factor on ultimate strength to the safety factor on yield strength (n_u/n_y = 1.18 for building type structures). Further details are as follows: a compression flange has two allowable stresses as shown in the yielding range of Table 2.10b, $F_{ay} = F_{cy}/n_y$ and $F_{au} = F_{tu}/n_u$. If the ultimate limit state governs, then $F_{au} \le F_{ay}$. Thus, $F_{tu}/n_u \le F_{cy}/n_y$, and then, $F_{tu}/F_{cy} \le n_u/n_y$. In this computation, all stresses are positive. However, if the width-to-thickness ratio (b/t) falls outside of the yielding range, the yield limit state may govern, since the two allowable stresses for a compression flange become closer as shown in the inelastic buckling range of Table 2.10b. For this reason, regardless of the slenderness factor, the varying safety factor on yield strength is larger than or equal to 1.65, as in the AA *Specification*. So for this group there is no difference between Procedures I and II.

In Figure 2.21b the third alloy-temper combination (6063-T5) in Table 2.4 is used. Similarly, since the ultimate to yield stress ratio (F_{tu}/F_{cy} = 1.4) is larger than the ratio of the safety factors (n_u/n_y = 1.18), the yield limit state governs for a compression flange. Thus, regardless of the slenderness factor, the safety factor on yield strength is a constant, 1.65 if Procedure I is used. When Procedure II is used, the safety factor varies, as expected.

In the aforementioned discussion, the governing limit state should also be examined with respect to a compressive web component element. However, with these types of cross-sections and material properties, it is found that the effect of the web element is insignificant, as shown in computational examples provided in the Appendix.

In Figure 2.21, it is found that the calculated member moment capacity by Procedure I is 9 to 13% more than that can be computed by the current AA

Specification. A constant safety factor on yield strength of 1.65 is maintained. Procedure II further increases the calculated member moment capacity for materials with a larger margin between the ultimate and yield stresses. Although this will result in a variation in the safety factor on yield strength, it should not cause any significant problem for maintaining a desirable strength margin for safety. Step-by-step computation procedures for the allowable moment capacity and the safety factor are provided in the Appendix for a sample cross-section.

2.10 Conclusions

For tension component elements, the AA *Specification* provides two different allowable stress (or factored limit state stress) expressions at the yield and ultimate limit states. However, for compression component elements, the allowable stress (or factored limit state stress) is provided only for the yield limit state. In this study, the limit state stress at the ultimate limit state is developed for compression component elements to take advantage of the ultimate-plastic capacity of compact aluminum members in bending.

An expression for the ultimate limit state stress for compression component elements is obtained from rigorous closed-form expressions derived for the ultimate shape factor for rectangular web elements integrating the stresses across the cross-section. The rigorous expression thus obtained is simplified for practical design purposes. A parametric study for component elements is conducted using the finite element method. Based on the above studies, the ultimate limit state stress equations are proposed for compression component elements. In addition, the empirically developed weighted average stress approach (WASA) is investigated, and a simple modification is proposed. Moreover, a more general approach denoted by the Total Moment Capacity Approach (TMCA) is developed.

The proposed approaches are more accurate for calculating the moment capacities of laterally supported flexural members. This is validated through a parametric study of I-shaped sections with a wide range of slenderness, using the finite element method. The proposed approaches are further supported by the flexural tests of standard sections.

For design purposes, two procedures are suggested. In Procedure I, the factor of safety on yield strength used in the current specification is maintained. In Procedure II, the safety factor is applied to the additional inelastic capacity. Procedure II is more reasonable in that the safety factor varies depending on the margin between the ultimate and yield stresses.

3. SYMMETRIC CROSS-SECTIONS WITH TAPERED THICKNESS COMPONENT ELEMENTS

Some standard sections listed in AA (2000b) have tapered thickness plate flanges, as shown in Figure 3.1a. Also custom shapes with tapered thickness flanges may be extruded as shown in Figure 3.1b.

(a)   (b)
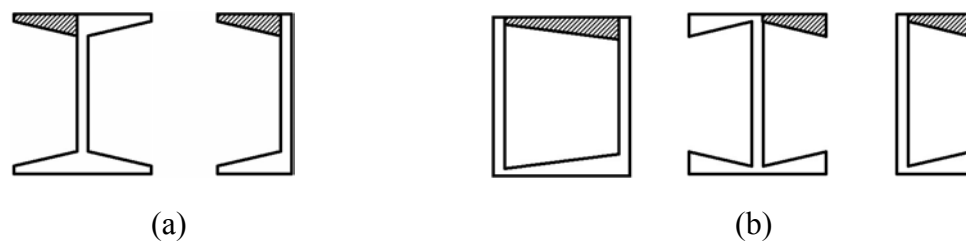
Figure 3.1 Examples of sections with tapered elements (a) standard extruded shapes (b) custom extruded shapes

The behavior of a component element with tapered thickness has been investigated for aircraft and structural member analysis by Pines et al. (1947), Wittrick et al. (1962), Chehil et al. (1973), Kobayashi et al. (1990), Mizusawa (1993) and Ohga et al. (1995). However, The behavior of tapered thickness elements has not been fully incorporated in both AISC (1998) and the AA *Specification* (2000a). Instead, an average thickness is used in design.

In this study, stiffness matrices for plates with tapered thickness are derived for use in the framework of an available finite strip analysis program. Using the program, plate buckling coefficients can be calculated taking into account thickness variation and boundary conditions. The plate buckling coefficients obtained are introduced into the current specification approach for aluminum structures to calculate more precise limit state stresses.

3.1 Introduction

Sections with tapered plate thickness shown in Figure 3.1a are commonly used sections made of steel or aluminum. However, the design equations for the behavior of such tapered plate elements have not been fully developed in specifications. In both AISC (1998) and the AA *Specification* (2000a), the treatment of a tapered component element as a uniform one using an average thickness is implied.

The buckling behavior of a plate element with tapered thickness has been studied primarily for aircraft design by Pines et al. (1947), Wittrick et al. (1962), and Chehil et al. (1973). The main focus has been on the buckling of a plate with a thickness variation in the same direction as the loading. However, since a plate element that is a component of a structural member is tapered in the direction perpendicular to loading as shown in Figure 3.2, these studies do not apply to the type of problem covered in this study.
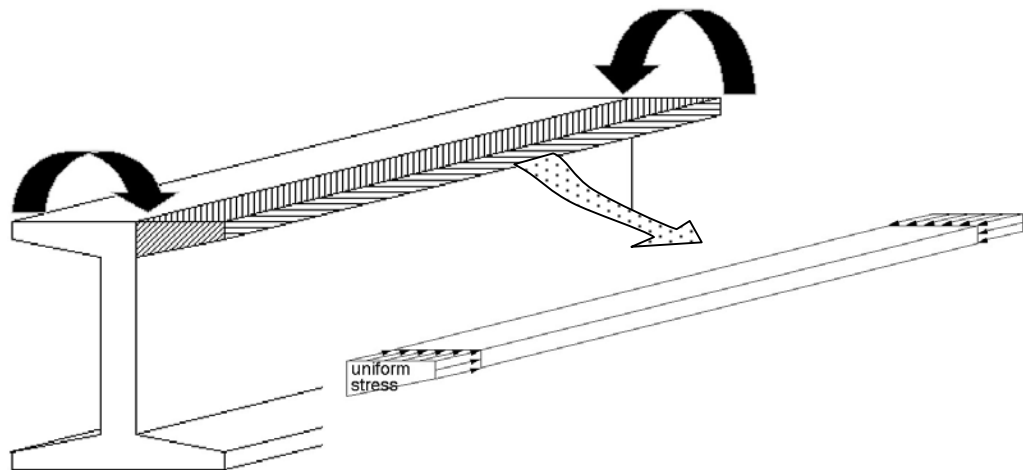
Figure 3.2 A tapered element separated from an I-section under bending

More recently, Kobayashi et al. (1990), Mizusawa (1993) and Ohga et al. (1995) have studied the behavior of plate elements tapered in the direction perpendicular to loading which is the same case as the problem in Figure 3.2.

However, the studies have focused on demonstrating theoretical approaches without any application to structural design codes.

In this study, stiffness matrices are derived for a plate element with tapered thickness based on the finite strip method. The derived stiffness matrices are incorporated into the CUFSM program developed by Schafer (1997) to compute the elastic buckling stress of arbitrary shapes containing tapered thickness component elements such as those in Figure 3.1. The program is also used to compute the plate buckling coefficients of an individual tapered thickness plate element with idealized boundary conditions. The plate buckling coefficients determined in this way are incorporated in the AA *Specification* (2000a) so that the limit state stresses of tapered plate elements are obtained rigorously instead of treating such elements as having a uniform thickness.

A parametric study of a wide variety of I-shaped sections with tapered thickness is conducted using non-linear inelastic finite element analyses to validate the limit state stress expressions based on the rigorously obtained plate buckling coefficients. Physical tests further support this approach. Allowable stress design equations are also suggested for application to the AA *Specification* (2000a) based on the proposed limit state stress equations. The framework for uniform thickness sections is maintained in the proposed approach for tapered thickness sections.

3.2   *Stiffness Matrices for a Tapered Finite Strip Element*

The CUFSM program computes the elastic buckling load factor and corresponding mode shapes using the finite strip method. However, since CUSFM is based on the uniform plate theory, a thickness variation cannot be considered directly. This study derives stiffness matrices for tapered finite strip elements.

The shape function used in CUFSM is based on Cheung (1976). The shape function is the multiplication of a width-direction shape function $X(x)$ and a longitudinal-direction shape function $Y(y)$.

$$N(x,y) = X(x)Y(y) \qquad (27)$$

For the plane stress part of the stiffness matrix, the width-direction shape function $X(x)$ is linear, which is the same as a truss element. For the plate bending part of the matrix, the width-direction shape function $X(x)$ is cubic, which is the same as a beam element. The longitudinal-direction shape function $Y(y)$ is a sine function, since the boundary condition at the loaded edges of the CUFSM program is limited to the simply-supported case. Only the width-direction shape functions are modified, since the thickness varies only in that direction. The exact shape functions for tapered truss and beam elements are based on McGuire et al. (2000).
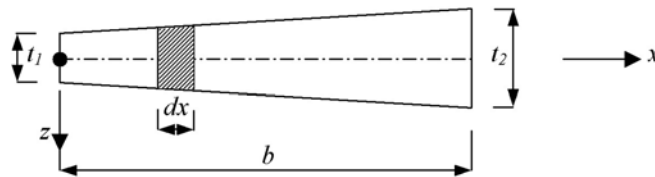
Figure 3.3 A tapered truss or beam element with unit width or a cross-section of a tapered plate element
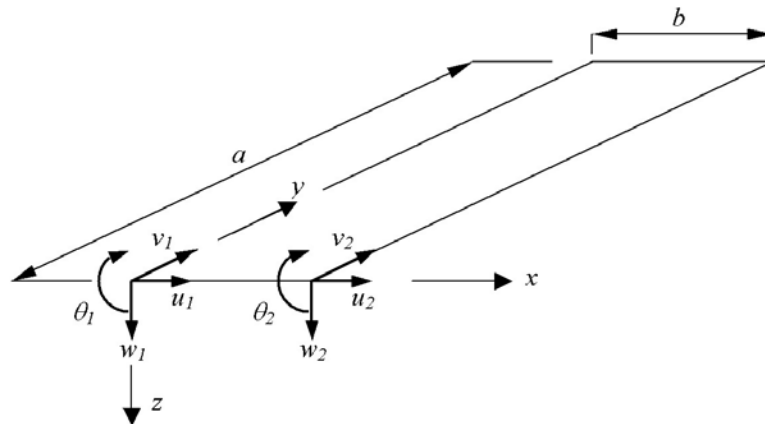
Figure 3.4 Degrees of freedom for a finite strip

For the axially loaded linearly tapered truss element shown in Figure 3.3, the equilibrium of an infinitesimal segment in the x-direction yields the following displacement field:

$$u(x) = \lfloor N_t(x) \rfloor \lfloor u_1 \quad u_2 \rfloor^T \tag{28}$$

$$\lfloor N_t(x) \rfloor = \lfloor 1 - f_1(x) \quad f_1(x) \rfloor \tag{29}$$

where $f_1(x) \equiv \dfrac{\ln\left(1 + \delta \frac{x}{b}\right)}{\ln(1+\delta)}$, $\delta = \dfrac{t_2 - t_1}{t_1}$ and $\lfloor N_t(x) \rfloor$ = the shape function for a tapered truss element.

Using Equation (29), the shape function for the plane stress is expressed in the form of Equation (27) within the displacement field:

$$\lfloor u(x,y) \quad v(x,y) \rfloor^T = [N_1(x,y)] \lfloor u_1 \quad v_1 \quad u_2 \quad v_2 \rfloor^T \tag{30}$$

$$[N_1(x,y)] = \begin{bmatrix} (1-f_1(x))Y_m(y) & 0 & f_1(x)Y_m(y) & 0 \\ 0 & (1-f_1(x))\dfrac{Y'_m(y)}{k_m} & 0 & f_1(x)\dfrac{Y'_m(y)}{k_m} \end{bmatrix} \tag{31}$$

where $Y_m(y) = \sin(k_m y)$, $k_m = m\pi/a$, m = number of half-waviness, and a = longitudinal length of the strip element (y-direction in Figure 3.4). The degrees of freedom in Equation (30) are defined in Figure 3.4.

The strain field is derived from the displacement field:

$$\lfloor \varepsilon_x \quad \varepsilon_y \quad \gamma_{xy} \rfloor^T = \left\lfloor \left(\dfrac{\partial u}{\partial x}\right) \quad \left(\dfrac{\partial v}{\partial y}\right) \quad \left(\dfrac{\partial u}{\partial y} + \dfrac{\partial v}{\partial x}\right) \right\rfloor^T = [B_1(x,y)] \lfloor u_1 \quad v_1 \quad u_2 \quad v_2 \rfloor^T \tag{32}$$

$$[B_1(x,y)] = \begin{bmatrix} -f'_1(x)Y_m(y) & 0 & f'_1(x)Y_m(y) & 0 \\ 0 & (f_1(x)-1)k_m Y_m(y) & 0 & -f_1(x)k_m Y_m(y) \\ (1-f_1(x))Y'_m(y) & -f'_1(x)\dfrac{Y'_m(y)}{k_m} & f_1(x)Y'_m(y) & f'_1(x)\dfrac{Y'_m(y)}{k_m} \end{bmatrix} \tag{33}$$

The initial stiffness matrix of the plane stress part is derived from the minimum potential energy:

$$[k_{plane-stress}] = \int_0^b \int_0^a t(x)[B_1]^T [E_p][B_1] dy dx \qquad (34)$$

where $[E_p] = \begin{bmatrix} E_1 & v_x E_2 & 0 \\ v_x E_2 & E_2 & 0 \\ 0 & 0 & G \end{bmatrix}$, $E_1 = \dfrac{E_x}{1-v_x v_y}$, $E_2 = \dfrac{E_y}{1-v_x v_y}$, $t(x) = t_1\left(1+\delta\dfrac{x}{b}\right)$, E_x,

E_y = Young's moduli, G = shear modulus, and v_x, v_y = Poisson's ratios.

For the linearly tapered beam element shown in Figure 3.3, the force equilibrium of an infinitesimal segment in the vertical direction (z) and the moment equilibrium with respect to the axis perpendicular to the cross-section (y) yield the following displacement field:

$$w(x) = \lfloor N_b(x) \rfloor \lfloor w_1 \quad \theta_1 \quad w_2 \quad \theta_2 \rfloor^T \qquad (35)$$

where $\lfloor N_b(x) \rfloor$ = the shape function for a tapered beam element

$$\lfloor N_b(x) \rfloor = \frac{1}{C} \left\{ \begin{array}{c} f_2(x) - \delta + (2+\delta)\ln\left(\dfrac{f_2(b)}{f_2(x)}\right) - \dfrac{f_2(b)}{f_2(x)} \\[2mm] \dfrac{b}{f_2(x)}\left[(\delta - \ln(1+\delta))\left(\dfrac{x}{b}\right)^2 + (C+\delta)\left(\dfrac{x}{b}\right)\right] - b\ln f_2(x) \\[2mm] -f_2(x) - \delta + (2+\delta)\ln f_2(x) + \dfrac{f_2(b)}{f_2(x)} \\[2mm] \dfrac{bf_2(b)}{f_2(x)}\left[\dfrac{(C+\delta\ln(1+\delta))}{2}\left(\dfrac{x}{b}\right)^2 + \delta\dfrac{x}{b}\right] - bf_2(b)\ln f_2(x) \end{array} \right\}^T \qquad (36)$$

where $C = -2\delta + (2+\delta)\ln(1+\delta)$, and $f_2(x) = 1 + \delta\dfrac{x}{b}$

Using Equation (36), the shape function for plate bending is expressed in the form of Equation (27) within the displacement field for a finite strip element:

$$w(x, y) = \lfloor N_2(x, y) \rfloor \lfloor w_1 \quad \theta_1 \quad w_2 \quad \theta_2 \rfloor^T \qquad (37)$$

$$\lfloor N_2(x,y) \rfloor = \lfloor N_b(x) \rfloor Y_m(y) \tag{38}$$

The degrees of freedom in Equation (37) are defined in Figure 3.4.

Using the displacement field in Equation (37), the strain field is computed:

$$\lfloor \varepsilon_x \quad \varepsilon_y \quad \gamma_{xy} \rfloor^T = \left\lfloor -\frac{\partial^2 w}{\partial x^2} \quad -\frac{\partial^2 w}{\partial y^2} \quad 2\frac{\partial^2 w}{\partial x \partial y} \right\rfloor^T = [B_2(x,y)] \lfloor w_1 \quad \theta_1 \quad w_2 \quad \theta_2 \rfloor^T \tag{39}$$

where $\left[B_2(x,y) \right] = \left[-[N_b''(x)]Y_m(y) \quad [N_b(x)]k_m^2 Y_m(y) \quad 2[N_b'(x)]Y_m'(y) \right]^T$.

The initial stiffness matrix of the plate bending part is also derived from the minimum potential energy:

$$[k_{plate-bending}] = \int_0^b \int_0^a [B_2]^T [E_b][B_2] dy dx \tag{40}$$

where $[E_b] = \dfrac{t^3(x)}{12}\left[E_p \right]$.

The complete initial stiffness matrix is a combination of Equations (34) and (40):

$$[k_e] = \begin{bmatrix} \left[k_{plane-stress} \right] & zeros(4 \times 4) \\ zeros(4 \times 4) & \left[k_{plate-bending} \right] \end{bmatrix} \tag{41}$$

The derivation of the geometric stiffness matrix follows Schafer (1997). The thickness variation is also incorporated in the geometric stiffness matrix. For a linearly varying applied stress,

$$\left[k_g \right] = \int_0^a \int_0^b \left(f_1 - (f_1 - f_2)\frac{x}{b} \right) t(x)[G]^T [G] dx dy \tag{42}$$

where $[G]\{d\} = \left\lfloor \dfrac{\partial u(x,y)}{\partial y} \quad \dfrac{\partial v(x,y)}{\partial y} \quad \dfrac{\partial w(x,y)}{\partial y} \right\rfloor^T$, f_1 and f_2 = stresses at the nodes of an element, $\{d\} = \lfloor u_1 \ v_1 \ u_2 \ v_2 \ w_1 \ \theta_1 \ w_2 \ \theta_2 \rfloor^T$, $\lfloor u(x,y) \ v(x,y) \rfloor^T$ = Equation (30), and $w(x,y)$ = Equation (37). The stiffness matrices derived in this manner are introduced into the CUFSM program.

In this program, after the initial stiffness matrix of Equation (41) is computed for each element, each stiffness matrix is transformed into a global coordinate system. The transformed stiffness matrices from all elements are assembled according to the global degrees of freedom. The same procedure is repeated for the geometric stiffness matrix of Equation (42). By solving the eigen-value problem of Equation (43), elastic buckling load factors (β) and corresponding mode shapes $\{\Delta\}$ are obtained for a given cross-section:

$$\left[K_e + \beta K_g \right]\{\Delta\} = \{0\} \qquad (43)$$

where K_e, K_g = the assembled initial and geometric stiffness matrices in a global coordinate system, respectively.

Due to the singularity of the width-direction shape functions in Equations (29) and (36) as the thickness variation ratio (δ) approaches zero, the stiffness matrices for a plate with tapered thickness are used only when the thickness variation ratio is larger than or equal to 5%. For a thickness variation ratio less than 5%, stiffness matrices for uniform thickness are used with an average thickness.

A version of the CUFSM program has been developed to accommodate the effect of tapered thickness based upon the theory developed in this study. This version of the program is called CUFSM-tap hereafter.

3.3 *The Plate Buckling Coefficient for a Tapered Thickness Plate Element and Application to the AA* Specification

In the AA *Specification* (2000a), the compressive limit state stress varies according to the equivalent slenderness ratio (λ_p), which falls into one of three ranges, the yielding, inelastic buckling, and post buckling ranges, as shown in Figure 2.4. The equivalent slenderness ratio (λ_p) is defined in Equation (5).

$$\lambda_p = \kappa \left(\frac{b}{t} \right), \text{ where } \kappa = \sqrt{\frac{12\left(1 - v^2\right)}{k_p}} \tag{5}$$

As seen in this equation, the equivalent slenderness ratio of each component element is dependent on the plate buckling coefficient (k_p).

However, for a plate element with tapered thickness, the equivalent slenderness is not provided in the current AA *Specification* (2000a), since the plate buckling coefficient is unknown. Examples of sections with tapered thickness are shown in Table 3.1. The shaded flange area of each cross-section is considered as an individual plate element under uniform compression with idealized boundary conditions.

Table 3.1 Idealization of sections with tapered elements

Flexural member – idealized tapered element under uniform compression is shaded	idealized boundary condition (IBC)	IBC designation
		SSSS
		SSFS
		SSSF
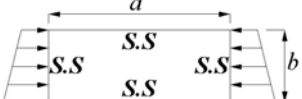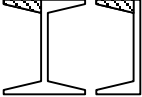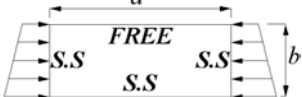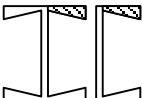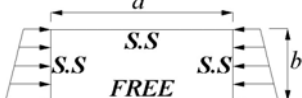
Since the thickness varies at the loaded edges, the distributed force per unit length shown in this table, which is the multiplication of the uniform compressive stress by the thickness, is not uniform. Using the CUFSM-tap program, the plate buckling coefficient is computed for each idealized plate element shown in Table 3.1. The computation is based on a given thickness variation ratio (δ), which is defined in Equation (44), and repeated for different ratios. The thickness variation ratio (δ) is an additional variable needed to evaluate a plate with tapered thickness:

$$\delta = \left(t_2 - t_1\right)/t_1 \tag{44}$$

The plate buckling coefficient (k_p^1) is computed based on the smallest thickness (t_1).

$$k_p^1\left(\delta\right) = \frac{12\left(1-v^2\right)\left(b/t_1\right)^2 F_{cr}}{\pi^2 E} \qquad (45)$$

The computed plate buckling coefficients are plotted in Figure 3.5. In the analysis, the plate is discretized into eight equally spaced strips.
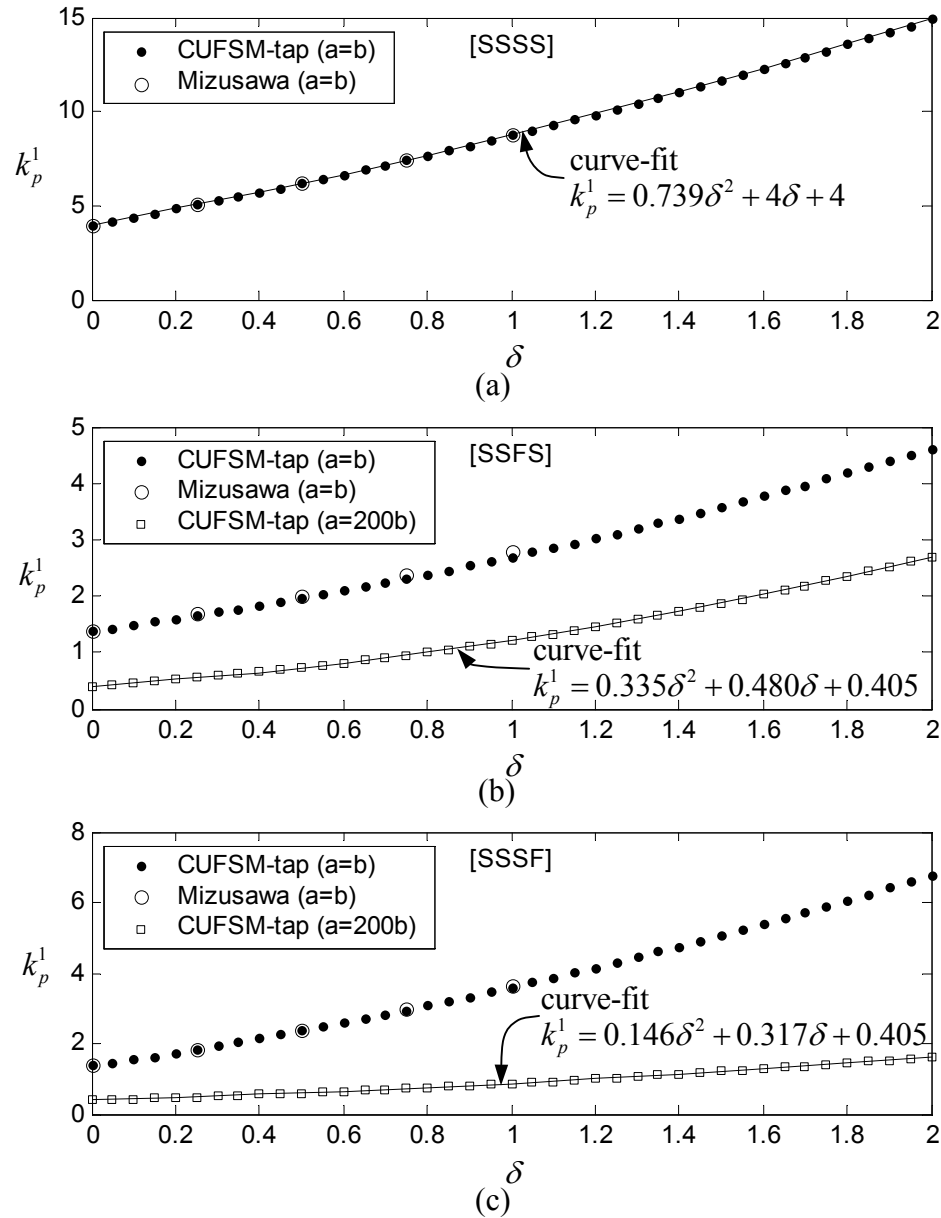
Note: $b/t_1 = 1000$ in Mizusawa (1993)

Figure 3.5 Plate buckling coefficient of tapered thickness plates for boundary condition (a) SSSS (b) SSFS (c) SSSF

The plate buckling coefficients calculated in this study are compared to Mizusawa (1993) as shown in Figure 3.5. Since the available data from Mizusawa (1993) is limited to the case where the width (*b*) is the same as the length (*a*), initial comparisons are made from buckling coefficients calculated for the same case. However, since the plate buckling coefficient decreases as the length-to-width ratio (*a/b*) increases under SSFS and SSSF boundary conditions, the results for a large length-to-width ratio (*a/b*) of 200 are also given. The plate buckling coefficient obtained from CUFSM by using this length-to-width ratio for a plate with uniform thickness is 0.405. This number is rather small compared to 0.425 or 0.43, which is found in other specifications. However, 0.405 is more consistent with the current AA *Specification* (2000a), since the equivalent slenderness of a uniform thickness plate under the SSFS (or SSSF) boundary condition is 5.13(*b/t*) according to the Aluminum Company of America (1958), from which the basis for the AA *Specification* (2000a) is obtained. See Equation (5) to obtain $\lambda_p = 5.13(b/t)$ from $k_p = 0.405$ when $\nu = 1/3$.

As the thickness variation ratio (δ) increases, the plate buckling coefficient (k_p^1) increases monotonically as seen in Figure 3.5. For this reason, quadratic equations are used for curve-fitting the relationship between the plate buckling coefficient and the thickness variation ratio. The error average between the computed and curve-fitted data is less than 0.1%, with a standard deviation of less than 0.5% for all cases.

The curve-fitted plate buckling coefficients in Figure 3.5 are based on the minimum thickness (t_1) as shown in Equation (45). However, it would be more useful for practical design purposes if the plate buckling coefficients were expressed in terms of the average thickness, as the current AA *Specification* is based on the average thickness. The relationship between the plate buckling coefficients based on the minimum and average thicknesses is obtained as follows:

$$k_p = 4k_p^1 \big/ (\delta + 2)^2 \qquad\qquad (46)$$

where k_p = the plate buckling coefficient based on the average thickness (t_{avg}).

Equation (46) is derived from the following relationships:

$$F_{cr} = \frac{k_p \pi^2 E}{12(1-v^2)(b/t_{avg})^2} = \frac{k_p^1 \pi^2 E}{12(1-v^2)(b/t_1)^2} \quad \text{and} \quad \frac{t_{avg}}{t_1} = \frac{t_1 + t_2}{2t_1} = \frac{1 + t_2/t_1}{2} = \frac{\delta + 2}{2} .$$

A comparison between the plate buckling coefficients of a uniform thickness plate and a tapered thickness plate using Equation (46) is shown in Figure 3.6.
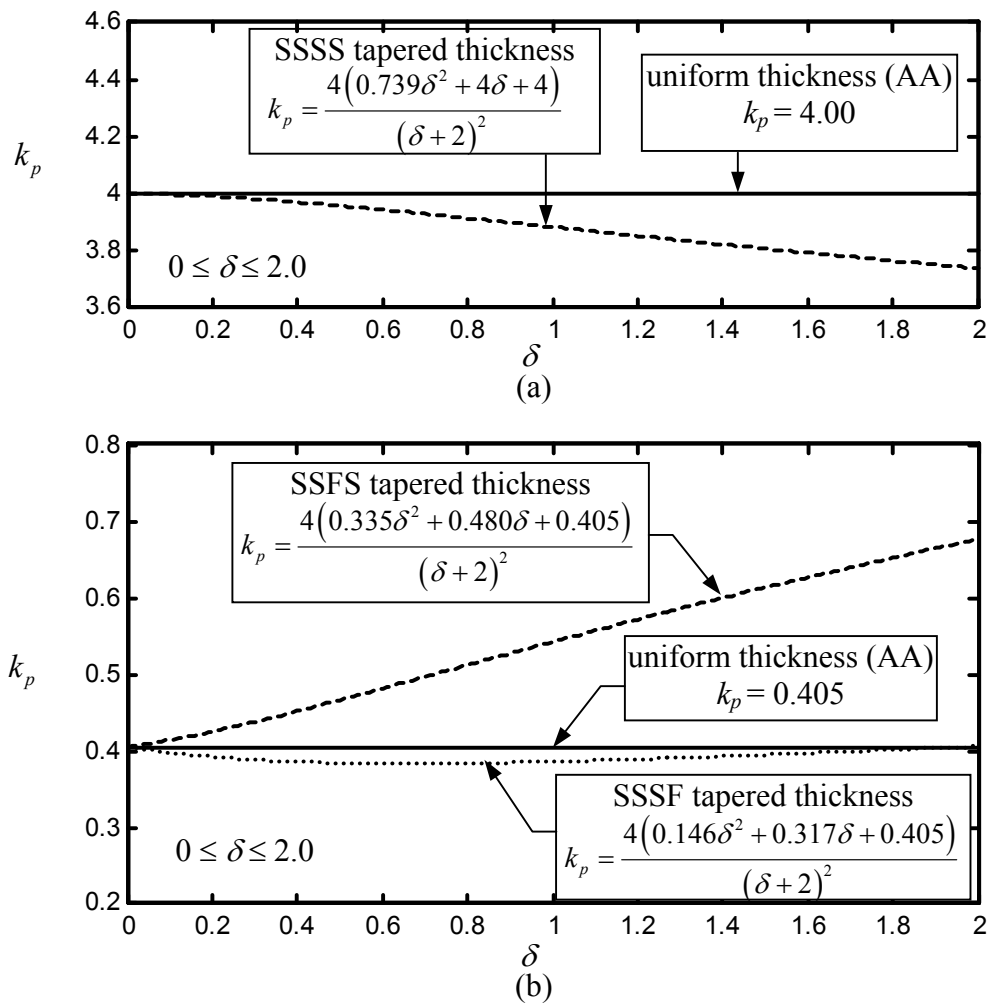
Figure 3.6 Rigorous plate buckling coefficient comparisons between tapered and uniform thickness plates based on average thickness with (a) SSSS (b) SSFS and SSSF boundary conditions

The rigorous plate buckling coefficient for tapered thickness plates increases as the thickness variation ratio (δ) increases in the SSFS boundary condition case, which implies that the current AA *Specification* is conservative. However, for other cases, the current AA *Specification* is not conservative.

The equivalent slenderness ratios of tapered thickness plate elements are obtained by introducing the rigorous plate buckling coefficients in Figure 3.6 into Equation (5), as shown in Table 3.2. The rigorous equivalent slenderness ratios are also linearly approximated in the table for design purposes. The errors due to linear approximations of the rigorous equivalent slenderness ratios are within ±2%. It is noted that since the curve-fitted equations are for a limited range, the range of the thickness variation ratio (δ) is limited as well. However, the thickness variation ratios of all standard I-shaped sections with tapered thickness in AA (2000b) fall within this range.

Table 3.2 Linear approximation of the equivalent slenderness ratio (λ_p) for tapered thickness elements under uniform compression ($0 < \delta \le 2.0$)

type of member	rigorous expression $\left(\lambda_p\right)$	linear approx. $\left(\lambda_p^L\right)$	AA *Spec.* $\left(\lambda_p^{AA}\right)$
[SSSS]	$\dfrac{1.633(\delta+2)}{\sqrt{0.739\delta^2 + 4(\delta+1)}}\left(\dfrac{b}{t_{avg}}\right)$	$(1.63+0.03\delta)\left(\dfrac{b}{t_{avg}}\right)$	$1.6\left(\dfrac{b}{t_{avg}}\right)$
[SSFS]	$\dfrac{1.633(\delta+2)}{\sqrt{0.335\delta^2 + 0.480\delta + 0.405}}\left(\dfrac{b}{t_{avg}}\right)$	$(5.1-0.6\delta)\left(\dfrac{b}{t_{avg}}\right)$	$5.1\left(\dfrac{b}{t_{avg}}\right)$
[SSSF]	$\dfrac{1.633(\delta+2)}{\sqrt{0.146\delta^2 + 0.317\delta + 0.405}}\left(\dfrac{b}{t_{avg}}\right)$	$5.2\left(\dfrac{b}{t_{avg}}\right)$	$5.1\left(\dfrac{b}{t_{avg}}\right)$
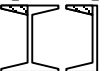
The limit state stress for a tapered flange element is determined by introducing the linearly approximated equivalent slenderness ratios in Table 3.2 into the equations in Table 3.3. The shape factors (α) in this table under the yield and ultimate limit states are provided in Table 2.5b.

Table 3.3 Limit state stress equations for a tapered flange element

approaches	limit state stress $\dfrac{b}{t_{avg}} \le S_1$	limit S_1	limit state stress $S_1 < \dfrac{b}{t_{avg}} \le S_2$	limit S_2	limit state stress $S_2 < \dfrac{b}{t_{avg}}$
AA *Specification*	$F_p^{AA} = \alpha F_{cy}$	$\dfrac{B - \alpha F_{cy}}{\kappa^{AA} D}$	$F_p^{AA} = B - D\lambda_p^{AA}$	$\dfrac{k_1 B}{\kappa^{AA} D}$	$F_p^{AA} = \dfrac{k_2 \sqrt{BE}}{\lambda_p^{AA}}$
proposed linear approximation	$F_p^{L} = \alpha F_{cy}$	$\dfrac{B - \alpha F_{cy}}{\kappa^{L} D}$	$F_p^{L} = B - D\lambda_p^{L}$	$\dfrac{k_1 B}{\kappa^{L} D}$	$F_p^{L} = \dfrac{k_2 \sqrt{BE}}{\lambda_p^{L}}$

Note: a. $\kappa^{AA} = \lambda_p^{AA}/\left(b/t_{avg}\right)$ and $\kappa^{L} = \lambda_p^{L}/\left(b/t_{avg}\right)$.

b. See Table 2.5b for α.
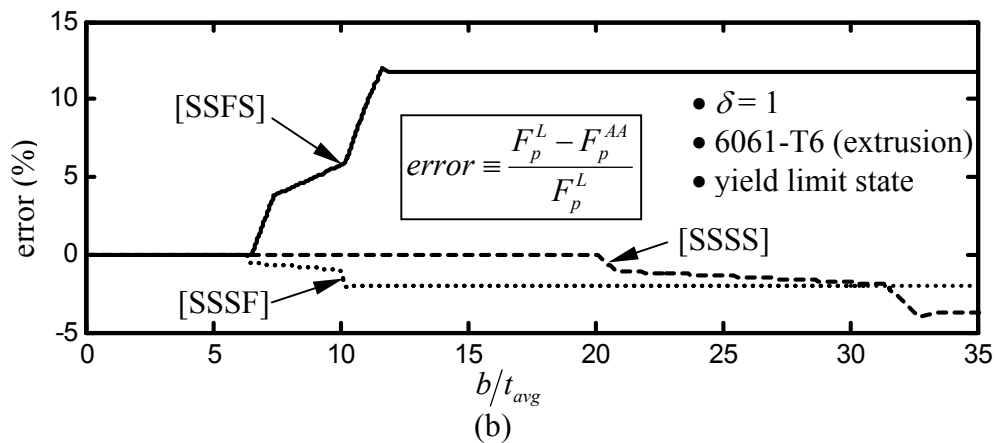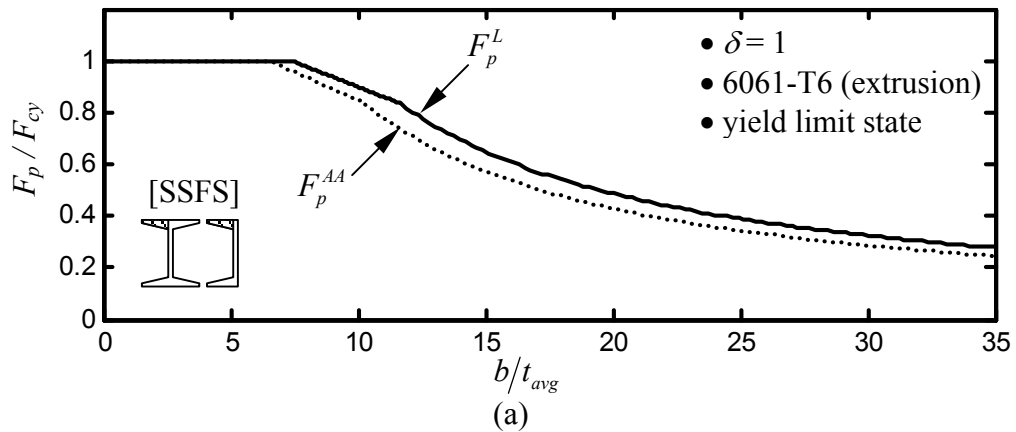
Figure 3.7 (a) The proposed limit state stress $\left(F_p^{L}\right)$ and current limit state stress $\left(F_p^{AA}\right)$ for linearly tapered elements under uniform compression and (b) error between the stresses ($\delta = 1$)

For a given material (extruded 6061-T6) and geometry ($\delta = 1$), limit state stresses (F_p) from both approaches in Table 3.3 are plotted in Figure 3.7a for the SSFS boundary condition. They confirm that the current AA *Specification* (2000a) is conservative for the SSFS boundary condition. The errors between both approaches are plotted in Figure 3.7b for all three boundary condition cases. The current AA *Specification* (2000a) is unconservative for the SSSS and SSSF boundary conditions, but the calculated errors for these boundary conditions are smaller than those for the SSFS boundary condition.

3.4 The Moment Capacity Evaluation Approaches

The moment capacity evaluation approaches shown in Section 2.6 can be used for the symmetric tapered thickness sections in Figure 3.1. However, the definition of h_c used in this section should be changed from the distance between centerlines to the distance between centroids of the flange areas (A_f) as shown in Figure 3.8.
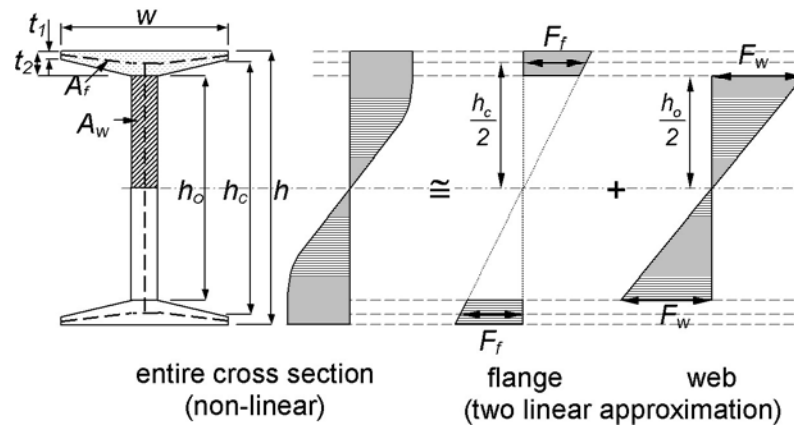
Figure 3.8 Contributions of component elements to the entire moment capacity of an I-shaped section with tapered thickness

3.5 Parametric Study of I-Shaped Sections with Tapered Thickness

The moment capacities are computed for all 36 standard I-shaped sections with tapered thickness listed in AA (2000b) using the approaches developed for the tapered

thickness element. Subsequently the same sections are analyzed using the finite element method. These sections are denoted by Series 1 in this parametric study. Since the slenderness factors, defined in Equation (22), of all Series 1 sections are in the stocky range (λ < 0.673) based on AISI (1996), additional series sections are created through reduction of the thickness of the standard sections by 60%. These sections are denoted by Series 2. Details of the dimensions for Series 1 and 2 sections are given in Section 6.4 of the Appendix.

The finite element model used for the parametric study is quite similar to that of Section 2.7 except for the following. Each member length is at least four times the member depth so that the end effects disappear at the middle of the member. The length is also set to 3 to 8 times the critical local buckling length, which results in the minimum buckling load. Twenty-noded quadratic hexahedral solid elements with reduced integration are used to fully take into account the thickness variation in the finite element model. The cross-sections used in the parametric study are extrusions of 6061-T6 with the minimum material properties in Table 2.4. Since the moment capacity variation resulting from the ultimate strain variation is not significant, as shown in Table 2.8, the ultimate strain is set to 8%, which is the same as the minimum percent elongation in AA (2000c).

The influence of employing the rigorous plate buckling coefficient for a tapered thickness plate is investigated, as shown in Figure 3.9. The abbreviations used in Figure 3.9 and Figure 3.10 are as follows. In the first category, M_{AA-UNI} and M_{AA-TAP} denote the moment capacities when the limit state stresses are computed by the specification approach based on the uniform average thickness (F_p^{AA} in Table 3.3) and the proposed approach based on the tapered thickness (F_p^L in Table 3.3), respectively. The second category is the limit state, either yield ($-_Y$) or ultimate ($-_U$), as given in Table 2.5 and Table 3.3 for the compression side. The third category indicates the moment capacity evaluation approach in Table 2.7 with a correction for h_c as

described in Section 3.4. On the vertical axis, the moment capacity from each finite element analysis is divided by the capacity obtained from the approach specified in the figure. As seen in Figure 3.9, considering the tapered thickness plate buckling coefficient significantly improves the member capacity for rather slender sections (Series 2 sections). This is because most Series 2 sections fall into the inelastic or post buckling range, in which the limit state stress is considerably affected by the equivalent slenderness ratio.

(a)

(b)
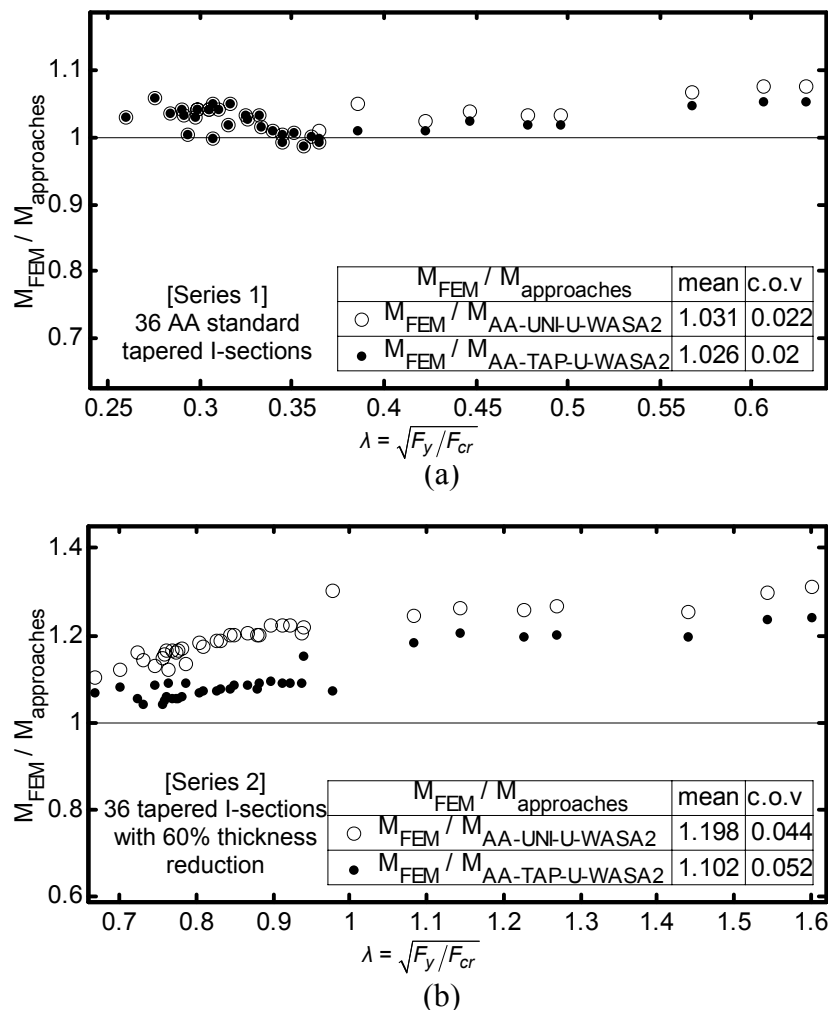
Figure 3.9 Influence of employing the plate buckling coefficient for a tapered thickness plate (a) Series 1 (b) Series 2

The two currently available approaches ($M_{AA\text{-}UNI\text{-}Y\text{-}MMCA}$ and $M_{AA\text{-}UNI\text{-}Y\text{-}WASA}$) in the AA *Specification* (2000a) are compared to the two proposed approaches ($M_{AA\text{-}}$

$_{\text{TAP-U-WASA2}}$ and $M_{\text{AA-TAP-U-TMCA}}$). The comparison is shown in Figure 3.10. The two proposed approaches predict the ultimate-plastic capacities of the cross-sections used in the parametric study more accurately than the two currently available approaches across a wide range of slenderness. In addition, the two proposed approaches show similar results. The moment capacities obtained with all four approaches and the finite element analyses normalized by the yield moment capacity are listed in Section 6.4.

$M_{\text{FEM}} / M_{\text{approaches}}$		mean	c.o.v
△	$M_{\text{FEM}} / M_{\text{AA-UNI-Y-MMCA}}$	1.27	0.039
+	$M_{\text{FEM}} / M_{\text{AA-UNI-Y-WASA}}$	1.211	0.032
○	$M_{\text{FEM}} / M_{\text{AA-TAP-U-WASA2}}$	1.026	0.02
●	$M_{\text{FEM}} / M_{\text{AA-TAP-U-TMCA}}$	1.016	0.019

(a)

$M_{\text{FEM}} / M_{\text{approaches}}$		mean	c.o.v
△	$M_{\text{FEM}} / M_{\text{AA-UNI-Y-MMCA}}$	1.43	0.088
+	$M_{\text{FEM}} / M_{\text{AA-UNI-Y-WASA}}$	1.257	0.041
○	$M_{\text{FEM}} / M_{\text{AA-TAP-U-WASA2}}$	1.102	0.052
●	$M_{\text{FEM}} / M_{\text{AA-TAP-U-TMCA}}$	1.099	0.055

(b)
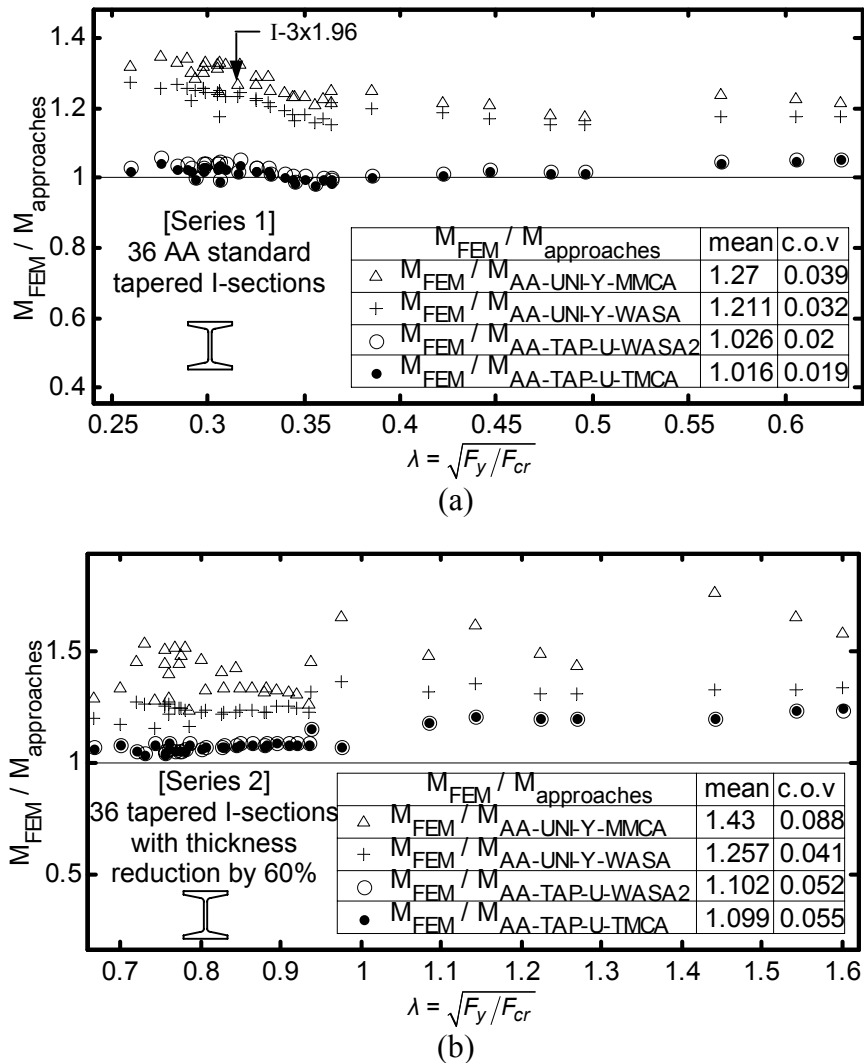
Figure 3.10 Comparison between current and proposed approaches (a) Series 1 (b) Series 2

3.6   Experiments and FEM Simulation

Flexural tests for three American Standard I-Beams with tapered thickness, I-3x1.96, listed in AA (2000b), have been conducted to further support the approaches proposed in this study. The dimensions of the section are shown in Section 6.4 of the Appendix. The test setup is quite similar to that used for the uniform thickness sections in Figure 2.16. It is simulated using the finite element method. All modeling issues are similar to those of the SOLID model in Section 2.8 except for different lateral support spacing, as shown in Figure 3.11, and different material properties, as shown in Table 6.27c in the Appendix.
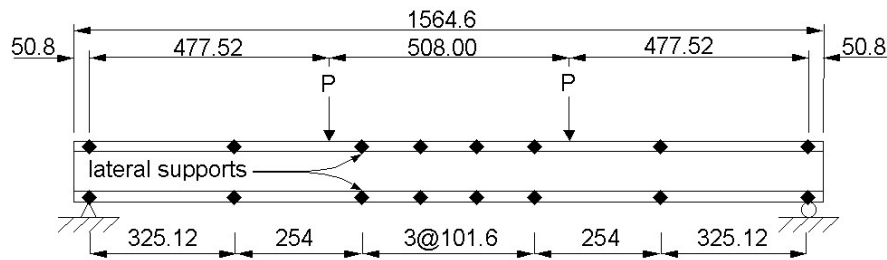
Note: all dimensions are in mm and not to scale

Figure 3.11 Schematic test setup (I-3x1.96)

In contrast to the uniform thickness sections of Section 2.8, almost no ripples were formed during the tests, as shown in Figure 3.12. The beam does not seem to be sensitive to such local deformations. The first test performed was unsuccessful due to a lack of stiffness at the lateral supports; large lateral S-shaped deformations occurred, as shown in Figure 3.12b. For this reason, the first tested beam reached the peak too early, as seen in Figure 3.13. The test setup was reinforced against lateral movements for the following tests, resolving the problem with the first test. However, the last two tests were discontinued at a vertical displacement between approximately 150mm and 170mm at the span center, due to the limitation of the test setup. Up to this stage, load factor continually increases as displacement increases, as observed in Figure 3.13.
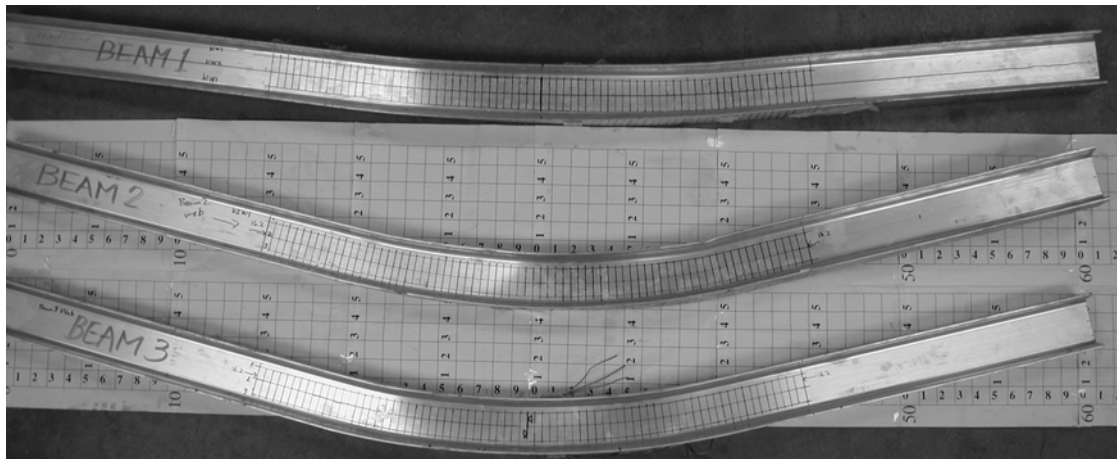
(a)
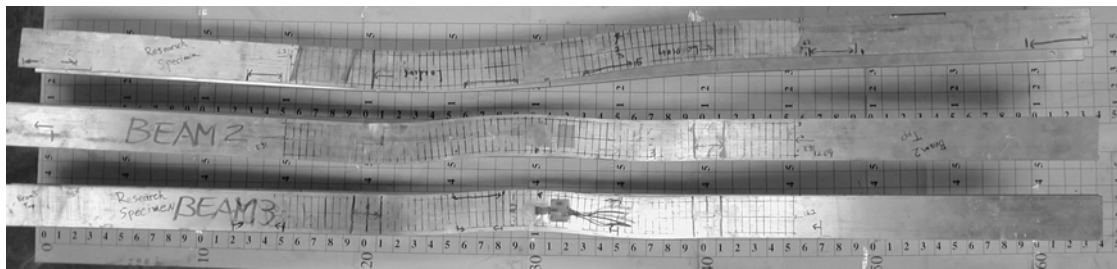
(b)

Figure 3.12 Residual deformation of tested specimens (I-3x1.96) (a) side (b) plan

DESCRIPTION		MAX-LF	DISP-XL
+	TEST 1	1.123	50.56
●	TEST 2	1.173	168.5
○	TEST 3	1.174	147.2
—	FEM	1.197	167.4

DISP-XL = Displacement at max LF
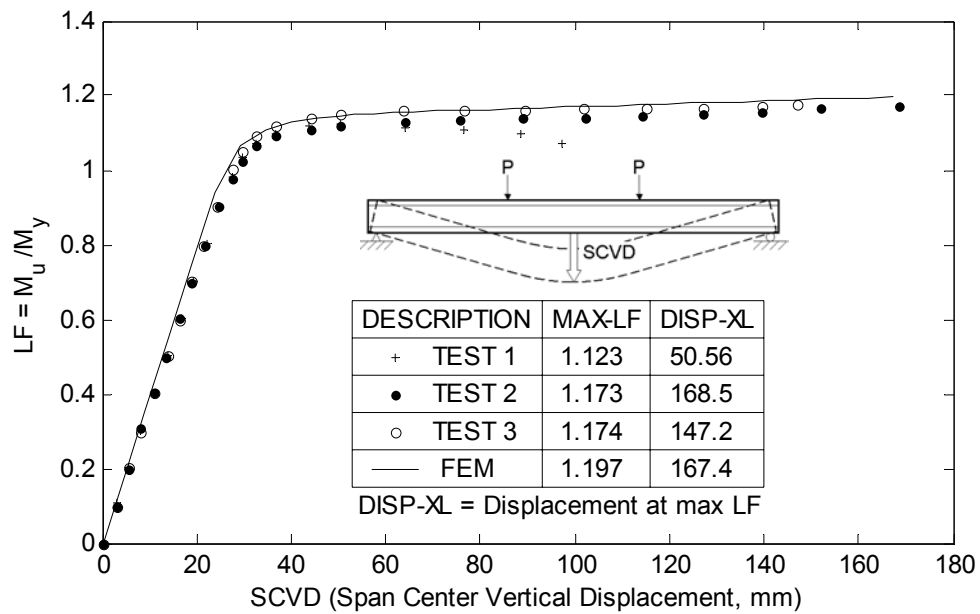
Figure 3.13 Load factor-displacement result comparison for I-3x1.96

The load factor-displacement curves obtained from the last two physical tests are closely matched by the finite element analysis, as shown in Figure 3.13. In the analysis, the Von Mises stress reaches the ultimate stress failure criteria without stability problems. At this stage, the peak load factor is determined, although the load factor is still increasing.

In Table 3.4, the average of the maximum moment capacities from the last two physical tests is compared with those from the approaches available in the current AA *Specification* (2000a) and those from the approaches developed in this study. The proposed approaches show closer agreement with the tests than the current approaches. Thus, in addition to the parametric study, the test results further validate the proposed approaches. The moment ratios from the tests in Table 3.4 are slightly smaller than from the finite element analyses in Figure 3.10 and Table 3.5, which may be due to the early discontinuation of the tests. Since the material properties used for the finite element analyses are not from the minimum values in AA (2000c) but from tensile tests in this study, the moment capacities based on the approaches in these tables are recalculated.

Table 3.4 Comparison of test results to the available approaches

current approaches		proposed approaches	
$\dfrac{M_{TESTS}}{M_{AA\text{-}UNI\text{-}Y\text{-}MMCA}}$	$\dfrac{M_{TESTS}}{M_{AA\text{-}UNI\text{-}Y\text{-}WASA}}$	$\dfrac{M_{TESTS}}{M_{AA\text{-}TAP\text{-}U\text{-}WASA2}}$	$\dfrac{M_{TESTS}}{M_{AA\text{-}TAP\text{-}U\text{-}TMCA}}$
1.174	1.141	0.967	0.960

Table 3.5 Comparison of finite element simulation to the available approaches

current approaches		proposed approaches	
$\dfrac{M_{FEM\text{-}SIMULATION}}{M_{AA\text{-}UNI\text{-}Y\text{-}MMCA}}$	$\dfrac{M_{FEM\text{-}SIMULATION}}{M_{AA\text{-}UNI\text{-}Y\text{-}WASA}}$	$\dfrac{M_{FEM\text{-}SIMULATION}}{M_{AA\text{-}TAP\text{-}U\text{-}WASA2}}$	$\dfrac{M_{FEM\text{-}SIMULATION}}{M_{AA\text{-}TAP\text{-}U\text{-}TMCA}}$
1.198	1.164	0.986	0.979

3.7 *Application to the AA* **Specification**

The allowable stress equations based on the yield and ultimate limit states are summarized for tapered thickness elements in Table 3.6. The equations given in this table are consistent with those proposed in Section 2.9 for uniform thickness elements. In addition, the governing allowable stress for sections with tapered thickness can also be determined by either Procedure I or Procedure II given in Table 2.9. Although Table 2.9 and Table 3.6 are based on the Allowable Stress Design, these tables can also be applied to the Load and Resistance Factor Design by replacing the reciprocal of each safety factor with the corresponding resistance factor.

Table 3.6 Proposed allowable stress equations for tapered thickness elements under uniform compression ($0 < \delta \le 2.0$) when sections are under bending

BC	allowable stress $\frac{b}{t_{avg}} \le S_1$	limit S_1	allowable stress $S_1 < \frac{b}{t_{avg}} \le S_2$	limit S_2	allowable stress $S_2 < \frac{b}{t_{avg}}$
SSSS	$F_{ay} = \dfrac{\alpha_y F_{cy}}{n_y}$ $F_{au} = \dfrac{\alpha_u F_{cy}}{n_u}$	$\dfrac{B - \alpha_y F_{cy}}{(1.63 + 0.03\delta)D}$ $\dfrac{B - \frac{n_y}{n_u}\alpha_u F_{cy}}{(1.63 + 0.03\delta)D}$	$F_{ay} = F_{au} =$ $\dfrac{\left\{ B - D(1.63 + 0.03\delta)\dfrac{b}{t_{avg}} \right\}}{n_y}$	$\dfrac{k_1 B}{(1.63 + 0.03\delta)D}$	$F_{ay} = F_{au} =$ $\dfrac{k_2\sqrt{BE}}{n_y(1.63 + 0.03\delta)\left(\dfrac{b}{t_{avg}}\right)}$
SSFS	$F_{ay} = \dfrac{\alpha_y F_{cy}}{n_y}$ $F_{au} = \dfrac{\alpha_u F_{cy}}{n_u}$	$\dfrac{B - \alpha_y F_{cy}}{(5.1 - 0.6\delta)D}$ $\dfrac{B - \frac{n_y}{n_u}\alpha_u F_{cy}}{(5.1 - 0.6\delta)D}$	$F_{ay} = F_{au} =$ $\dfrac{1}{n_y}\left\{ B - D(5.1 - 0.6\delta)\dfrac{b}{t_{avg}} \right\}$	$\dfrac{k_1 B}{(5.1 - 0.6\delta)D}$	$F_{ay} = F_{au} =$ $\dfrac{k_2\sqrt{BE}}{n_y(5.1 - 0.6\delta)\left(\dfrac{b}{t_{avg}}\right)}$
SSSF	$F_{ay} = \dfrac{\alpha_y F_{cy}}{n_y}$ $F_{au} = \dfrac{\alpha_u F_{cy}}{n_u}$	$\dfrac{B - \alpha_y F_{cy}}{5.2D}$ $\dfrac{B - \frac{n_y}{n_u}\alpha_u F_{cy}}{5.2D}$	$F_{ay} = F_{au}$ $= \dfrac{1}{n_y}\left(B - 5.2D\dfrac{b}{t_{avg}} \right)$	$\dfrac{k_1 B}{5.2D}$	$F_{ay} = F_{au} =$ $\dfrac{k_2\sqrt{BE}}{n_y 5.2\left(\dfrac{b}{t_{avg}}\right)}$

Note. See Section 2.9 for details.

3.8   Conclusions

Initial and geometric stiffness matrices for a plate with tapered thickness are derived for the finite strip analysis program, CUFSM. Using the CUFSM program with the derived stiffness matrices, parametric studies are conducted to find the relationship between the plate buckling coefficient and the thickness variation ratio. Using the relationship thus obtained, limit state stress equations are proposed for tapered thickness elements, while the framework of the AA *Specification* (2000a) is maintained.

Another parametric study is conducted for I-sections with tapered thickness for the verification of the proposed limit state stress equations. The moment capacity evaluation approaches that are developed for uniform thickness sections are also employed for the sections used in the parametric study. From the comparisons with the finite element analyses, it has been found that the proposed approaches work much better than the current specification approaches. Experimental study additionally supports the proposed approaches.

The limit state stress equations developed for tapered thickness elements are improved primarily within the inelastic and post buckling ranges. For this reason, the proposed approaches could also be used to develop more slender cross-sections with tapered thickness than the current standard cross-sections, which mostly fall within the yielding range.

4. NUMERICAL SLENDERNESS APPROACH FOR COMPLEX ALUMINUM EXTRUSIONS UNDER FLEXURAL LOADING

One of the most attractive aspects of aluminum as a structural material is that it can be extruded. Through extrusion, the cross-section can be a wide range of shapes, and combination of shapes. For example, extrusion is the best process for producing the geometric shape shown in Figure 4.1b, in which additional component elements are attached to the flanges of a simple I-shaped section. Sections containing such component elements are common among extruded aluminum shapes and provide additional functions such as screw chases and grooves.
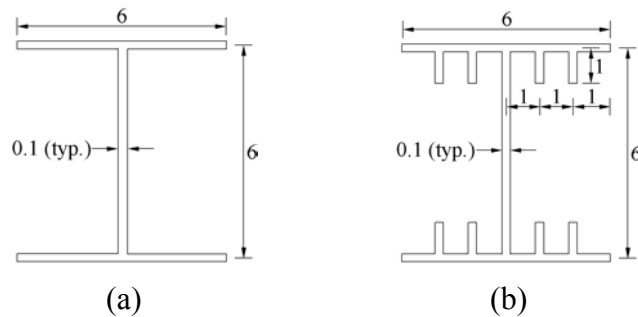
Note: All dimensions are in inches and not to scale.

Figure 4.1 (a) Simple I-shaped section (b) complex extrusion
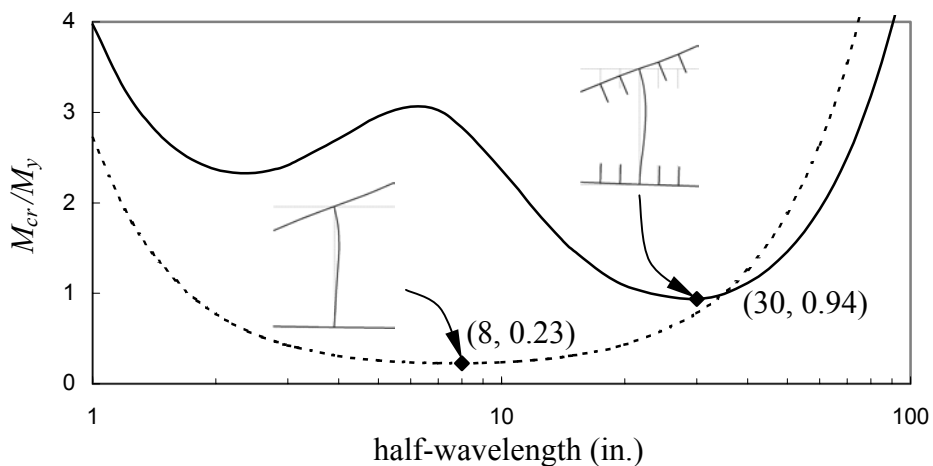
Figure 4.2 Buckling analyses by CUFSM for simple and complex extrusions

As shown in Figure 4.2, the local buckling capacity of a complex extrusion (Figure 4.1b) is usually much larger than a simple extrusion (Figure 4.1a) due to the additional component elements. However, the advantage of increased member capacity is usually disregarded due to the difficulty of considering all possible geometric variations in the specifications. For example, in order to calculate the compressive allowable stress (or factored limit state stress) of the complex extrusion in Figure 4.1b using the AA *Specification* (2000a), the geometry should be simplified to the one shown in Figure 4.1a.

To consider all possible geometric variations of aluminum extrusions, a numerical analysis is desirable. Thus, a new design approach based on a numerical analysis is developed. In this approach, the framework of the current specification is maintained, with only the equivalent slenderness ratio being determined by local buckling analysis. Since the geometric shape does not limit the numerical buckling analysis, practically all aluminum extrusions can be evaluated. In this approach, rigorously obtained plate buckling stress values are used instead of the minimum plate buckling coefficients implicit in the AA *Specification* (2000a).

In addition, since the current methodologies to compute moment capacities based on the determined limit state stresses are over-simplified for unsymmetric sections, more precise approaches are formulated. A shape factor for a rectangular web element is also developed for unsymmetric sections. Results of physical tests and non-linear finite element analyses are compared to the approaches developed in this study.

4.1   *Numerical Slenderness Approach for Component Elements*

In the AA *Specification* (2000a), the limit state (or allowable) stress for a compressive component element varies according to the equivalent slenderness ratio (λ_p), which falls into one of three ranges, the yielding, inelastic buckling, and post buckling ranges, as shown in Figure 2.4. The equivalent slenderness ratio is defined in Equation (5).

$$\lambda_p = \kappa \left(\frac{b}{t} \right), \text{ where } \kappa = \sqrt{\frac{12\left(1 - v^2\right)}{k_p}} \qquad (5)$$

In the AA *Specification* (2000a), boundaries between component elements are idealized as simply-supported, for which plate buckling coefficients (k_p) are generally known. It has been shown in Chapters 2 and 3 that this idealization is satisfactory for sections with simple geometry such as in Figure 2.1 and Figure 3.1. Although the AA *Specification* (2000a) provides limit state stress equations for additional types of cross-sections, they are insufficient to cover the wide range of possible geometric shapes through extrusion.

The Numerical Slenderness Approach (abbreviated as NSA hereafter) is developed to provide a design approach for complex extrusions, in which the aforementioned boundary idealization is not applicable or appropriate. In this approach the equivalent slenderness ratio is determined using a numerical buckling analysis tool such as CUFSM. The CUFSM program developed by Schafer (1997) is designed to determine the minimum elastic buckling stress and a corresponding mode shape for a given length of a member. By varying the member length, several mode shapes such as local, distortional, and lateral buckling can be detected. Examples of the buckling analysis results are shown in Figure 4.2. A complete manual for CUFSM can be found in Schafer (1997), although the name of the program has changed since then from CUSTRIP to CUFSM.

An alternative form of the equation for the equivalent slenderness ratio based on the numerically determined minimum buckling stress F_{cr} is derived from the relationship given in Equation (6):

$$\lambda_p = \pi \sqrt{\frac{E}{F_{cr}}} \qquad (47)$$

Since the geometric shape is not limited to simple cases when performing a numerical analysis, the equivalent slenderness ratio can be obtained for a wide range of possible geometries. There is only one unique minimum buckling stress corresponding to a given cross-section, as shown in Figure 4.2. Thus, the equivalent slenderness ratios for all component elements are equal. In addition, in the use of the NSA there is no need to idealize boundaries between component elements as simply-supported, which is necessary in the AA *Specification* (2000a). Using Equation (47), the limit state stress equations are provided in Table 4.1. The equations in this table are identical to those in Figure 2.4 for the AA *Specification* (2000a), except for the expression for the equivalent slenderness ratio.

Table 4.1 Limit state stress equations for a component element

Limit state stress for $\lambda_p \leq S_1$	S_1	Limit state stress for $S_1 \leq \lambda_p \leq S_2$	S_2	Limit state stress for $S_2 \leq \lambda_p$
$F_p = \alpha F_{cy}$	$\dfrac{B - \alpha F_{cy}}{D}$	$F_p = B - D\lambda_p$	$\dfrac{k_1 B}{D}$	$F_p = \dfrac{k_2 \sqrt{BE}}{\lambda_p}$

Note: B, D, k_1 and k_2 are the factors provided in the AA *Specification* (2000a). These factors differ for flanges and webs. F_p = limit state stress for flange (F_f) or web (F_w). See Table 2.5b for shape factors (α) of symmetric cross-sections. For unsymmetric sections, see Table 4.8c.

4.2 Rigorous Ultimate Shape Factor for Rectangular Web Elements with Neutral Axis Not at Mid-Depth

As shown in Section 2.5, the cut-off of the AA *Specification* (2000a) seen in Figure 2.4 can be raised up to the ultimate shape factor (α_u) times the yield stress to

take into account the ultimate limit state of bending members. In this study, the closed form solution of the ultimate shape factor for rectangular web elements when the neutral axis is located at mid-depth is obtained using analytic integration of the stress distribution.

However, when the neutral axis is not at mid-depth, as is the case where the section is not symmetric with respect to the bending axis, the shape factor for the web element given in Equation (14) is not appropriate.
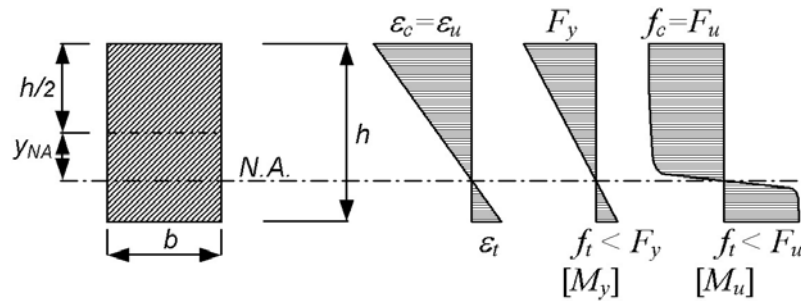
Figure 4.3 Stress distributions corresponding to yield and ultimate moment capacities when neutral axis (N.A.) is not located at mid-depth

Figure 4.3 shows the strain and stress distributions of a rectangular web element, of which the neutral axis is not at mid-depth. Based on Figure 4.3, the closed-form ultimate moment capacity and shape factor of a rectangular section with an arbitrary neutral axis is derived using an analytical approach similar to the one for symmetric sections in Section 2.3:

$$M_u = b \left(\frac{h/2 + y_{NA}}{\varepsilon_c} \right)^2 \left(\frac{f_c^3 + f_t^3}{3E^2} + \frac{n\left(f_c^{2n+1} + f_t^{2n+1}\right)}{500^2 \left(2n+1\right) F_y^{2n}} + \frac{\left(n+1\right)\left(f_c^{n+2} + f_t^{n+2}\right)}{500\left(n+2\right) F_y^n E} \right) \quad (48)$$

$$M_y = \frac{F_y b}{3\left(h/2 + y_{NA}\right)} \left(\frac{h^3}{4} + 3 y_{NA}^2 h \right) \quad (49)$$

$$\alpha_u = \alpha_w = \frac{M_u}{M_y} = \frac{3\left(h/2 + y_{NA}\right)^3}{F_y \varepsilon_c^2 \left(h^3/4 + 3 y_{NA}^2 h\right)} \left(\frac{f_c^3 + f_t^3}{3E^2} + \frac{n\left(f_c^{2n+1} + f_t^{2n+1}\right)}{500^2 \left(2n+1\right) F_y^{2n}} + \frac{\left(n+1\right)\left(f_c^{n+2} + f_t^{n+2}\right)}{500\left(n+2\right) F_y^n E} \right) \quad (50)$$

where y_{NA} is the distance from the neutral axis to the mid-depth. α_w denotes the ultimate shape factor of a rectangular web element with a neutral axis not at mid-depth (for an unsymmetric section). For a symmetric section, another denotation (α_{wo}) has been used, as shown in Equation (14).

In Equation (50), either the compression or tension extreme fiber stress (f_c, f_t) should be the ultimate stress. If the compressive extreme fiber stress and strain (f_c, ε_c) are the ultimate stress and strain (F_u, ε_u), respectively, the tension side extreme fiber stress (f_t) must also be determined to use this equation. This can be done by the following procedure. After the tension side extreme fiber strain (ε_t) is computed by similar triangles, the strain is introduced into the Ramberg-Osgood equation, Equation (7), to determine the tension side extreme fiber stress (f_t) using increasing trial values. It should be noted that Equation (14) is a special case ($y_{NA} = 0$, $\varepsilon_c = \varepsilon_t = \varepsilon_u$ and $f_c = f_t = F_u$) of Equation (50).

4.3 *Simplified Ultimate Shape Factor for Rectangular Web Elements with Neutral Axis Not at Mid-Depth*

Since Equation (50) requires the aforementioned additional iterative steps to find the tension side extreme fiber stress, a simplification of this process is necessary for application to practical design. Thus, using Equation (50), the shape factors are computed and curve-fitted with respect to the location of the neutral axis, as shown in Figure 4.4, for 6061-T6 alloy and temper. The curve-fitted expression in the figure, shown again in Equation (51), is simple and accurate for any alloy and temper if the two coefficients a and m are known. In Equation (51), α_{wo} can be determined from Equation (14).

$$\alpha_u = \alpha_w = a\left(\frac{y_{NA}}{h}\right)\left(0.5 - \frac{y_{NA}}{h}\right)^m + \alpha_{wo}, \quad \left(0 \le \frac{y_{NA}}{h} \le 0.5\right) \tag{51}$$
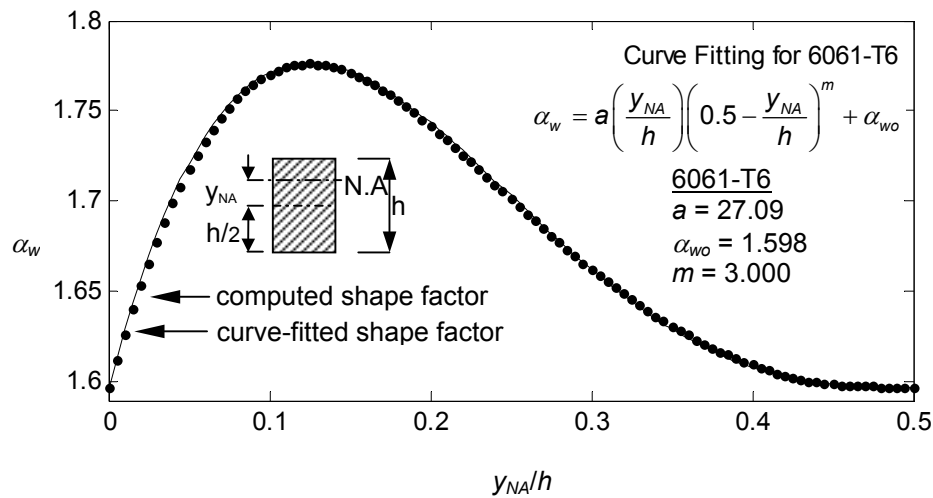
Figure 4.4 Ultimate shape factor for web with neutral axis not at mid-depth (Individual Curve-Fitting)

Table 4.2 Material properties and coefficients of individual curve-fitting for ultimate shape factor of solid rectangular sections for some 6000 series alloys

alloy-temper	F_y (MPa) [a]	E (MPa) [b]	F_u (MPa) [a]	ε_u [c]	a [e]	α_{wo} [d]	m [e]
6005-T5, 6105-T5, 6351-T5 & 6061-T6, -T6510, & -T6511	241.15	68900	261.82	0.04	27.094	1.5975	3.00
6063-T5 [f]	110.24	68900	151.58	0.04	30.563	1.9467	3.03
6063-T5 [g]	103.35	68900	144.69	0.04	31.087	1.9766	3.04
6063-T6, T62 & 6463-T6	172.25	68900	206.70	0.04	28.423	1.7361	3.01
6066-T6, -T6510, & -T6511	310.05	68900	344.50	0.04	28.167	1.6224	3.05
6070-T6, -T62	310.05	68900	330.72	0.03	28.232	1.5617	3.09

Note: a. Minimum values from AA (2000c).

    b. These are average values, which are 689 MPa (100 ksi) lower than compression.

    c. ε_u is assumed to be half of the minimum percent elongation listed in AA (2000c).

    d. See Equation (14).

    e. Coefficients obtained for Equation (51) using Individual Curve-Fitting.

    f. Test coupon diameter or thickness up through 12.7mm.

    g. Test coupon diameter or thickness between 12.7 and 25.4mm.

To determine the two coefficients in Equation (51), an iterative procedure is employed until the best curve-fitting is obtained. This procedure is denoted by "Individual Curve-Fitting" hereafter. For each 6000 series alloy listed in Table 4.2, the coefficients are computed individually through this procedure. It is possible to tabulate these coefficients for use in design. However, because of the continued increase in the

variety of alloy-temper combinations, a simpler method is desired. Thus, an alternative approach is proposed, using the results from the Individual Curve-Fitting method. The two coefficients are first determined for the same 986 alloy-temper combinations in AA (2000c) used to obtain Equation (16). The results are plotted in Figure 4.5 with respect to the ultimate stress to yield stress ratio. The results are curve-fitted with rounded numbers for practical design purposes. This approach is denoted by "Unified Curve-Fitting" hereafter.

$$a = 14\frac{F_{tu}}{F_{ty}} + 13 \qquad (52)$$

$$m = 3 \qquad (53)$$
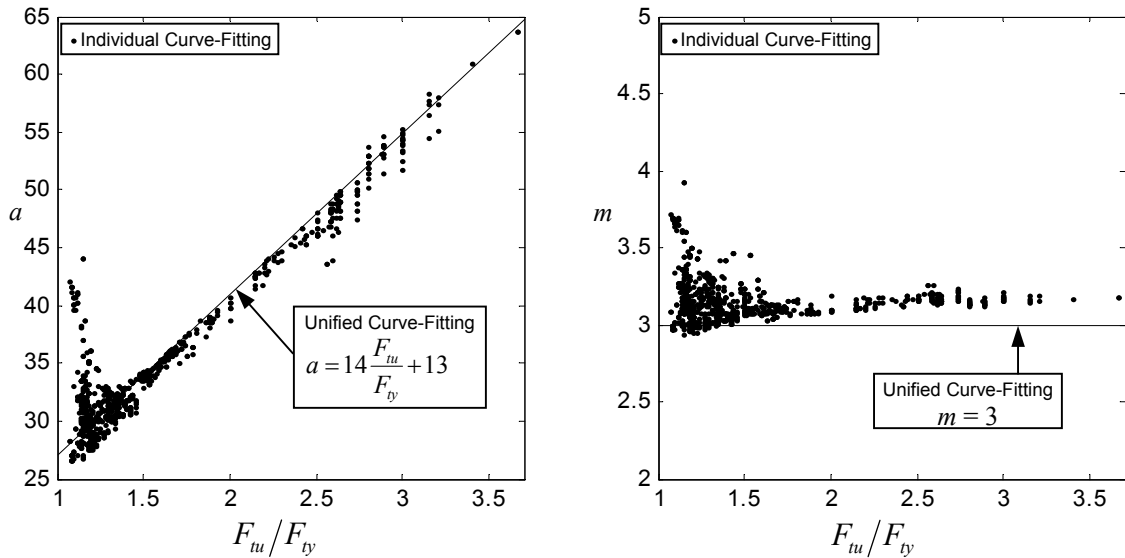
Figure 4.5 Unified Curve-Fitting parameters *a* and *m*

Introducing Equations (16), (52), and (53) into Equation (51), the final form of the shape factor is obtained using the Unified Curve-Fitting:

$$\alpha_u = \alpha_w = \left(14\frac{F_{tu}}{F_{ty}} + 13\right)\left(\frac{y_{NA}}{h}\right)\left(0.5 - \frac{y_{NA}}{h}\right)^3 + \left(1.25\frac{F_{tu}}{F_{ty}} + 0.2\right), \left(0 \le \frac{y_{NA}}{h} \le 0.5\right) \qquad (54)$$

In Figure 4.6, the shape factor obtained from the Individual Curve-Fitting for each material is divided by that from the Unified Curve-Fitting to investigate the accuracy

of the latter. Since the shape factor changes as the location of the neutral axis changes, the range of the neutral axis variation $(0 \leq y_{NA}/h \leq 0.5)$ is divided into 20 equal intervals. In this figure, the two solid dots connected by a solid line represent the maximum and minimum ratios for each alloy-temper combination. Most of the shape factors obtained from the Unified Curve-Fitting approximate those from the Individual Curve-Fitting reasonably well. Thus, Equation (54) based on the Unified Curve-Fitting is suggested for the AA *Specification* (2000a). For the complete NSA limit state stress equations, the ultimate shape factor for a web element (α_u) implicit in Table 4.1, which is Equation (16), should be replaced with that represented by Equation (54).
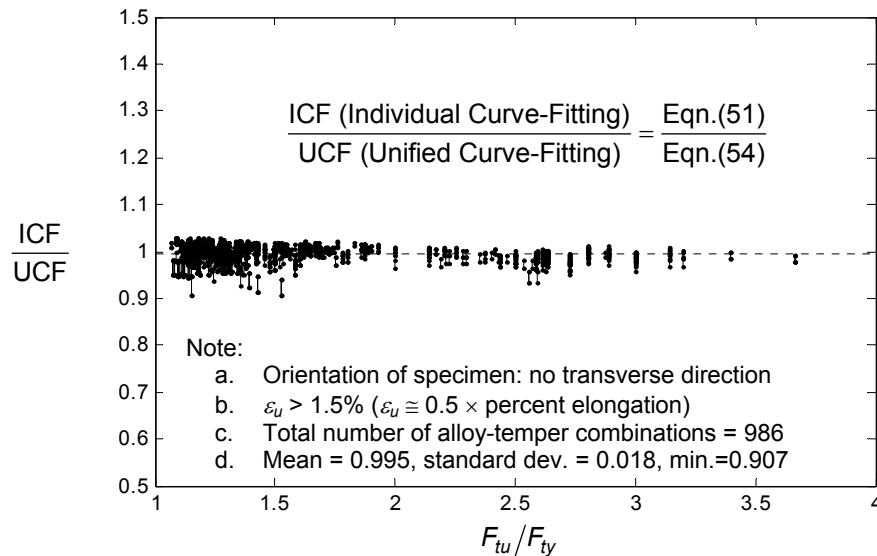
Figure 4.6 Comparison between shape factors from Individual Curve-Fitting and Unified Curve-Fitting

4.4   *Moment Capacity Evaluation Approaches*

Once the allowable stresses (or factored limit state stresses) for component elements are obtained in actual design, the moment capacity can be computed using one of the following approaches. However, instead of the allowable stresses (or

factored limit state stresses), limit state stress values have been used in the parametric study that follows in Section 4.5.

4.4.1 Minimum Moment Capacity Approach (MMCA)

The MMCA is one approach described in AA (2000b), as explained in Section 2.6. However, for sections unsymmetric with respect to the bending axis, the calculation sequence is slightly different from the symmetric case. First, the allowable stress (or factored limit state stress) from each component element is multiplied by the elastic section modulus of the entire cross-section to compute the moment capacity. Among the obtained moment capacities, the minimum value is chosen as the allowable moment capacity of the member. In this computation, the section modulus of the entire cross-section is not uniform among component elements. This is because the section modulus is the moment of inertia of the entire cross-section (I) divided by the distance from the neutral axis to the location where the allowable stress (or factored limit state stress) of each component element is evaluated. For the cross-section given in Figure 4.7, the allowable moment capacity is

$$M_u = \min(F_{cf}I/c_{cf}, F'_{tf}I/c_{tf}, F_{cw}I/c_{cw}, F_{tw}I/c_{tw}, F_{cs}I/c_{cs}) \qquad (55)$$

where F_{cf}, F'_{tf}, F_{cw}, F_{tw}, and F_{cs} are the limit state (or allowable) stress of compression flange, tension flange, compression web, tension web, and compression edge-stiffener, respectively. Other notations are given in Figure 4.7. This approach is demonstrated in AA (2000b) through the Illustrative Examples of Design (Part VIII, Example 22) for a similar type of unsymmetric cross-section.

4.4.2 Weighted Average Stress Approach (WASA)

The WASA is an alternative approach in the AA *Specification* (2000a) to compute the moment capacity, as explained in Section 2.6. For symmetric sections with edge-stiffeners such as C or Z-sections (Figure 4.10c), additional terms for the

edge-stiffener are added, as shown in Table 4.3. The modification factor (h/h_c) is also recommended for this type of cross-section as is done in Section 2.6.

Table 4.3 Correction in WASA for symmetric edge-stiffened C or Z sections

current WASA (WASA)	proposed WASA (WASA2)
$M_u = \dfrac{F_f A_f + F_w \frac{1}{3} A_w + F_s A_s}{A_f + \frac{1}{3} A_w + A_s} S$	$M_u = \dfrac{F_f A_f + F_w \frac{1}{3} A_w + F_s A_s}{A_f + \frac{1}{3} A_w + A_s} \left(\dfrac{h}{h_c} \right) S$

where F_f, F_w, F_s = limit state (allowable) stress for flange, web, and stiffener, respectively; A_f = entire compression side flange area, A_w = half of web area, A_s = entire compression side stiffener area, S = section modulus = $I/(h/2)$, h = entire depth of a section, and h_c = depth of a section measured between the centroids of compression and tension flanges.

However, for sections with a neutral axis not at the mid-depth (or unsymmetric sections), this approach is not applicable because the simplification procedure used in Equation (19) is based on the assumption that the cross-section is symmetric so the weighted average stress cannot be calculated using Equation (18).

4.4.3 Total Moment Capacity Approach (TMCA)

The TMCA introduced in Section 2.6 can be extended to most possible cross-sectional geometries. For example, the sections shown in Figure 4.10 can be divided into the web group (shaded area) and the flange group (unshaded area). The first three cross-sections have the elastic neutral axis at the mid-depth, while the remaining two cross-sections do not.

For cross-sections with a neutral axis located far from mid-depth, the use of a single linear stress distribution for both tension and compression flanges would not be realistic. For example, in Figure 4.7 the tension limit state stress (F'_{tf}) obtained from a linear stress distribution based on the compression limit state stress (F_{cf}) could cause a significant difference from the actual tension limit state stress (F_{tf}). For this reason, the flange group may be subdivided into two groups, resulting in a total of three groups in an entire cross-section, i.e., the compression flange group, tension flange group, and web group. This approach is denoted by TMCA2. The moment capacity

based on TMCA2 is expressed in Equation (56) using the notations given in Figure 4.7.

$$M_u = M_{cf} + M_{tf} + M_w = F_{cf}S_{cf} + F_{tf}S_{tf} + F_{cw}S_w = \frac{F_{cf}I_{cf}}{c_{cf}} + \frac{F_{tf}I_{tf}}{c_{tf}} + \frac{F_{cw}I_w}{c_{cw}} \qquad (56)$$

When calculating the moment of inertia for each group, it is recommended that the simple groups be computed first, e.g., I_{cf} and I_w in Figure 4.7. Then the remaining moment of inertia for the complicated group (I_{tf} in this figure) can be obtained by subtracting the sum of the previously calculated groups from the moment of inertia of the entire cross-section (I), which is generally provided by the manufacturer:

$$I_{tf} = I - (I_{cf} + I_w) \qquad (57)$$
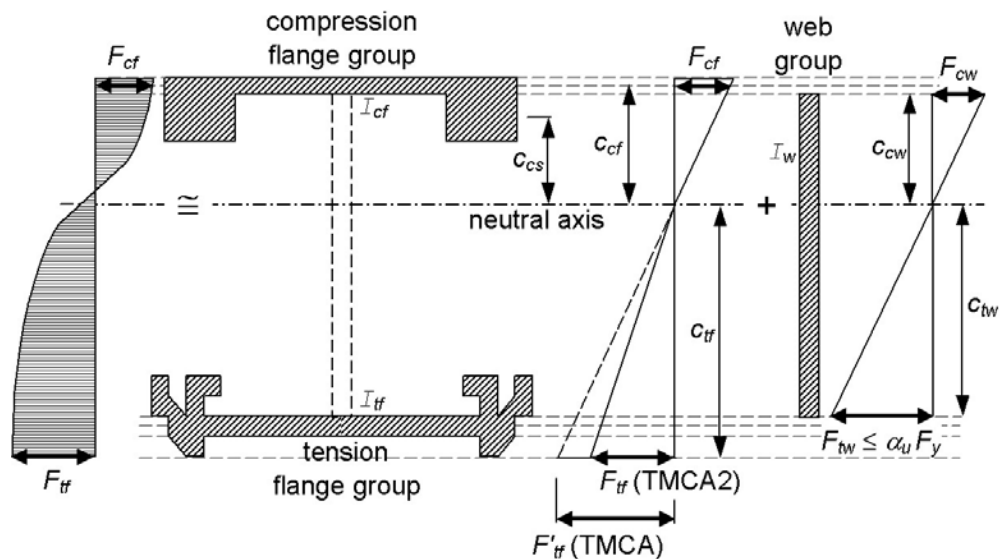
Figure 4.7 Linear approximations of an actual non-linear stress distribution of a mullion section

In this example the moment capacity could not have been computed properly with the WASA2, due to the complex tension flange and the location of the neutral axis. In contrast, Equations (56) and (57) show the versatility of the TMCA2 in tackling complex cross-sections, although the following additional steps are required to compute the limit state stress of the tension flange. First, the stain corresponding to

the compressive limit state stress is computed using the Ramberg-Osgood equation shown in Equation (7). A linear strain distribution is then drawn from the calculated strain through the neutral axis to the tension extreme fiber. The strain thus determined at the tension extreme fiber is introduced into the Ramberg-Osgood equation to obtain the limit state stress for the tension flange (extreme fiber) by an iterative process. For either the flange or web stress distribution, the tension side extreme fiber stress (tension limit state stress) must be limited to a maximum value of the corresponding shape factor times the yield stress. This limitation of the maximum extreme fiber stress is not necessary for the case of symmetric sections because the symmetry itself imposes limitations.

TMCA2 becomes the same as TMCA when the cross-section is symmetric with respect to the bending axis. In addition, TMCA2 becomes TMCA as the slenderness increases, because the non-linear stress distribution becomes linear due to a loss of the inelastic reserve capacity. In the use of TMCA2, the stress of each component element given in Equation (56) (F_{cf}, F_{tf}, and F_{cw}) should not be the allowable stress (or factored limit state stress) but the limit state stress, for the following reason. If each limit state stress is first divided by the safety factor (or multiplied by the resistance factor), the non-linearity of the stress distribution decreases, resulting in almost no difference between TMCA and TMCA2. Therefore, the moment capacity is computed using the limit state stresses after which the entire moment capacity should be divided by the safety factor (or multiplied by the resistance factor). See Table 6.19 in the Appendix for a step-by-step procedure.

4.4.4   Moment Capacity Based on Elasto-Plastic Stress Distribution (EPMC)

An approach to computing the moment capacity using the elasto-plastic stress distribution is available in AISI (1996). In AISI (1996), the ultimate compressive

strain is calculated with a factor proposed by Reck, Peköz, and Winter (1975) based on the slenderness of the compression flange.

However, the use of this factor in calculating the ultimate compressive strain is not necessary in the present study. Instead, the ultimate compressive strain can be directly determined from the Ramberg-Osgood equation, Equation (7), since the compressive limit state stress for the flange element is known based on either the NSA or the AA *Specification* (2000a). The strain distribution is determined based on the compressive limit state strain and an assumed neutral axis location, which is set as an unknown variable. The stress distribution is determined from the linear stress-strain relationship, unless the strain is larger than the yield strain, in which case it is assumed to be equal to the yield stress. The neutral axis location is computed from the force equilibrium with respect to the longitudinal direction. The moment capacity is then computed on an element-by-element basis. Since this approach uses the elasto-plastic stress distribution without strain hardening, it is expected to be somewhat conservative for some compact sections.

Although this approach seems straightforward, it becomes complicated when there are additional elements between compression and tension flanges, such as edge-stiffeners. This is because depending on the location of the neutral axis the stress distribution at the edge-stiffener changes. For each possible case, equilibrium of the stress distribution is used to determine the neutral axis, which is then compared with the initially assumed location. For the edge-stiffened singly-symmetric section shown in Figure 4.10d, a total of seven cases must be evaluated to find the neutral axis location, as shown in Figure 4.8. However, for different cross-sections, different cases must be evaluated, limiting the practicality of this approach.

Note: strain zone that is not yielded is shaded.
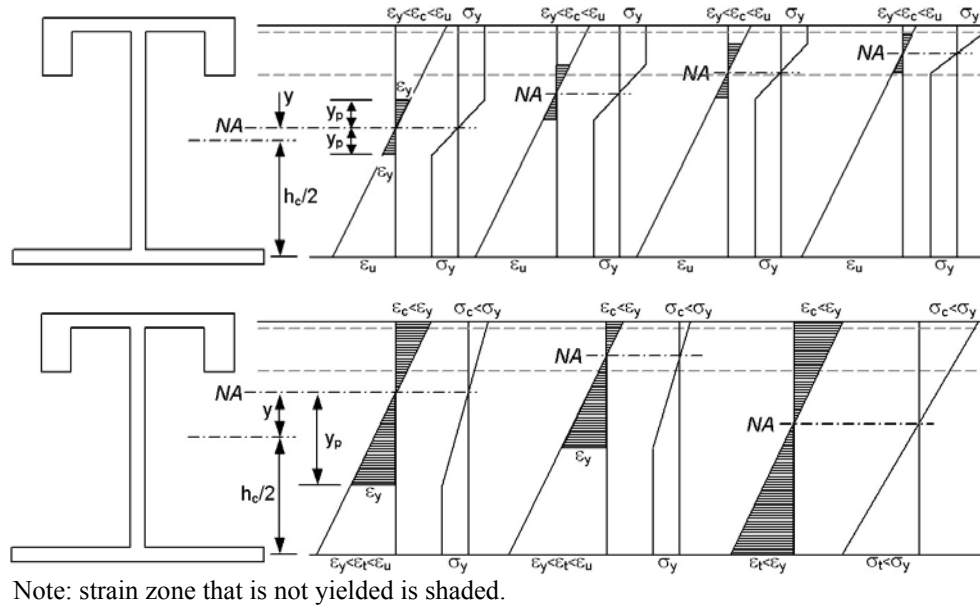
Figure 4.8 Possible cases using EPMC

4.4.5 Moment Capacity Based on Ramberg-Osgood Stress Distribution (ROMC)

The ROMC uses the Ramberg-Osgood equation, Equation (7), to determine the stress distribution from the strain distribution. The stress distribution obtained is analytically integrated to compute the moment capacity. In the sense that the approach computes the location of the neutral axis from the equilibrium and relies on a linear strain distribution, it is similar to the EPMC. The following describes the overall procedure of this approach, based on an example given in Figure 4.9.

Depending on whether the tension or compression yields first, two possible stress distribution cases are considered, as shown in Figure 4.9. For either stress distribution case, the compression limit state stress (f_c) is computed first. Using the Ramberg-Osgood equation, the corresponding compression strain (ε_c) is obtained from Equation (60). Based on the strain and the unknown distance between the mid-depth and the neutral axis (y_{NA}), a linear strain distribution is assumed. The tension side strain (ε_t) is determined from the strain distribution. Using the Ramberg-Osgood equation, a

relationship between the tension side strain (ε_t) and the tension limit state stress (f_t) is obtained:

$$\varepsilon_t = \frac{f_t}{E} + 0.002\left(\frac{f_t}{F_y}\right)^n \qquad (58)$$
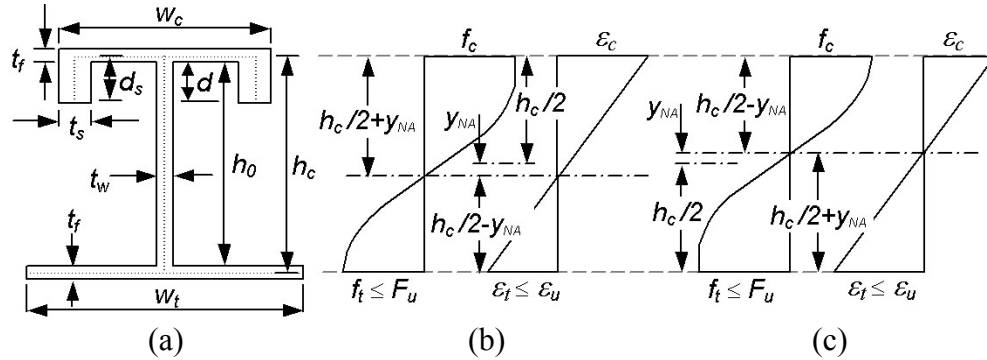
Figure 4.9 Notations for edge-stiffened singly symmetric section (a) cross-section (b) compression yield first (c) tension yield first

The assumed stress distribution needs to satisfy the force equilibrium with respect to the longitudinal direction:

$$\int_A f\,dA = 0 \qquad (59)$$

Since there are two unknowns, f_t and y_{NA}, and two equations, Equations (58) and (59), the unknowns can be solved. However, due to the highly non-linear nature of the equations, the procedure for obtaining solutions is iterative.

In some cases of Figure 4.9c, the computed tension limit state stress (f_t) could be larger than the ultimate stress. In this case, the tension limit state stress (f_t) should be reduced to the ultimate stress. According to the reduced tension limit state stress (f_t), the entire strain stress distribution is reduced. The compression limit state stress is then back calculated from this reduced strain distribution with the Ramberg-Osgood equation:

$$\varepsilon_c = \frac{f_c}{E} + 0.002\left(\frac{f_c}{F_y}\right)^n \qquad (60)$$

In this case, the unknowns are f_c and y_{NA}, which can be solved by two equations: Equations (59) and (60).

After the stress distributions and the location of the neutral axis are determined, a rather rigorous moment capacity can be obtained using classical beam theory:

$$M_u = \int_A f \cdot y \, dA \qquad (61)$$

or using the notations given in Figure 4.9,

$$M_u = f_c t_f w_c \left(\frac{h_c}{2} + y_3 \right) + f_t \, t_f w_t \left(\frac{h_c}{2} - y_3 \right) + f_c t_s d \left(2 - \frac{d_s}{\frac{h_c}{2} + y_3} - \frac{\frac{t_f}{2}}{\frac{h_c}{2} + y_3} \right) \left(z_1 + \frac{h_c}{2} + y_3 - d_s \right)$$

$$+ t_w \left(\frac{\frac{h_c}{2} - y_3}{\varepsilon_t} \right)^2 \left(\frac{f_c^3 + f_t^3}{3E} + \frac{(n+1)\left(f_c^{n+2} + f_t^{n+2} \right)}{500(n+2) F_y^n E} + \frac{n\left(f_c^{2n+1} + f_t^{2n+1} \right)}{500^2 (2n+1) F_y^{2n}} \right) \qquad (62)$$

where z_1 is the distance from the neutral axis to the centroid of the stress distribution on the stiffener, which is assumed to be linear.

The ROMC should be the most accurate approach among those developed in this study, since a non-linear stress distribution is used to compute the neutral axis, rather than a linear elastic stress distribution. However, this approach is rather complicated due to the iterative nature of the procedure. In addition, the equations for finding the neutral axis location and moment capacity, Equation (62), need to be re-derived for different types of cross-sections. Thus, this approach is not appropriate for practical design.

4.5 Parametric Studies

4.5.1 Types of Analyses Used

The approaches to computing the moment capacity of an aluminum member proposed in this study and presented in the AA *Specification* (2000a) are summarized in Table 4.4.

Table 4.4 Types of analysis approaches (a) specification applicable (b) specification non-applicable

(a)

design categories	AA *Specification*		proposed design approaches		
	$M_{AA-Y-MMCA}$	$M_{AA-Y-WASA}$	$M_{NSA-U-WASA2}$	$M_{NSA-U-TMCA}$	$M_{NSA-U-TMCA2}$
limit state	yielding	yielding	ultimate	ultimate	ultimate
equivalent slenderness ratio	AA	AA	NSA	NSA	NSA
neutral axis	LENA	LENA	LENA	LENA	LENA
moment capacity	MMCA	WASA	WASA2	TMCA	TMCA2
recommended cross-section	symmetric or unsymmetric	symmetric	symmetric	symmetric or unsymmetric	symmetric or unsymmetric

(b)

design categories	proposed design approaches	
	$M_{NSA-U-EPMC}$	$M_{NSA-U-ROMC}$
limit state	elasto-plastic	ultimate
equivalent slenderness ratio	NSA	NSA
neutral axis	computed from equilibrium	computed from equilibrium
moment capacity	EPMC (element-by-element basis)	ROMC (Equation (62))
recommended cross-section	symmetric or unsymmetric	symmetric or unsymmetric

Note: LENA = a neutral axis determined from a linear elastic stress distribution.
    MMCA = Minimum moment capacity approach in Section 4.4.1.
    WASA = Weighted average stress approach in Section 4.4.2.
    WASA2 = Modified weighted average stress approach in Section 4.4.2.
    TMCA = Total moment capacity approach (2 groups) in Section 4.4.3.
    TMCA2 = Total moment capacity approach (3 groups) in Section 4.4.3.
    EPMC = Moment capacity based on elasto-plastic stress distribution in Section 4.4.4.
    ROMC = Moment capacity based on Ramberg-Osgood stress distribution in Section 4.4.5.

The first three proposed approaches in this table are suited for application in design, while the remaining two are somewhat too complicated. The first category in Table 4.4 defines the limit state used in each approach, which is described in Section 2.1. The second category indicates whether the equivalent slenderness ratio (as well as the compressive limit state stress) for each component element is determined using the AA *Specification* (2000a, Section 2.2) or the Numerical Slenderness Approach (NSA, Section 4.1). The third category represents whether the neutral axis is directly calculated from equilibrium or determined based on the linear elastic stress distribution (LENA). The final category indicates the method used to calculate the moment capacity.

4.5.2   Cross-Sections Used in Parametric Study

A parametric study is performed for five types of sections, as shown in Figure 4.10. The first two sections are simple extrusions, which can be designed accurately following the proposed approaches in Chapter 2 and 3. However, these sections are included in this study so that the applicability of the NSA to the simple extrusions can also be examined. The NSA is originally designed for complex extrusions, as explained in Section 4.1.

| (a) | (b) | (c) | (d) | (e) |
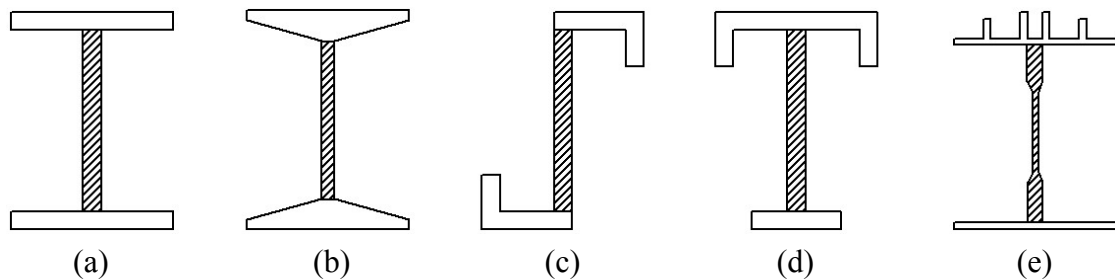
Note: web group area is shaded.

Figure 4.10 Cross-sections used in the parametric study

Although there is a provision in the AA *Specification* (2000a) for the edge-stiffened sections shown in Figure 4.10c and Figure 4.10d, unlike the more general

NSA, it does not deal with cross-sections with different flange and stiffener thicknesses. In addition, it is limited to the yield limit state. There is no provision in the AA *Specification* (2000a) for taking into account multiple intermediate stiffeners and variation in thickness within one component element, as is the case for the cross-section in Figure 4.10e.

The slenderness of the cross-sections used in the parametric study is rather low, such that the equivalent slenderness ratios of component elements mostly fall into the yielding or inelastic buckling ranges defined in Figure 2.4. This is because the slenderness of most of the standard sections in AA (2000b) also falls within these ranges. Fixed dimensions of the cross-sections are given below, and the varied dimensions used in the parametric study can be found in Section 6.4 of the Appendix.

4.5.2.1 Symmetric I-Shaped Sections with Uniform Thickness (Figure 4.10a)

The cross-sections used in this parametric study are the same as in Section 2.7. The depth between flange center-lines and the width of the flanges are maintained at 254mm (10 in.), while the thicknesses are varied. The length is set to ten times the depth. The width-to-thickness ratio for the flange ranges from 2.70 to 9.75, and from 8.33 to 38.0 for the web. This covers most of the width-to-thickness ratios of the standard doubly symmetric I-sections listed in AA (2000b).

4.5.2.2 Symmetric I-Shaped Sections with Tapered Thickness (Figure 4.10b)

The cross-sections used in this parametric study are the same as in Section 3.5. All the 36 standard I-sections with tapered thickness listed in AA (2000b) are used for Series 1. Since all of these sections are rather stocky, additional sections are created through reduction of the thickness of the standard sections by 60% that constitute Series 2. Width-to-average thickness ratio for the flange ranges from 3.5 to 21.6, while width-to-thickness ratio for the web ranges from 6.6 to 81.5. Each member length is set to more than or equal to four times the member depth.

4.5.2.3 Edge-Stiffened Z-Sections (Figure 4.10c)

Depth and flange width along the mid-thickness are maintained at 91.44mm (3.6 in.) and 45.72mm (1.8 in.), respectively, while the thicknesses for each component element are varied. Width-to-thickness ratio for the flange ranges from 2.2 to 21, and ranges from 6.3 to 43 for the web. In Series 1, thicknesses of all component elements are the same. In Series 2 stiffeners are twice as thick as the other elements, as shown in Figure 4.11. Since the dimensions of tension elements are identical to those of compression elements and the sections are laterally supported, the behavior of edge-stiffened Z-sections should be similar to the edge-stiffened C-sections. Thus, this type of section is considered as symmetric when design approaches are applied. Member length is taken as three times the half-wavelength corresponding to the minimum distortional buckling stress mode obtained from buckling analyses.
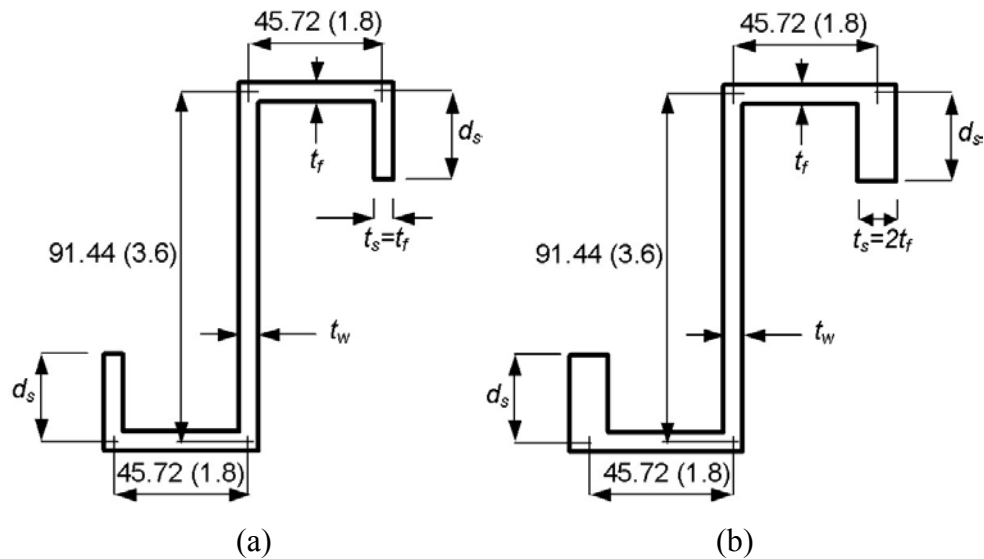
Note: All dimensions are in mm (and inches inside parenthesis) and not to scale.

Figure 4.11 Model geometry and dimensional notations for edge-stiffened Z-sections (a) Series 1 (b) Series 2

4.5.2.4 Singly Symmetric Edge-Stiffened Sections (Figure 4.10d)

Two different series of cross-sections used in the parametric study are investigated. For both series, the width of the compression flange is 228.6mm (9 in.),

the depth of the member is 279.4mm (11 in.), and the length of the stiffener is 63.5mm (2.5 in.) when measured through mid-thickness. Tension flange width varies from 25.4 mm (1 in.) to 431.8mm (17 in.). The varying width is used to evaluate the influence of the location of the neutral axis on each approach. The thickness of the flanges and web is 25.4mm (1 in.) for one series and 7.62mm (0.3 in.) for the other. The thickness of edge-stiffeners is set to twice the flange thickness. The length of the member is set to three times the half-wavelength corresponding to the minimum distortional buckling stress mode obtained from buckling analyses.
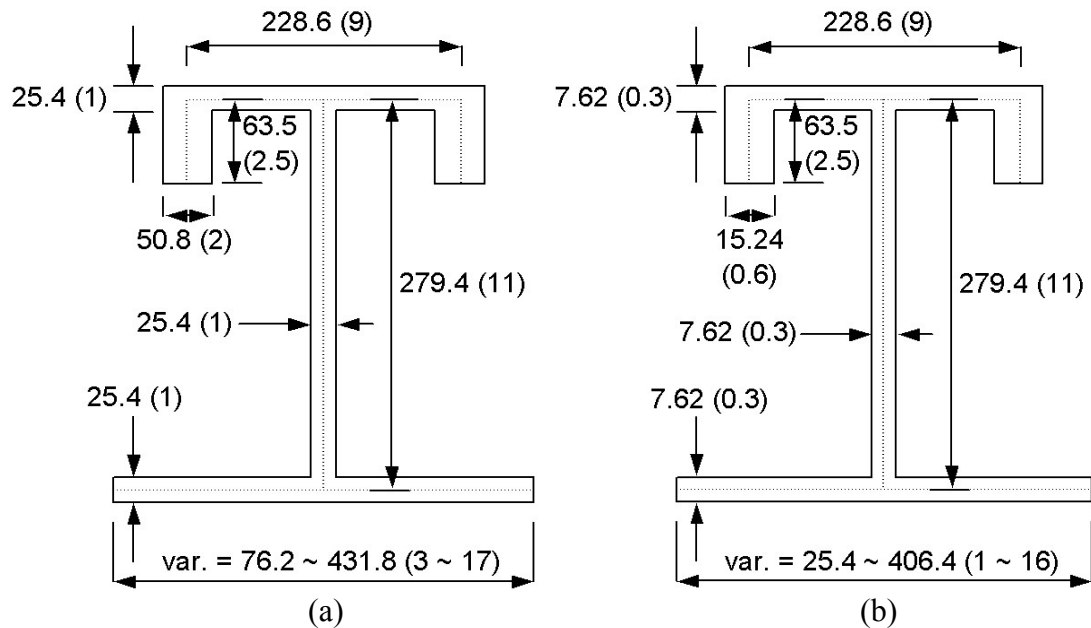
Note: all dimensions are in mm (and inches inside parenthesis) and not to scale.

Figure 4.12 Model geometry and dimensional notations for edge-stiffened singly-symmetric sections (a) Series 1 (b) Series 2

4.5.2.5 Dome-strut sections (Figure 4.10e)

There are two series of cross-sections used in this parametric study. In Series 2, the web-flange junction is protruded, while it is not protruded in Series 1, as shown in Figure 4.13. The depth measured between mid-thicknesses of the flanges and the

width of flanges remain constant at 127 mm (5 in.). Interior intermediate stiffeners are 12.7 mm (0.5 in.) long, while exterior stiffeners are 10.16mm (0.4 in.) long. Width-to-thickness ratio for the flange ranges from 4.1 to 27.2 if the intermediate stiffeners are ignored. Width-to-thickness ratio for the web ranges from 12 to 86.4 if the portions protruding from the web-flange junctions are ignored. The thickness of the thicker portion of the web (t_{w2}) is set to three times the thinner portion (t_w). The length of the thicker portion of the web (d_w) is set to one-eighth of the section depth. All the thicknesses are varied for this parametric study. The length of the member is set to three times the half wavelength corresponding to the minimum distortional buckling stress mode obtained from the buckling analyses.
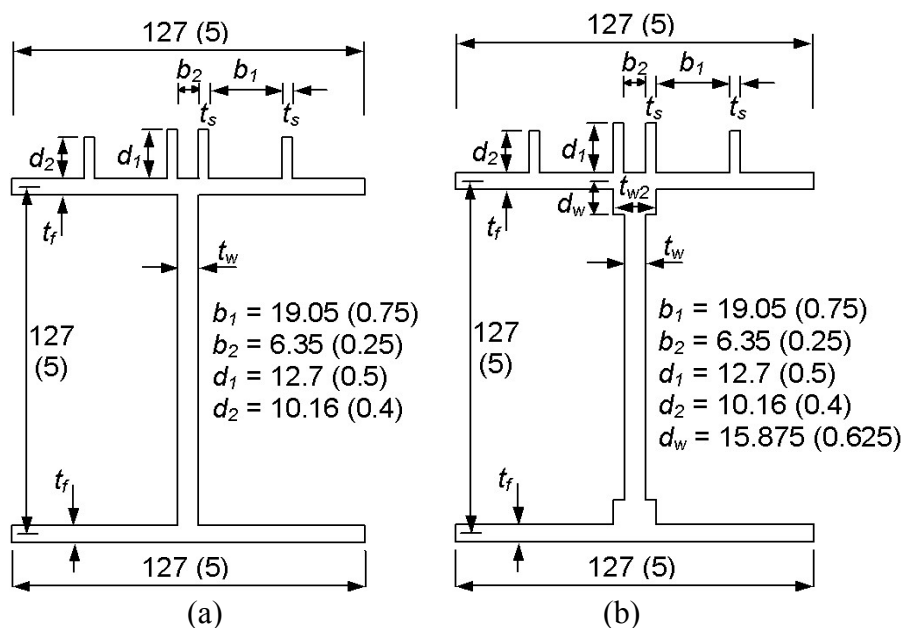
Note: all dimensions are in mm (and inches inside parenthesis) and not to scale.

Figure 4.13 Model geometry and dimensional notations for dome-strut sections (a) Series 1 (b) Series 2

4.5.3   Finite Element Modeling

Second order inelastic non-linear finite element analyses are conducted using ABAQUS, developed by Hibbitt, Karlsson & Sorensen, Inc. (1998), for comparison

with the design approaches proposed in this study and those presented in the AA *Specification* (2000a) as summarized in Table 4.4.

For all cross-sections used in the parametric study except type (c) sections, rigid beam elements are attached at the ends of the member so that a plane section can remain plane during bending. For these sections, equal and opposite concentrated moments are applied at both ends to simulate pure bending conditions. For type (c) sections, consistent nodal forces are applied to simulate pure bending conditions. Lateral supports are attached at web-flange junctions so that lateral buckling is prevented. Initial geometric imperfections are generated using elastic buckling analyses with the maximum amplitude based on the standard flatness tolerance provided in AA (2000c).

For type (b) sections, twenty-noded quadratic hexahedral solid elements with reduced integration are used to fully take into account the tapered thickness. For all other types of sections, shell elements are used. Further details regarding finite element modeling can be found in Section 2.5.

4.5.4 Material Properties

The cross-sections used in the parametric study are extrusions of 6061-T6 with the minimum material properties tabulated in AA (2000c) and shown in Table 2.4. Based on these properties, a tensile stress-strain curve is fitted by the Ramberg-Osgood equation given in Equation (7). The stress-strain curve for compression is assumed to be the same as for tension. The ultimate strain, which is not defined in AA (neither 2000a, 2000b or 2000c), is set to 8%, based on the discussion set forth in Section 2.3.

4.5.5 Idealization of Type (e) Sections in the AA *Specification* (2000a) and NSA

The dome-strut section shown in Figure 4.10e is one of the most common types of extrusion. It consists of a doubly symmetric I-shaped portion and multiple stiffeners on one of the flanges. The stiffeners are intended for use as a screw chase to hold the exterior panels of a dome structure. The behavior of sections with (Figure 4.10e) and without stiffeners (Figure 4.10a) is significantly different, which is also demonstrated in Figure 4.2. This difference affects the calculated member capacity.
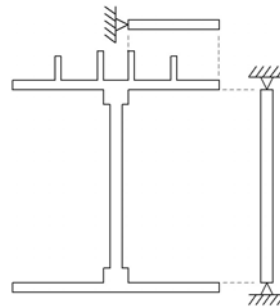
Figure 4.14 Idealization in the AA *Specification* (2000a) for a dome strut section

However, the AA *Specification* (2000a) does not have provisions for multiple stiffeners as in this dome-strut section. In addition, the variation in the web thickness near the web-flange junctions cannot be taken into account in the specification. A possible idealization made for the limit state (or allowable) stress computation of component elements using the AA *Specification* (2000a) is shown in Figure 4.14. In contrast, the NSA can account for the irregularities of the section. However, the thickness variation in the web is not considered when the shape factor is computed, because it is based on uniform thickness as shown in Figure 4.3.

4.5.6 Results

The ultimate moment capacity obtained from each finite element analysis for each section given in Figure 4.10 is divided by that from each approach in the AA *Specification* (2000a) and proposed in this study. The results are shown in Figure 4.15

with respect to the slenderness factor (λ), as defined in Equation (22), in the horizontal axis. Since AISI (1996) defines a component element as fully effective when λ is less than or equal to 0.673, it would be reasonable to consider 0.673 as the border between the slender and stocky ranges. However, the slenderness factor is not used in design procedures but for visual convenience only.

For all sections, the proposed approaches using the NSA show a performance superior to the approaches in the AA *Specification* (2000a). The differences amongst the approaches are summarized in Table 4.4. For the stocky range ($\lambda \leq 0.673$), the difference between the proposed and specification-based approaches should be mainly due to the choice of limit state (ultimate or yield). In this range, proposed approaches predict the ultimate-plastic capacities quite precisely for all type of sections, when they are compared to the finite element analyses. On the other hand, for the slender range ($\lambda > 0.673$), the accuracy of the approach should depend more on the method that the equivalent slenderness ratio is determined. For this reason, when the limit state stress is computed based on highly idealized geometry as shown in Figure 4.14, the bending capacity cannot be computed accurately using the current specification approach as shown in Figure 4.15e; the moment capacity computed is at times less than half of that computed using the FEM analysis for some cross-sections.

In addition, the proposed approaches based on the WASA2, TMCA or TMCA2 show a closer agreement with the finite element analysis than the specification approaches based on the MMCA or WASA. This supports the accuracy of the proposed approaches. Especially for unsymmetric cross-sections, the MMCA is the only specification-based approach that can be used as explained in Section 4.4.2. Since contributions from all component elements cannot be fully incorporated in the MMCA as opposed to the other aforementioned approaches, the deviation between this approach and the finite element analysis is larger for unsymmetric cross-sections.

The following subsections further elaborate on the results of the parametric study for each type of cross-section shown in Figure 4.10.

4.5.6.1 Symmetric I-Shaped Sections with Uniform Thickness (Figure 4.10a)

For this type of cross-section, the approaches using the NSA in Figure 4.15a show almost the same performance as the proposed approaches in Figure 2.14. This implies that the idealization of the web-flange junction as being simply-supported is quite accurate for simple I-shaped sections with uniform thickness.

4.5.6.2 Symmetric I-Shaped Sections with Tapered Thickness (Figure 4.10b)

For use in the NSA, the buckling stress of the tapered thickness sections is computed using CUFSM-tap, which is the version of the CUFSM program modified for the tapered element based on the study in Section 3.2. For this type of cross-section, the idealization of simply-supported boundaries between component elements is quite accurate if the equivalent slenderness ratio developed in Section 3.3 for simple I-shaped sections with tapered thickness is used, which is almost the same conclusion made for the I-sections with uniform thickness.

4.5.6.3 Edge-Stiffened Z-Sections (Figure 4.10c)

For this type of cross-section, the results based on the AA *Specification* (2000a) are not significantly different from those based on the NSA in the slender range ($\lambda > 0.673$). The approach available in the AA *Specification* (2000a) for edge-stiffened sections seems reasonable.

4.5.6.4 Singly Symmetric Edge-Stiffened Sections (Figure 4.10d)

For the singly symmetric edge-stiffened section, it is noted that the moment capacity based on the Ramberg-Osgood equation (ROMC) shows excellent agreement with the non-linear finite element analysis as shown in Figure 4.15d. In this figure,

although the proposed approach based on the TMCA is still much better than that of the AA *Specification* (2000a), the difference from the results of the finite element analysis increases as the distance from the neutral axis to the mid-depth (y_{NA}) increases. On the other hand, the other proposed approach using the TMCA2 shows considerable improvement compared to the approach using the TMCA, because the TMCA2 uses three linearized stress distributions. Thus, the use of TMCA2 is recommended for unsymmetric sections.

4.5.6.5 Dome-Strut Sections (Figure 4.10e)

In order to investigate the effect of the idealizations shown in Figure 4.14, type (e) sections are analyzed at the yield limit state in Figure 4.16. As seen in this figure, a more significant difference between the approach based on the AA *Specification* (2000a) and the proposed approach is observed in the larger slenderness range, where the limit state stress is more sensitive to the equivalent slenderness ratio. In addition, Series 2 sections show more deviation from the finite element analysis than Series 1 sections due to the additional idealization in the web element. Thus, the equivalent slenderness ratio computed through the NSA should be applied to the design of complex extrusions.

Finally, the performance improvement from the use of both the ultimate limit state and the TMCA2 is demonstrated in Figure 4.15e. Although the results for the TMCA and TMCA2 are similar for large slenderness factors, as the slenderness of the cross-section decreases the difference between these two methods becomes more prominent. This is because as the slenderness increases the stress distribution becomes more linear due to the lack of non-linear inelastic reserve capacity.
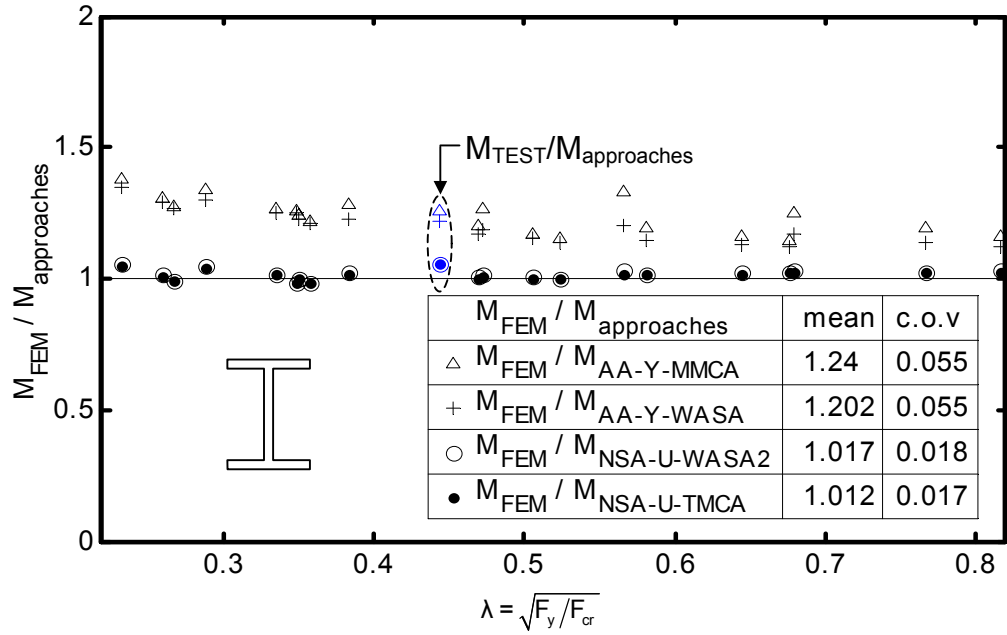
(a)
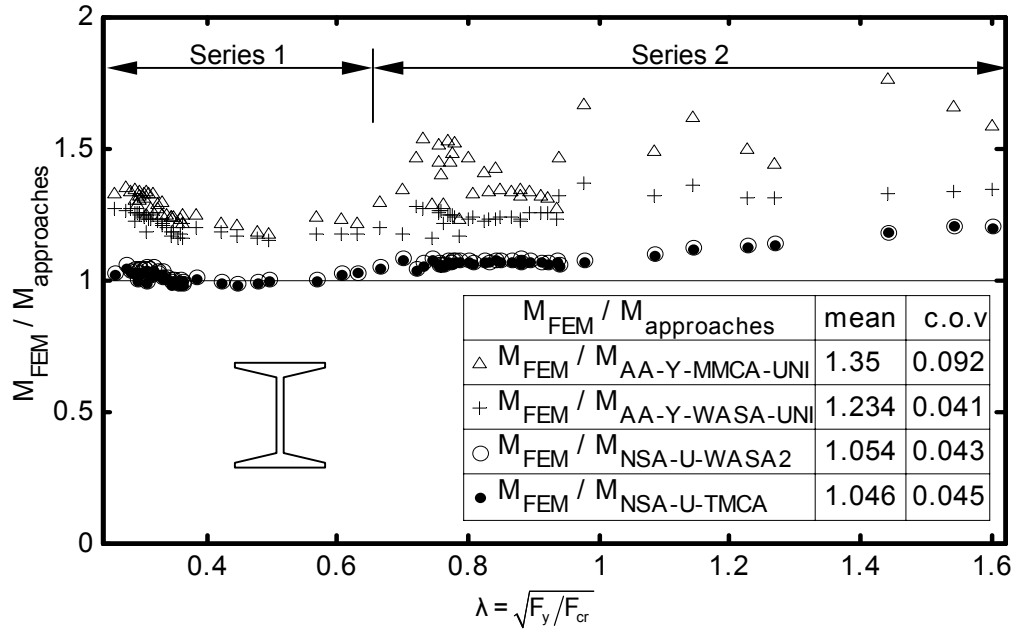
(b)

Figure 4.15 Parametric study results

Figure 4.15 (Continued)

The figure (c) shows a scatter plot with axis $M_{FEM}/M_{approaches}$ (vertical, 0 to 2) versus $\lambda = \sqrt{F_y/F_{cr}}$ (horizontal, 0.2 to 1.2), with the following legend table:

$M_{FEM}/M_{approaches}$	mean	c.o.v
$\triangle$ $M_{FEM}/M_{AA-Y-MMCA}$	1.175	0.103
$+$ $M_{FEM}/M_{AA-Y-WASA}$	1.077	0.095
$\circ$ $M_{FEM}/M_{NSA-U-WASA2}$	0.976	0.039
$\bullet$ $M_{FEM}/M_{NSA-U-TMCA}$	0.979	0.039

(c)

The figure (d) shows a scatter plot with axis $M_{FEM}/M_{approaches}$ (vertical, 0 to 2) versus $\lambda = \sqrt{F_y/F_{cr}}$ (horizontal, 0.2 to 0.65), divided into Series 1 and Series 2, with y_{NA}=large and y_{NA}=small regions, with the following legend table:

$M_{FEM}/M_{approaches}$	mean	c.o.v
$\triangle$ $M_{FEM}/M_{AA-Y-MMCA}$	1.431	0.149
$\circ$ $M_{FEM}/M_{NSA-U-TMCA}$	1.174	0.095
$\bullet$ $M_{FEM}/M_{NSA-U-TMCA2}$	1.002	0.053
$\square$ $M_{FEM}/M_{NSA-U-EPMC}$	1.072	0.045
$+$ $M_{FEM}/M_{NSA-U-ROMC}$	1.001	0.024

(d)

Figure 4.15 (Continued)

(e)

Figure 4.16 Effect of idealization for dome-strut sections

4.6   Flexural Tests

The average of the three bending test results for an Aluminum Association Standard I-Beam with uniform thickness (I-3x1.64), described in Section 2.8, is included in Figure 4.15a within the dashed-line oval. The average of two other bending test results for an American Standard I-Beam with tapered thickness (I-3x1.96), listed in AA (2000b), is compared to the current and proposed approaches in Table 4.5. From the comparisons, it can be seen that the proposed approaches are in better agreement with the test results than the current approaches. Further details regarding the tests are given in Section 3.6.

Table 4.5 Comparison of test results to proposed approaches for I-section with tapered thickness (I-3x1.96)

current approaches		proposed approaches	
$\dfrac{M_{TESTS}}{M_{AA\text{-}UNI\text{-}Y\text{-}MMCA}}$	$\dfrac{M_{TESTS}}{M_{AA\text{-}UNI\text{-}Y\text{-}WASA}}$	$\dfrac{M_{TESTS}}{M_{NSA\text{-}U\text{-}WASA2}}$	$\dfrac{M_{TESTS}}{M_{NSA\text{-}U\text{-}TMCA}}$
1.174	1.141	0.967	0.960

Additionally, flexural tests are conducted for a complex extrusion type cross-section. This cross-section is not a standard section but a mullion section made by Kawneer Co., which is similar to the cross-section shown in Figure 4.7. The exact dimensions of the cross-section cannot be presented here due to patent issues.

Before bending tests are conducted, the test setup is simulated using the finite element method. The same solid elements are used to take into account the complex geometry of the mullion section as those used for tapered thickness I-sections in Section 3.6. On the assumption that the failure shape would be symmetric, only half of the member is analyzed with longitudinal restraints at the cross-section cut. From the analyses, the lateral support spacing is determined as shown in Figure 4.17 so that continuous lateral support can be properly simulated. The test setup is designed for typical two-point bending tests. Except for the spacing of the lateral supports specified

in this figure, details of the test setup are quite similar to those for the uniform thickness I-sections shown in Figure 2.16.
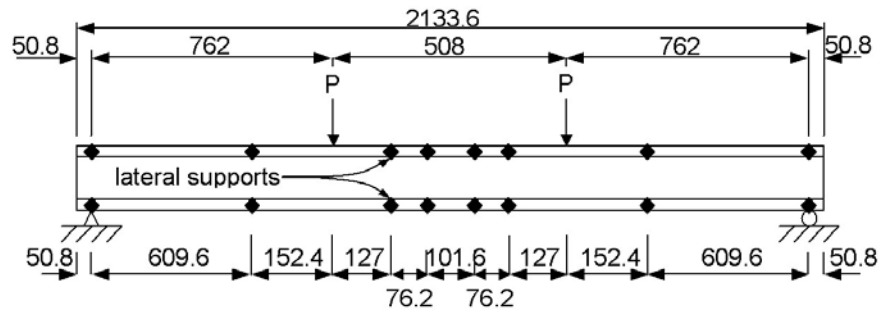
Figure 4.17 Schematic bending test setup for mullion section

The residual deformations of the tested mullion sections are shown in Figure 4.18. In the first test, a single wave was formed near the middle of the span; this is very similar to the assumption made for the finite element analysis that the failure shape would be symmetric. On the other hand, in the second test, two waves were formed; one is at the middle and the other is between two neighboring lateral supports.

(a)

(b)

(c)

(d)
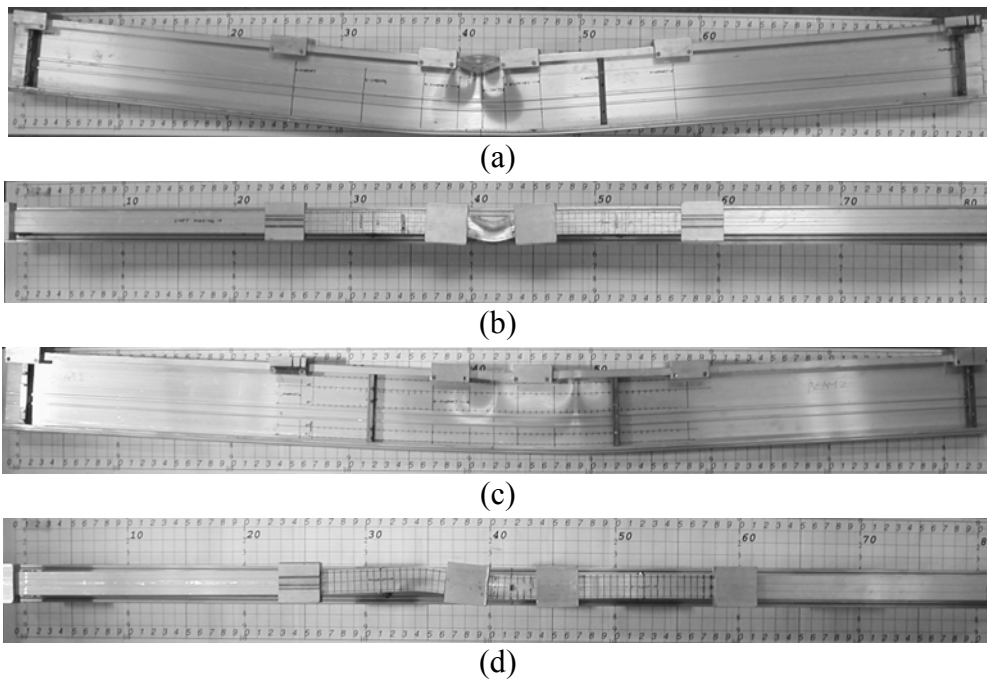
Figure 4.18 Residual deformation of tested mullion specimens (a) side view at Test 1 (b) plan view at Test 1 (c) side view at Test 2 (d) plan view at Test 2

Tests results are plotted and compared to the finite element analysis in Figure 4.19. Although there are some differences, the overall results are in good agreement. The moment capacities from the tests and finite element simulation are compared to those from the specification-based and proposed approaches in Table 4.6 and Table 4.7, respectively. From the tables, it is clear that the proposed approaches are in better agreement with both the finite element analysis and the experimental test results than current specification-based approaches for the mullion section.
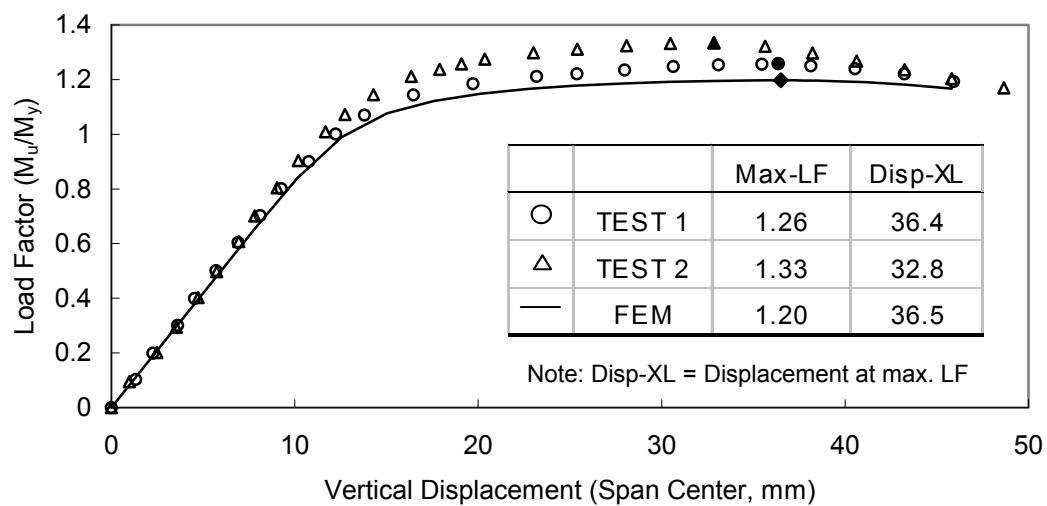
Note. The maximum load factors are shown as solid shapes.

Figure 4.19 Test results for a mullion section

Table 4.6 Comparison of test results for mullion

current approaches	proposed approaches	
$\dfrac{M_{TESTS}}{M_{AA\text{-}Y\text{-}MMCA}}$	$\dfrac{M_{TESTS}}{M_{NSA\text{-}U\text{-}TMCA}}$	$\dfrac{M_{TESTS}}{M_{NSA\text{-}U\text{-}TMCA2}}$
1.295	1.096	1.106

Note. M_{TESTS} is the average of the two maximum load factors from the tests.

Table 4.7 Comparison of finite element simulation results for mullion

current approaches	proposed approaches	
$\dfrac{M_{FEM}}{M_{AA\text{-}Y\text{-}MMCA}}$	$\dfrac{M_{FEM}}{M_{NSA\text{-}U\text{-}TMCA}}$	$\dfrac{M_{FEM}}{M_{NSA\text{-}U\text{-}TMCA2}}$
1.205	1.020	1.029

Before the tests are conducted, initial geometric imperfections were measured on the compression flange and web as shown in Figure 6.5 in the Appendix. The maximum imperfection on the flange is somewhat larger than the standard flatness tolerance in AA (2000c), while the maximum imperfection on the web is much less than the tolerance.

Uniaxial tension tests have also been conducted using seven test coupons obtained from a portion adjacent to the specimens used for the bending tests. In Table 6.27d in the Appendix, the results are compared to the standard values listed in AA (2000b). The median of the seven test results is introduced into the finite element analysis.

4.7 *Application to the AA* Specification

In Section 2.9, two procedures are proposed for the governing allowable stress equations for symmetric sections. In these procedures, the proposed allowable stress equations for component elements are based on the AA *Specification* (2000a). By replacing the allowable stress equations for component elements with the NSA, the governing allowable stress equations can employ the NSA. In other words, Table 2.10 is replaced by Table 4.8.

It should be noted that the width-to-thickness ratio is not used for the slenderness in Table 4.8. Instead, the equivalent slenderness ratio (λ_p) is used directly to determine the allowable stress. The equivalent slenderness ratio (λ_p) is a function of the buckling stress (F_{cr}), as shown in Equation (47). The buckling stress is the minimum value that can be obtained from any numerical buckling analysis program. Further details regarding the NSA can be found in Section 4.1. Although Table 4.8 is based on the Allowable Stress Design, this table can also be applied to the Load and Resistance Factor Design by replacing the reciprocal of each safety factor with the corresponding resistance factor.

Table 4.8 Allowable stress equations of NSA for (a) tension component element (b) compression component element and (c) shape factors

(a)

AA Section	allowable stress
3.4.2 3.4.4	$F_{ay} = \alpha_y F_{ty}/n_y$
	$F_{au} = \alpha_u F_{ty}/(k_i n_u)$

(b)

AA Section	[c] allowable stress $\lambda_p \leq S_1$	limit S_1	allowable stress $S_1 \leq \lambda_p \leq S_2$	limit S_2	allowable stress $S_2 \leq \lambda_p$
3.4.15 3.4.16 3.4.16.2 3.4.16.3 3.4.18, 3.4.19	$F_{ay} = \dfrac{\alpha_y F_{cy}}{n_y}$ $F_{au} = \dfrac{\alpha_u F_{cy}}{n_u}$	$\dfrac{B - \alpha_y F_{cy}}{D}$ $\dfrac{B - \frac{n_y}{n_u}\alpha_u F_{cy}}{D}$	$F_{ay} = F_{au} =$ $\dfrac{1}{n_y}\left(B - D\lambda_p\right)$	$\dfrac{k_1 B}{D}$	$F_{ay} = F_{au} =$ $\dfrac{k_2\sqrt{BE}}{n_y \lambda_p}$

(c)

AA Section	[c] yield shape factor	ultimate shape factor
3.4.2	$\alpha_y = 1.0$	$\alpha_u = F_{tu}/F_{ty}$
3.4.4	$\alpha_y = 1.3$	$\alpha_u = \left(14\dfrac{F_{tu}}{F_{ty}} + 13\right)\left(\dfrac{y_{NA}}{h}\right)\left(0.5 - \dfrac{y_{NA}}{h}\right)^3 + \left(1.25\dfrac{F_{tu}}{F_{ty}} + 0.2\right)$ [a]
3.4.15, 3.4.16 3.4.16.2, 3.4.16.3	$\alpha_y = 1.0$	$\alpha_u = F_{tu}/F_{cy}$ [b]
3.4.18	$\alpha_y = 1.3$	$\alpha_u = \left(14\dfrac{F_{tu}}{F_{cy}} + 13\right)\left(\dfrac{y_{NA}}{h}\right)\left(0.5 - \dfrac{y_{NA}}{h}\right)^3 + \left(1.25\dfrac{F_{tu}}{F_{cy}} + 0.2\right)$ [b]

Note: B, D, k_1 and k_2 are the factors provided in the AA *Specification* (2000a). These factors differ for flanges and webs. F_{au} = ultimate allowable stress. F_{ay} = yield allowable stress. y_{NA} = the distance from the neutral axis to the mid-depth. See Equation (47) for λ_p.

a. In the AA *Specification* (2000a), $\alpha_u = 1.42 F_{tu}/F_{ty}$.

b. Not available in the AA *Specification* (2000a).

c. The allowable stress equations corresponding to the AA Section numbers indicated here can be replaced with the NSA. In the following sections, flanges are under uniform compression, while webs are under bending in own plane.

AA 3.4.2: tension flange

AA 3.4.4: tension web

AA 3.4.15: compression flange with one edge supported and the other edge free

AA 3.4.16: compression flange with both edges supported

AA 3.4.16.2: compression flange with one edge supported and the other edge with stiffener

AA 3.4.16.3: compression flange with both edges supported and with an intermediate stiffener

AA 3.4.18: compression web with both edges supported

AA 3.4.19: compression web with both edges supported with a horizontal stiffener

For cross-sections with the neutral axis not at mid-depth, the ultimate shape factor of rectangular web elements (α_u) varies according to the location of the neutral axis as shown in Equation (54). The maximum shape factor is obtained from one of two solutions of $\partial\alpha_w/\partial y_{NA} = 0$, which is when $y_{NA} = 0.125h$ (y_{NA} = distance between the neutral axis and the mid-depth of the web element. h = depth of the web element). Introducing this into Equation (54) results in the maximum ultimate shape factor of rectangular web elements when the neutral axis is not at mid-depth (unsymmetric sections):

$$\max\left(\alpha_u\right) = \alpha_u\big|_{y_{NA}=0.125h} = 1.34\frac{F_{tu}}{F_{ty}} + 0.286 \qquad (63)$$
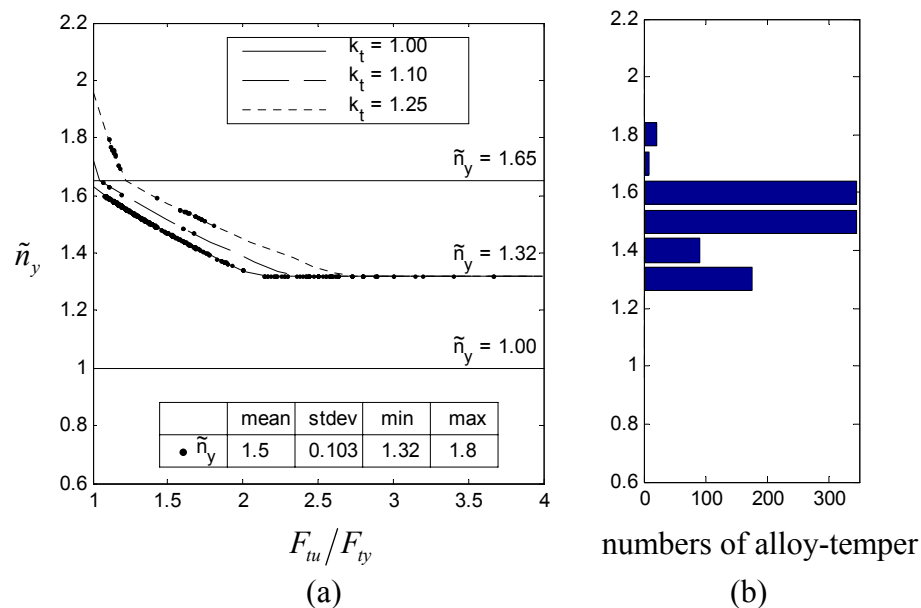
Figure 4.20 Safety factor on yield strength of the tensile allowable stress (AA Section 3.4.4) for a plate under bending when Procedure II is used

Using Equation (63), the safety factors on yield strength based on Procedure II are computed for the previously selected 986 alloy-temper combinations as is done in Section 2.9 for symmetric sections. Compared to the safety factor on yield strength in the AA *Specification* (n_y =1.65), the average of the varying safety factor ($\tilde{n}_y$ =1.50) is

9.1% smaller for unsymmetric cross-sections as shown in Figure 4.20. The average is also somewhat smaller than that for symmetric cross-sections in Figure 2.20, as a result of using a larger shape factor in Equation (63). However, the safety factor on ultimate strength (n_u = 1.95 for building and similar type of structures) given in the AA *Specification* (2000a) is maintained, since only a specified percentage of the ultimate allowable stress is used, as explained in Section 2.9.

4.8   Conclusions

The Numerical Slenderness Approach (NSA) is developed in this study to provide a design approach for complex extrusions, in which the simply-supported boundary idealization between component elements is not applicable or appropriate. Since this approach computes the limit state (or allowable) stresses of component elements using the numerically determined buckling stress, practically all aluminum extrusions can be evaluated. The framework of the limit state (or allowable) stress equations used for the AA *Specification* (2000a) is maintained in the NSA, with only the expression for the equivalent slenderness ratio being changed.

For all cross-sections used in the parametric study, the proposed approaches based on the NSA show a performance better than or equal to the approaches in the AA *Specification* (2000a). The NSA shows a superior performance especially for dome strut sections, in which intermediate stiffeners and variations in thickness are ignored in the specification-based approaches. It is found that the NSA can be used for the type of cross-sections that are presently covered by the AA *Specification* (2000a). In addition, a wide variety of extruded aluminum sections that are not covered in the specification can also be analyzed using the NSA.

Due to the flexibility of the extrusion process, many aluminum cross-sections are not symmetric with respect to the bending axis or have a neutral axis that is not at mid-depth. For these types of cross-sections, the rigorously determined shape factor of

rectangular web elements developed for symmetric sections in Section 2.3 is not appropriate. Therefore, a rigorously determined shape factor based on the neutral axis location for unsymmetric sections is developed in this chapter. The rigorous expression is greatly simplified through curve-fittings for practical design purposes.

The Total Moment Capacity Approach (TMCA) developed for symmetric sections in Section 2.6 is further extended to more general cross-sections in this study. For sections with the neutral axis not at the mid-depth, TMCA2 is suggested, in which the actual non-linear stress distribution is approximated by three linear stress distributions. When the ultimate limit state is employed, TMCA2 shows good agreement with the finite element analysis for the unsymmetric sections.

Moment capacity evaluation approaches relying on elasto-plastic stress distribution (EPMC) and Ramberg-Osgood stress distribution (ROMC) are also developed for unsymmetric sections. Although these approaches are quite accurate, they are not appropriate for practical design approaches due to their complicated procedures.

The approaches developed in this chapter are verified through parametric studies using finite element analyses. In addition, the approaches are further validated through physical flexural tests. In these tests, lateral supports are provided so that lateral buckling is prevented.

Based on the NSA, the final form of the allowable stress equations has been provided. The two procedures for calculating the governing allowable stress (or factored limit state stress) suggested for symmetric sections have also been used for unsymmetric sections in this chapter.

The ultimate shape factor for rectangular web elements with a neutral axis not at mid-depth and the TMCA2 can also be employed in the modified specification-based approaches in Chapter 2.

5. CONCLUSIONS

Aluminum is a structural material with "a thousand faces," which are combinations of a wide variety of both geometric shapes and material properties. This wide range of variety distinguishes aluminum from other metals such as steel. To make use of all the advantages of aluminum as a structural material, the variety should be properly recognized.

In the study presented here, it is found that physical tests could be replaced with numerical tools. Using numerical tools, a wide variety of virtual experiments can be conducted. Most of the current specification approaches are based on physical tests and analytical studies and it may not be appropriate to replace the whole specification with results from numerical tools. Instead, if at least portions that are not covered in the specification can be filled with the results of some simple numerical tools, significant benefits can be expected. This study shows that linear elastic buckling analyses using computers can improve the current specification in the application to a wide variety of cross-sections obtained through extrusion.

In addition, the use of a uniform safety factor applied only to the yield strength provided in the specification could be overconservative for certain alloy-temper combinations that have a great margin between the ultimate stress and yield stress. For this reason, a new design approach is proposed so that a larger inelastic reserve capacity is recognized for such materials. This approach should provide a way to make the current specifications more flexible with respect to material variations with a varying safety factor on yield strength, while maintaining the usual safety factor on ultimate strength.

In Chapter 2, equations are developed for the compressive limit state stress at the ultimate limit state. The rigorous closed-form expression derived for the ultimate shape factor using analytic integration shows that the current shape factor available in

the AA *Specification* (2000a) is unconservative for materials with a large ultimate to yield stress ratio. Thus, a better shape factor expression, simplified for practical design purposes, has been proposed. In addition, the parametric study for component elements shows that the existing limit state stress equations for the inelastic buckling range can be extended linearly up to the shape factor times the yield stress. A parametric study for I-shaped sections using the proposed approaches shows good agreement with the finite element analysis. The study is also further supported by the flexural tests of a standard section.

For practical design purposes, two procedures are suggested for specifications. In Procedure I, the safety factor on yield strength used in the current AA *Specification* (2000a) is maintained. In Procedure II, the safety factor is applied to the additional inelastic capacity. Procedure II is more reasonable in that the safety factor varies depending on the margin between the ultimate and yield stresses.

In Chapter 3, initial and geometric stiffness matrices for plates with tapered thickness are derived for a finite strip analysis program. The buckling coefficients obtained by this program show good agreement with previous research results. Expressions for the plate buckling coefficients of tapered plates are proposed with respect to the thickness variation ratio. Using the expressions, limit state stress equations are suggested for tapered thickness elements within the framework of the current specification. A parametric study validates the developed equations for tapered thickness plate flanges. Physical test results also agree well with the proposed approaches.

In Chapter 4, the Numerical Slenderness Approach (NSA) is developed in this study to provide a design approach for complex extrusions, in which the simply-supported boundary idealization between component elements is not applicable or appropriate. Since in this approach the limit state (or allowable) stresses of component elements are computed using the numerically determined buckling stress, a wider

range of geometric shapes of the cross-section can be covered. The framework of the limit state (or allowable) stress equations used for the specification is maintained in the NSA, with only the expression for the equivalent slenderness ratio being changed. For all cross-sections used in the parametric study, the proposed approaches based on the NSA show a performance better than or equal to the modified specification-based approaches in Chapters 2 and 3. In addition, a rigorous shape factor based on the neutral axis location is developed, and it is greatly simplified for practical design purposes. The Total Moment Capacity Approach (TMCA) developed for symmetric sections in Chapter 2 is further extended to unsymmetric sections in the TMCA2, where the actual non-linear stress distribution is approximated by three linear stress distributions. Moment capacity evaluation approaches relying on elasto-plastic stress distribution (EPMC) and Ramberg-Osgood stress distribution (ROMC) are also developed for unsymmetric sections. Although these approaches are quite accurate, they are not practical for use in design due to complicated procedures. The approaches developed in this chapter are verified through parametric studies using finite element analyses and physical flexural tests.

6. APPENDIX

6.1 Computational Example (1)

The following examples provide step-by-step computations of the moment capacities based on the currently available two approaches in the AA *Specification* (2000a) and two procedures proposed in Table 2.9. The safety factors on yield strength corresponding to the moment capacities are also computed. The cross sectional geometry is given in Figure 6.1, which is one of the cross-sections used in the parametric study in Table 2.8.
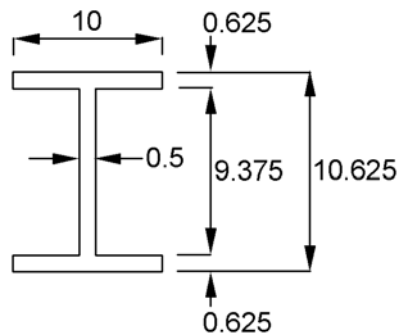
Note: All dimensions are in inches and not to scale

Figure 6.1 Geometry of cross-section for Computational Example (1)

Given:

Cross section: Figure 6.1

Alloy-temper: 6061-T6. See the first alloy-temper combination in Table 2.4.

Required:

Allowable moment capacities and safety factors on yield strength

Solution:

In Table 6.1, sectional properties are calculated for the cross-section given in Figure 6.1. For the computations of the ultimate shape factor for web (α_u), the expression in the AA *Specification*, Equation (15), should be used, if the moment capacity computation is based on the AA *Specification*. Similarly, the proposed shape

factor expression, Equation (16), should be used, if the moment capacity is based on the proposed approaches. However, such consistency is not maintained in this example, because the shape factors computed from the two equations do not differ significantly for the material used here. Thus, Equation (16) is only used in this example. The following computations are based on the sequence of table numbers (from Table 6.1 to Table 6.6).

Table 6.1 Geometrical and material properties

geometrical properties	material properties
$I_f = (10)(10.625^3 - 9.375^3)/12 = 312.91 \text{ in}^4$	$F_{tu} = 38 \text{ ksi}$
$I_w = (0.5)(9.375^3)/12 = 34.33 \text{ in}^4$	$F_{ty} = 35 \text{ ksi}$
$I = I_f + I_w = 347.24 \text{ in}^4$	$F_{cy} = 35 \text{ ksi}$
$S = I/(h/2) = 65.36 \text{ in}^3$	$E = 10100 \text{ ksi}$ (for compression)
$S_f = I_f/(h_c/2) = 62.58 \text{ in}^3$	
$S_w = I_w/(h_o/2) = 7.324 \text{ in}^3$	
$A_f = (10)(0.625) = 6.25 \text{ in}^2$	
$A_w = (0.5)(9.375)/2 = 2.344 \text{ in}^2$	
$b = (10 - 0.5)/2 = 4.75 \text{ in}$	
$b/t_f = 4.75/0.625 = 7.6$	
$h_o/t_w = 9.375/0.5 = 18.75$	

Table 6.2 Buckling constants, shape factors, and slenderness limits (from Table 2.10)

flange	web
$B_p = 45.04$	$B_{br} = 66.76$
$D_p = 0.3008$	$D_{br} = 0.6648$
$k_1 = 0.35$	$k_1 = 0.5$
$k_2 = 2.27$	$k_2 = 2.04$
$\alpha_u = 38/35 = 1.0857$	$\alpha_u = 1.25(38/35) + 0.2 = 1.557$
ultimate limit state	ultimate limit state
$S_1^u = \dfrac{45.04 - \frac{1.65}{1.95}(1.0857)(35)}{5.1(0.3008)} = 8.40$	$S_1^u = \dfrac{66.76 - \frac{1.65}{1.95}(1.557)(35)}{0.67(0.6648)} = 46.36$
yield limit state	yield limit state
$S_1^y = \dfrac{45.04 - 35}{5.1(0.3008)} = 6.54$	$S_1^y = \dfrac{66.76 - 1.3(35)}{0.67(0.6648)} = 47.73$
$S_2 = \dfrac{0.35(45.04)}{5.1(0.3008)} = 10.28$	$S_2 = \dfrac{0.5(66.76)}{0.67(0.6648)} = 74.94$

Note: B_p, D_p, B_{br}, D_{br}, k_1, and k_2 are from AA (2000a)

Table 6.3 Allowable stresses for component elements (from Table 2.10)

flange	web
For tension side, $F_{ay} = \dfrac{35}{1.65} = 21.21 \; ksi$ $F_{au} = \dfrac{(1.0857)(35)}{1.95} = 19.49 \; ksi$ For compression side, since $S_1^y < b/t_f < S_2$, $F_{ay} = \dfrac{45.04 - (0.3008)(5.1)(7.6)}{1.65} = 20.23 \; ksi$ since $b/t_f < S_1^u < S_2$, (not in AA) $F_{au} = \dfrac{(1.0857)(35)}{1.95} = 19.49 \; ksi$	For tension side, $F_{ay} = \dfrac{(1.3)(35)}{1.65} = 27.58 \; ksi$ $F_{au} = \dfrac{(1.557)(35)}{1.95} = 27.95 \; ksi$ For compression side, since $h_o/t_w < S_1^y < S_2$, $F_{ay} = \dfrac{(1.3)(35)}{1.65} = 27.58 \; ksi$ since $h_o/t_w < S_1^u < S_2$, (not in AA) $F_{au} = \dfrac{(1.557)(35)}{1.95} = 27.95 \; ksi$

Table 6.4 Member and governing allowable stresses (Table 2.7 and Table 2.9)

approaches	member allowable stress
AA-MMCA	$F_a = \min(19.49, 21.21, 20.23, 27.95, 27.58, 27.58) = 19.49 \; ksi$
AA-WASA	Tension $F_{ay} = \dfrac{21.21(6.25) + 27.58(2.344)/3}{6.25 + 2.344/3} = 21.92 \; ksi$ $F_{au} = \dfrac{19.49(6.25) + 27.95(2.344)/3}{6.25 + (2.344)/3} = 20.43 \; ksi$ Compression $F_{ay} = \dfrac{20.23(6.25) + 27.58(2.344)/3}{6.25 + (2.344)/3} = 21.05 \; ksi$ Entire section $F_a = \min(21.92, 20.43, 21.05) = 20.43$
Procedure I - WASA2	Tension $F_{ay} = 21.92(10.625/10) = 23.29 \; ksi$ $F_{au} = 20.43(10.625/10) = 21.71 \; ksi$ Compression $F_{ay} = 21.05(10.625/10) = 22.37 \; ksi$ $F_{au} = \dfrac{19.49(6.25) + 27.95(2.344)/3}{6.25 + (2.344)/3}\left(\dfrac{10.625}{10}\right) = 21.71 \; ksi$ Entire section $F_a = \min(23.29, 21.71, 22.37, 21.71) = 21.71 \; ksi$

Table 6.4 (Continued)

Procedure I - TMCA	Tension $$F_{ay} = \frac{21.21(62.58) + 27.58(7.324)}{65.36} = 23.40 \; ksi$$ $$F_{au} = \frac{19.49(62.58) + 27.95(7.324)}{65.36} = 21.79 \; ksi$$ Compression $$F_{ay} = \frac{20.23(62.58) + 27.58(7.324)}{65.36} = 22.46 \; ksi$$ $$F_{au} = \frac{19.49(62.58) + 27.95(7.324)}{65.36} = 21.79 \; ksi$$ Entire section F_a = min (23.40, 21.79, 22.46, 21.79) = 21.79 ksi
Procedure II - WASA2	Tension F_a = 23.29+0.25(21.71 – 23.29) = 22.90 < min{1.25(23.29), 21.71}? → No! $\therefore F_a$ = 21.71 ksi (due to the second safeguard) Compression F_a = 21.71 ksi (due to the second safeguard) Entire section F_a = 21.71 ksi
Procedure II - TMCA	Tension F_a = 21.79 ksi (due to the second safeguard) Compression F_a = 21.79 ksi (due to the second safeguard) Entire section F_a = 21.79 ksi

Table 6.5 Moment capacity based on the yield limit state stresses and TMCA

yield limit state stresses- TMCA	$F_{LS} = F_{ay} \, n_y$ Tension F_{LSt} = 23.40(1.65) = 38.61 ksi Compression F_{LSc} = 22.46(1.65) = 37.06 ksi Entire section F_{LS} = min (38.61, 37.06) = 37.06 ksi M_{LS} = 37.06(65.36) = 2422.2 in-k

Note: To obtain F_{LS}, F_{ay} in Table 6.4 is multiplied by the yield safety factor (1.65).

Table 6.6 Allowable moment capacity and varying safety factor on yield strength

	approaches	allowable moment capacity $\left(M_a = F_a S\right)$	safety factor on yield strength $\left(\tilde{n}_y = M_{LS}/M_a\right)$
current AA	AA-MMCA	19.49(65.36) = 1273.9 *in-k*	2422.2/1273.9 = 1.90
	AA-WASA	20.43(65.36) = 1335.3 *in-k*	2422.2/1335.3 = 1.81
proposed procedures	P1-WASA2	21.71(65.36) = 1419.0 *in-k*	2422.2/1419.0 = 1.71
	P1-TMCA	21.79(65.36) = 1424.2 *in-k*	2422.2/1424.2 = 1.70
	P2-WASA2	21.71(65.36) = 1419.0 *in-k*	2422.2/1419.0 = 1.71
	P2-TMCA	21.79(65.36) = 1424.2 *in-k*	2422.2/1424.2 = 1.70

Note: In actual design computations, it is not necessary to compute the safety factors. However, the safety factors are computed here just for comparison purposes.

6.2 *Computational Example (2)*

Given:

Cross section: Figure 6.1

Alloy-temper: 6063-T5 (test coupon diameter or thickness from 0.5 to 1.0 in.).

See the third alloy-temper combination in Table 2.4.

Required:

Allowable moment capacities and safety factors on yield strength

Solution:

All comments are the same as Computational Example (1). The following computations are based on the sequence of table numbers (Table 6.7 to Table 6.12).

Table 6.7 Geometrical and material properties

geometrical properties	material properties
$I_f = (10)(10.625^3 - 9.375^3)/12 = 312.91$ in^4 $I_w = (0.5)(9.375^3)/12 = 34.33$ in^4 $I = I_f + I_w = 347.24$ in^4 $S = I/(h/2) = 65.36$ in^3 $S_f = I_f/(h_c/2) = 62.58$ in^3 $S_w = I_w/(h_o/2) = 7.324$ in^3 $A_f = (10)(0.625) = 6.25$ in^2 $A_w = (0.5)(9.375)/2 = 2.344$ in^2 $b = (10 - 0.5)/2 = 4.75$ in $b/t_f = 4.75/0.625 = 7.6$ $h_o/t_w = 9.375/0.5 = 18.75$	$F_{tu} = 15$ *ksi* $F_{ty} = 21ksi$ $F_{cy} = 15$ *ksi* $E = 10100$ *ksi* (for compression)

Table 6.8 Buckling constants, shape factors, and slenderness limits (from Table 2.10)

flange	web
$B_p = 18.25$ $D_p = 0.0775$ $k_1 = 0.35$ $k_2 = 2.27$ $\alpha_u = 21/15 = 1.4$ ultimate limit state $S_1^u = \dfrac{18.25 - \frac{1.65}{1.95}(1.4)(15)}{5.1(0.0775)} = 1.22$ yield limit state $S_1^y = \dfrac{18.25 - 15}{5.1(0.0775)} = 8.22$ $S_2 = \dfrac{0.35(18.25)}{5.1(0.0775)} = 16.16$	$B_p = 26.37$ $D_p = 0.1650$ $k_1 = 0.5$ $k_2 = 2.04$ $\alpha_u = 1.25(21/15) + 0.2 = 1.95$ ultimate limit state $S_1^u = \dfrac{26.37 - \frac{1.65}{1.95}(1.95)(15)}{0.67(0.1650)} = 14.65$ yield limit state $S_1^y = \dfrac{26.37 - 1.3(15)}{0.67(0.1650)} = 62.14$ $S_2 = \dfrac{0.5(26.37)}{0.67(0.1650)} = 119.27$

Table 6.9 Allowable stress for component elements (from Table 2.10)

flange	web
For tension side, $F_{ay} = \dfrac{15}{1.65} = 9.09 \; ksi$ $F_{au} = \dfrac{(1.4)(15)}{1.95} = 10.77 \; ksi$ For compression side, since $b/t_f < S_1^y < S_2$, $F_{ay} = \dfrac{15}{1.65} = 9.09 \; ksi$ since $S_1^u < b/t_f < S_2$, $F_{au} = \dfrac{18.25 - (0.0775)(5.1)(7.6)}{1.65}$ $= 9.24 \; ksi$	For tension side, $F_{ay} = \dfrac{(1.3)(15)}{1.65} = 11.82 \; ksi$ $F_{au} = \dfrac{(1.95)(15)}{1.95} = 15 \; ksi$ For compression side, since $h_o/t_w < S_1^y < S_2$, $F_{ay} = \dfrac{(1.3)(15)}{1.65} = 11.82 \; ksi$ since $S_1^u < h_o/t_w < S_2$, $F_{au} = \dfrac{26.37 - (0.1650)(0.67)(18.75)}{1.65}$ $= 14.73 \; ksi$

Table 6.10 Member and governing allowable stresses (Table 2.7 and Table 2.10)

approaches	member allowable stress
AA-MMCA	F_a = min (9.09, 10.77, 9.09, 11.82, 15, 11.82) = 9.09 ksi
AA-WASA	Tension $$F_{ay} = \frac{9.09(6.25)+11.82(2.344)/3}{6.25+(2.344)/3} = 9.39\ ksi$$ $$F_{au} = \frac{10.77(6.25)+15(2.344)/3}{6.25+(2.344)/3} = 11.24\ ksi$$ Compression $$F_{ay} = \frac{9.09(6.25)+11.82(2.344)/3}{6.25+(2.344)/3} = 9.39\ ksi$$ Entire section F_a = min (9.39, 11.24, 9.39) = 9.39 ksi
Procedure I - WASA2	Tension $$F_{ay} = 9.39(10.625/10) = 9.98\ ksi$$ $$F_{au} = 11.24(10.625/10) = 11.94\ ksi$$ Compression $$F_{ay} = 9.39(10.625/10) = 9.98\ ksi$$ $$F_{au} = \frac{9.24(6.25)+14.73(2.344)/3}{6.25+(2.344)/3}\left(\frac{10.625}{10}\right) = 10.47\ ksi$$ Entire section F_a = min (9.98, 11.94, 9.98, 10.47) = 9.98 ksi
Procedure I - TMCA	Tension $$F_{ay} = \frac{9.09(62.58)+11.82(7.324)}{65.36} = 10.03\ ksi$$ $$F_{au} = \frac{10.77(62.58)+15(7.324)}{65.36} = 11.99\ ksi$$ Compression $$F_{ay} = \frac{9.09(62.58)+11.82(7.324)}{65.36} = 10.03\ ksi$$ $$F_{au} = \frac{9.24(62.58)+14.73(7.324)}{65.36} = 10.49\ ksi$$ Entire section F_a = min (10.03, 11.99, 10.03, 10.49) = 10.03 ksi

Table 6.10 (Continued)

Procedure II - WASA2	Tension F_a = 9.98+0.25(11.94 – 9.98) = 10.47 < min{1.25(9.98), 11.94} Compression F_a = 9.98+0.25(10.47 – 9.98) = 10.10 < min{1.25(9.98), 10.47} Entire section F_a = min(10.47, 10.10) = 10.10 *ksi*
Procedure II - TMCA	Tension F_a = 10.03+0.25(11.99 – 10.03) = 10.52 < min{1.25(10.03), 11.99} Compression F_a = 10.03+0.25(10.49 – 10.03) = 10.15 < min{1.25(10.03), 10.49} Entire section F_a = min(10.52, 10.15) = 10.15 *ksi*

Table 6.11 Moment capacity based on the yield limit state stresses and TMCA

yield limit state stresses- TMCA	$F_{LS} = F_{ay} n_y$ Tension F_{LSt} = 10.03(1.65) = 16.55 *ksi* Compression F_{LSc} = 10.03(1.65) = 16.55 *ksi* Entire section F_{LS} = min (16.55, 16.55) = 16.55 *ksi* M_{LS} = 16.55(65.36) = 1081.7 *in-k*

Note: F_{ay} from [Procedure I –TMCA] in Table 6.10 is multiplied by the safety factor on yield strength.

Table 6.12 Allowable moment capacity and varying safety factor on yield strength

	approaches	allowable moment capacity $(M_a = F_a S)$	safety factor on yield strength $(\tilde{n}_y = M_{LS}/M_a)$
current AA	AA-MMCA	9.09(65.36) = 594.1 *in-k*	1081.7/594.1 = 1.82
	AA-WASA	9.39(65.36) = 613.7 *in-k*	1081.7/613.7 = 1.76
proposed procedures	P1-WASA2	9.98(65.36) = 652.3 *in-k*	1081.7/652.3 = 1.66
	P1-TMCA	10.03(65.36) = 655.6 *in-k*	1081.7/655.6 = 1.65
	P2-WASA2	10.10(65.36) = 660.1 *in-k*	1081.7/660.1 = 1.64
	P2-TMCA	10.15(65.36) = 663.4 *in-k*	1081.7/663.4 = 1.63

Note: In actual design computations, it is not necessary to compute the safety factors. However, the safety factors are computed here just for comparison purposes.

6.3 Computational Example (3)

The following examples provide step-by-step computations of the moment capacities using the approaches based on the AA *Specification* (2000a) and the Numerical Slenderness Approach. The results from these approaches without safety factors are compared to the finite element analysis results. The cross sectional geometry is given in Figure 6.2, which is one of the cross-sections used in the parametric study in Chapter 4.

Note: All dimensions are in inches and not to scale

Figure 6.2 Geometry of cross section for Example (3)

Given:

Cross section: Figure 6.2

Alloy-temper: 6061-T6. See the first alloy-temper combination in Table 2.4.

Required:

Allowable moment capacities

Solution:

In Table 6.13, the sectional properties are calculated for the cross-section given in Figure 6.2. The following computations are based on the sequence of table

numbers: from Table 6.13 to Table 6.16 for the AA *Specification* approach and from

Table 6.17 to Table 6.20 for the proposed approach.

Table 6.13 Geometrical and material properties

geometrical properties	material properties
I_{cf} = 4.390 in^4 (all compression flange group) I_{tf} = 4.932 in^4 (all tension flange group) I_f = 9.322 in^4 (all flange group) I_w = 1.628 in^4 (all web group) I = 10.950 in^4 (all) S = (10.950)/(2.5 + 0.309 + 0.125/2) =3.813 in^3 $M_y = F_y S$ = (35)(3.813) = 133.47 *in-k* b = (5 – 0.2343)/2 = 2.383 in b/t_f = 2.383/0.125 = 19.1 h_o = 5 – 0.125 = 4.875 in h_o/t_w = 4.875/0.0781 = 62.4 y_{NA} = 0.309	F_{tu} = 38 *ksi* F_{ty} = 35 *ksi* F_{cy} = 35 *ksi* E = 10100 *ksi* (for compression)

Table 6.14 Buckling constants, shape factors, and slenderness limits for AA (from Table 2.10)

flange	web
B_p = 45.04 D_p = 0.3008 k_1 = 0.35 k_2 = 2.27 α_u = 38/35 = 1.0857 ultimate limit state $S_1^u = \dfrac{45.04 - \frac{1.65}{1.95}(1.0857)(35)}{5.1(0.3008)} = 8.40$ yield limit state $S_1^y = \dfrac{45.04 - 35}{5.1(0.3008)} = 6.54$ $S_2 = \dfrac{0.35(45.04)}{5.1(0.3008)} = 10.28$	B_{br} = 66.76 D_{br} = 0.6648 k_1 = 0.5 k_2 = 2.04 a = 14x38/35+13 = 28.2: from Equation (52) m = 3: from Equation (53) y_{NA}/h = 0.309/(5-0.125) = 0.0634 α_{wo} = 1.25x38/35 + 0.2 = 1.557 α_u = (28.2)(0.0634)(0.5-0.0634)^3 + 1.557 = 1.706 ultimate limit state $S_1^u = \dfrac{66.76 - \frac{1.65}{1.95}(1.706)(35)}{0.67(0.6648)} = 36.45$ yield limit state $S_1^y = \dfrac{66.76 - 1.3(35)}{0.67(0.6648)} = 47.73$ $S_2 = \dfrac{0.5(66.76)}{0.67(0.6648)} = 74.94$

Note: B_p, D_p, B_{br}, D_{br}, k_1, and k_2 are obtained from AA (2000a)

Table 6.15 Allowable stresses for component elements (from Table 2.10)

flange	web
For tension side, $F_{ay} = \dfrac{35}{1.65} = 21.21 \, ksi$ $F_{au} = \dfrac{(1.0857)(35)}{1.95} = 19.49 \, ksi$ For compression side, since $b/t_f > S_2$, $F_{au} = F_{ay} = \dfrac{2.27\sqrt{(45.04)(10100)}}{1.65(5.1)(19.06)}$ $= 9.55 \, ksi$	For tension side, $F_{ay} = \dfrac{(1.3)(35)}{1.65} = 27.58 \, ksi$ $F_{au} = \dfrac{(1.706)(35)}{1.95} = 30.62 \, ksi$ For compression side, since $S_1^u < S_1^y < h_o/t_w < S_2$, $F_{au} = F_{ay} = \dfrac{66.76 - (0.6648)(0.67)(62.4)}{1.65}$ $= 23.62 \, ksi$

Table 6.16 Member and governing allowable moments (from Table 2.7 and Table 2.9)

approaches	member allowable moment
AA-MMCA	tension flange $M_{ay} = \dfrac{21.21(10.950)}{2.5 + 0.309 + 0.125/2} = 80.88 \, in\text{-}k$ $M_{au} = \dfrac{19.49(10.950)}{2.5 + 0.309 + 0.125/2} = 74.32 \, in\text{-}k$ compression flange $M_{ay} = \dfrac{9.55(10.950)}{2.5 - 0.309} = 47.73 \, in\text{-}k$ compression stiffeners (it is assumed that they reach the maximum) $M_{ay} = \dfrac{21.21(10.950)}{2.5 - 0.309 + 0.125/2 + 0.5} = 84.35 \, in\text{-}k$ tension web $M_{ay} = \dfrac{27.58(10.950)}{2.5 + 0.309 - 0.125/2} = 110.0 \, in\text{-}k$ $M_{au} = \dfrac{30.62(10.950)}{2.5 + 0.309 - 0.125/2} = 122.1 \, in\text{-}k$ compression web $M_{ay} = \dfrac{23.62(10.950)}{2.5 - 0.309 - 0.125/2} = 121.5 \, in\text{-}k$ $M_a = \min(80.88, 74.32, 47.73, 84.35, 110.0, 122.1, 121.5)$ $\quad = 47.73 \, in\text{-}k$
AA-WASA	Not appropriate

Table 6.17 Buckling constants, shape factors, and slenderness limits for NSA (from Table 4.8)

Flange group	Web group
B_p, D_p, k_1, k_2, α_u are the same as those for AA in Table 6.14.	B_{br}, D_{br}, k_1, k_2, α_u are the same as those for AA in Table 6.14.
ultimate limit state	ultimate limit state
$S_1^u = \dfrac{45.04 - \frac{1.65}{1.95}(1.0857)(35)}{0.3008} = 42.84$	$S_1^u = \dfrac{66.76 - \frac{1.65}{1.95}(1.706)(35)}{(0.6648)} = 24.42$
yield limit state	yield limit state
$S_1^y = \dfrac{45.04 - 35}{(0.3008)} = 33.38$	$S_1^y = \dfrac{66.76 - 1.3(35)}{(0.6648)} = 31.98$
$S_2 = \dfrac{0.35(45.04)}{(0.3008)} = 52.41$	$S_2 = \dfrac{0.5(66.76)}{(0.6648)} = 50.21$

Note: B_p, D_p, B_{br}, D_{br}, k_1, and k_2 are obtained from AA (2000a)

(11, 1.02)
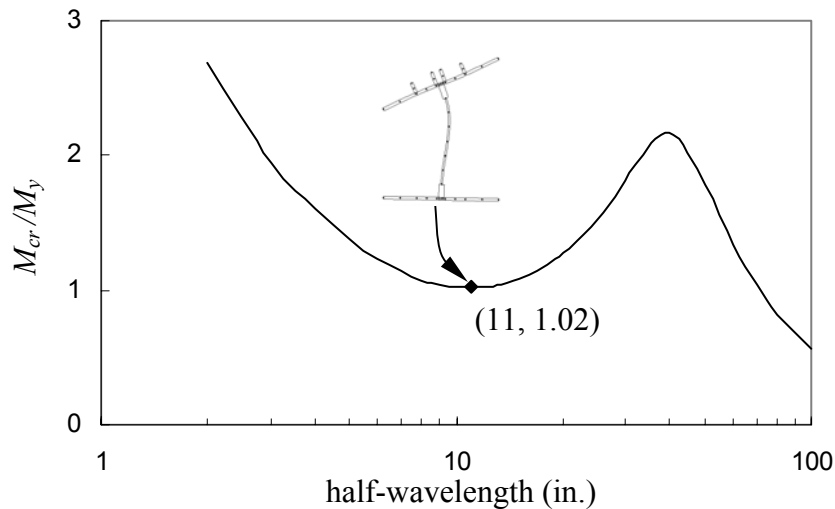
Figure 6.3 CUFSM analysis results finding minimum local bukling stress

From the CUFSM analysis results shown in Figure 6.3, the minimum buckling stress is $F_{cr} = 1.02 F_y = 35.7$ *ksi*. Thus, from Equation (47), $\lambda_p = \pi\sqrt{E/F_{cr}} = \pi\sqrt{10100/35.7}$ = 52.8. This is the equivalent slenderness ratio used in the NSA, which is the same for all elements.

Table 6.18 Allowable stresses for component elements (from Table 4.8)

flange group	web group
For tension side, $F_{ay} = \dfrac{35}{1.65} = 21.21 \, ksi$ $F_{au} = \dfrac{(1.0857)(35)}{1.95} = 19.49 \, ksi$ For compression side, since $\lambda_p > S_2$, $F_{au} =$ $F_{ay} = \dfrac{2.27\sqrt{(45.04)(10100)}}{1.65(52.8)} = 17.57 \, ksi$	For tension side, $F_{ay} = \dfrac{(1.3)(35)}{1.65} = 27.58 \, ksi$ $F_{au} = \dfrac{(1.706)(35)}{1.95} = 30.62 \, ksi$ For compression side, since $\lambda_p > S_2$, $F_{au} =$ $F_{ay} = \dfrac{2.04\sqrt{(66.76)(10100)}}{1.65(52.8)} = 19.20 \, ksi$

Table 6.19 Member and governing allowable moments (Table 2.7 and Table 2.9)

NSA-TMCA-Procedure I	Flange group tension flange $M_{ay} = \dfrac{21.21(9.322)}{2.5 + 0.309 + 0.125/2} = 68.86 \, in\text{-}k$ $M_{au} = \dfrac{19.49(9.322)}{2.5 + 0.309 + 0.125/2} = 63.27 \, in\text{-}k$ compression flange $M_{ay} = M_{au} = \dfrac{17.57(9.322)}{2.5 - 0.309} = 74.75 \, in\text{-}k$ compression stiffeners (it is assumed that they reach the maximum) $M_{ay} = \dfrac{21.21(9.322)}{2.5 - 0.309 + 0.125/2 + 0.5} = 71.81 \, in\text{-}k$ $M_{au} = \dfrac{19.49(9.322)}{2.5 - 0.309 + 0.125/2 + 0.5} = 65.98 \, in\text{-}k$ $M_f = \min(68.86, 63.27, 74.75, 71.81, 65.98) = 63.27 \, in\text{-}k$ Web group tension web $M_{ay} = \dfrac{27.58(1.628)}{2.5 + 0.309 - 0.125/2} = 16.35 \, in\text{-}k$ $M_{au} = \dfrac{30.62(1.628)}{2.5 + 0.309 - 0.125/2} = 18.15 \, in\text{-}k$ compression web $M_{ay} = M_{au} = \dfrac{19.20(1.628)}{2.5 - 0.309 - 0.125/2} = 14.69 \, in\text{-}k$ $M_w = \min(16.35, 18.15, 14.69) = 14.69 \, in\text{-}k$ Entire section $M_a = M_f + M_w = 63.27 + 14.69 = 77.96 \, in\text{-}k$

Table 6.19 (Continued)

NSA-TMCA-Procedure II	Flange group M_{ay} = min(68.86, 74.75, 71.81) = 68.86 *in-k* M_{au} = min(63.27, 74.75, 65.98) = 63.27 *in-k* M_f = 63.27 *in-k* (due to a safeguard of Procedure II) Web group M_{ay} = min(16.35, 14.69) = 14.69 *in-k* M_{au} = min(18.15, 14.69) = 14.69 *in-k* M_w = 14.69 *in-k* Entire section $M_a = M_f + M_w$ = 63.27 + 14.69 = 77.96 *ksi* (same as Procedure I)
NSA-TMCA2-Procedure I	All computations should be done without yield safety factor (1.65). Stress values computed here are based on the yield limit state Flange group F_{cf} = 1.65(17.57) = 28.99 ksi From Ramberg-Osgood equation with ε_u = 8% assumption ε_{cf} = 28.99/10100+0.002(28.99/35)$^{44.27}$ = 0.00287 From similar triangles, ε_{tf} = 0.00287(2.5+0.309+0.125/2)/(2.5-0.309)=0.00376 By monotonically increasing trial values of stress using Ramberg-Osgood equation, 0.00376 ≅ 33.8/10100+0.002(33.8/35)$^{44.27}$ F_{tf} = 33.8 ksi Web group F_{cw} = (19.2)1.65 = 31.68 ksi Element moment capacities M_{cf} = (28.99)(4.390)/(2.5-0.309) = 58.09 *in-k* M_{tf} = (33.8)(4.932)/(2.5+0.309+0.125/2) = 58.05 *in-k* M_{cw} = (31.68)(1.628)/(2.5-0.309-0.125/2) = 24.23 *in-k* M_{tw} = (27.58x1.65)(1.628)/(2.5+0.309-0.125/2) = 26.97 *in-k* M_w = min(24.23, 26.97) = 24.23 *in-k* Entire section $M_u = M_{cf} + M_{tf} + M_w$ = 58.09 + 58.05 + 24.23 = 140.37 *in-k*

Table 6.20 Comparison of computed moment capacities

	approaches	allowable moment capacity (M_a)	moment capacity without safety factor (M_u)
current AA	AA-MMCA	47.73 *in-k*	47.73x1.65 = 78.75 *in-k*
proposed procedures	P1-, P2-TMCA	77.96 *in-k*	77.96 x 1.65 = 128.63 *in-k*
	P1-TMCA2	140.37/1.65 = 85.07 *in-k*	140.37 *in-k*
	FEM		1.06(133.47) = 141.5 *in-k*

6.4 Dimensions and Moment Capacities of Parametric Study Sections

The tables and figures in this section provide detailed dimensions and analysis results of the cross-sections used in the parametric studies in this report.
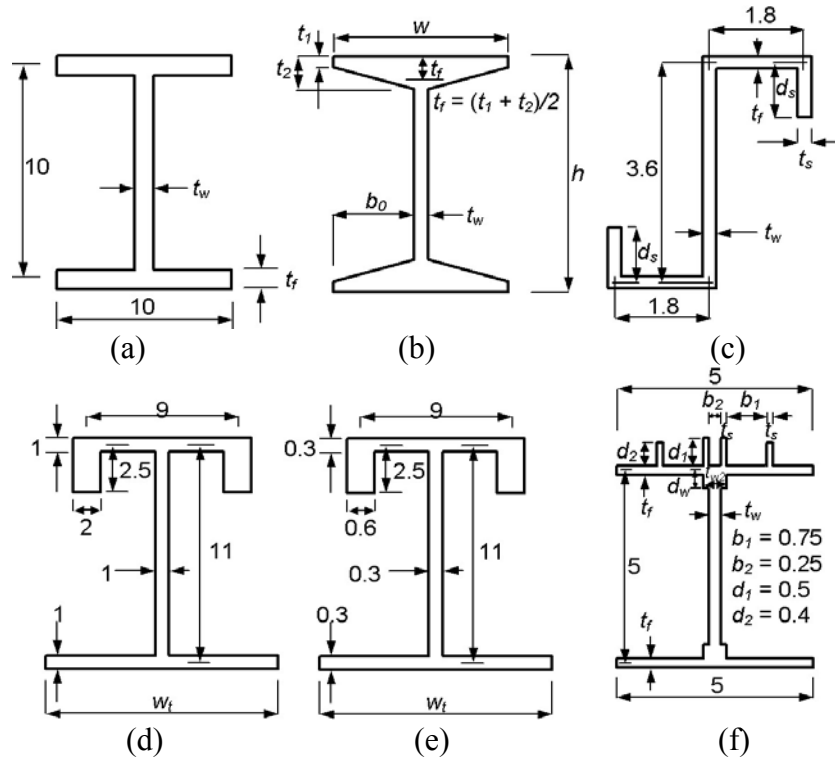
Note: All dimensions are in inches and not to scale.

Figure 6.4 Cross-sections used in the parametric study

Table 6.21 I-sections with uniform thickness for Figure 4.15a (Figure 6.4a)

t_w	t_f	$\dfrac{M_{NSA-U-WASA2}}{M_y}$	$\dfrac{M_{NSA-U-TMCA}}{M_y}$	t_w	t_f	$\dfrac{M_{NSA-U-WASA2}}{M_y}$	$\dfrac{M_{NSA-U-TMCA}}{M_y}$
25.4	42.3	1.309	1.316	8.46	42.3	1.282	1.284
25.4	31.8	1.277	1.285	8.46	31.8	1.241	1.244
25.4	21.2	1.249	1.259	8.46	21.2	1.164	1.167
25.4	15.9	1.213	1.224	8.46	15.9	1.075	1.079
25.4	12.7	1.156	1.167	8.46	12.7	1.002	1.005
12.7	42.3	1.289	1.292	6.35	42.3	1.278	1.280
12.7	31.8	1.251	1.255	6.35	31.8	1.236	1.238
12.7	21.2	1.194	1.199	6.35	21.2	1.150	1.152
12.7	15.9	1.119	1.125	6.35	15.9	1.053	1.056
12.7	12.7	1.059	1.065	6.35	12.7	0.971	0.974

Note: The moment capacities obtained by $M_{AA-Y-MMCA}$, $M_{AA-Y-WASA}$, $M_{AA-U-WASA2}$, and $M_{AA-U-TMCA}$ are given in Table 2.8. All dimensions are in mm.

Table 6.22 I-sections with tapered thickness for Figure 3.10 (Figure 6.4b)

(a) Series 1

Designation	h	w	t_f (mean)	t_w	$\frac{(t_2-t_1)}{b_0}$	$\frac{M_{UNI\text{-}Y\text{-}MMCA}}{M_y}$	$\frac{M_{UNI\text{-}Y\text{-}WASA}}{M_y}$	$\frac{M_{TAP\text{-}U\text{-}WASA2}}{M_y}$	$\frac{M_{TAP\text{-}U\text{-}TMCA}}{M_y}$	$\frac{M_{FEM}}{M_y}$	$\lambda = \sqrt{\frac{F_y}{F_{cr}}}$
WF2x1.43	2.0	2.00	0.232	0.188	1/11.4	1.000	1.027	1.280	1.289	1.286	0.293
WF2.5x1.8	2.5	2.00	0.247	0.250	1/7.00	1.000	1.040	1.282	1.296	1.323	0.259
WF4x4.76	4.0	4.00	0.370	0.313	1/11.3	1.000	1.029	1.249	1.257	1.249	0.364
WF5x6.49	5.0	5.00	0.415	0.313	1/13.6	1.000	1.027	1.203	1.209	1.217	0.422
WF6x7.85	6.0	5.93	0.451	0.250	1/15.6	1.000	1.021	1.153	1.157	1.176	0.496
WF6x8.30	6.0	6.00	0.451	0.313	1/15.6	1.000	1.026	1.162	1.167	1.184	0.478
WF6x9.18	6.0	6.13	0.451	0.438	1/15.6	1.000	1.034	1.178	1.185	1.208	0.446
WF8x11.2	8.0	7.94	0.458	0.313	1/18.9	0.922	0.956	1.063	1.066	1.121	0.629
WF8x11.8	8.0	8.00	0.458	0.375	1/18.9	0.922	0.961	1.073	1.077	1.131	0.606
WF8x13.0	8.0	8.13	0.458	0.500	1/18.9	0.922	0.972	1.091	1.096	1.143	0.567
I3x1.96	3.0	2.33	0.257	0.170	1/18.9	1.000	1.029	1.245	1.254	1.268	0.315
I3x2.25	3.0	2.41	0.257	0.251	1/6.00	1.000	1.039	1.265	1.277	1.303	0.297
I3x2.59	3.0	2.51	0.257	0.349	1/6.00	1.000	1.050	1.284	1.301	1.333	0.284
I4x2.64	4.0	2.66	0.289	0.190	1/6.00	1.000	1.034	1.235	1.245	1.271	0.325
I4x3.28	4.0	2.80	0.289	0.326	1/6.00	1.000	1.052	1.266	1.282	1.322	0.298
I5x3.43	5.0	3.00	0.323	0.210	1/6.00	1.000	1.038	1.231	1.240	1.250	0.333
I5x4.23	5.0	3.14	0.323	0.347	1/6.00	1.000	1.055	1.261	1.277	1.314	0.305
I5x5.10	5.0	3.28	0.323	0.494	1/6.00	1.000	1.070	1.287	1.308	1.344	0.290
I6x4.30	6.0	3.33	0.355	0.230	1/6.00	1.000	1.041	1.229	1.238	1.243	0.339
I6x5.10	6.0	4.44	0.355	0.343	1/6.00	1.000	1.044	1.237	1.249	1.250	0.386
I6x5.96	6.0	3.57	0.355	0.465	1/6.00	1.000	1.068	1.276	1.294	1.331	0.299
I7x5.27	7.0	3.66	0.389	0.250	1/6.00	1.000	1.044	1.227	1.237	1.235	0.344
I7x6.05	7.0	3.76	0.389	0.345	1/6.00	1.000	1.055	1.248	1.261	1.289	0.325
I7x6.92	7.0	3.86	0.389	0.450	1/6.00	1.000	1.066	1.267	1.284	1.332	0.306
I8x6.35	8.0	4.00	0.421	0.270	1/6.00	1.000	1.045	1.227	1.236	1.235	0.351
I8x7.96	8.0	4.17	0.421	0.441	1/6.00	1.000	1.065	1.260	1.275	1.326	0.316
I8x8.81	8.0	4.26	0.421	0.532	1/6.00	1.000	1.073	1.275	1.293	1.328	0.305
I9x7.51	9.0	4.33	0.453	0.290	1/6.00	1.000	1.047	1.226	1.236	1.211	0.356
I10x8.76	10	4.66	0.487	0.310	1/6.00	1.000	1.048	1.225	1.235	1.228	0.360
I10x10.4	10	4.80	0.487	0.447	1/6.00	1.000	1.063	1.251	1.265	1.293	0.332
I10x12.1	10	4.94	0.487	0.594	1/6.00	1.000	1.076	1.274	1.292	1.328	0.309
I12x11.0	12	5.00	0.538	0.350	1/6.00	1.000	1.055	1.225	1.235	1.217	0.364
I12x12.1	12	5.08	0.538	0.428	1/6.00	1.000	1.063	1.245	1.258	1.236	0.345
I12x14.1	12	5.25	0.653	0.460	1/6.00	1.000	1.055	1.244	1.256	1.243	0.306
I12x15.6	12	5.36	0.653	0.565	1/6.00	1.000	1.064	1.259	1.273	1.301	0.291
I12x17.3	12	5.48	0.653	0.687	1/6.00	1.000	1.072	1.274	1.291	1.349	0.275

Note: 1. The designations given here represent the original ones in AA (2000b).

2. All dimensions are in inches.

Table 6.22 (Continued)
(b) Series 2 (60% thickness reduction)

Desig-nation	h	w	t_f (mean)	t_w	$\dfrac{(t_2-t_1)}{b_0}$	$\dfrac{M_{\text{UNI-Y-MMCA}}}{M_y}$	$\dfrac{M_{\text{UNI-Y-WASA}}}{M_y}$	$\dfrac{M_{\text{TAP-U-WASA2}}}{M_y}$	$\dfrac{M_{\text{TAP-U-TMCA}}}{M_y}$	$\dfrac{M_{\text{FEM}}}{M_y}$	$\lambda = \sqrt{\dfrac{F_y}{F_{cr}}}$
WF2x1.43	2.0	2.00	0.093	0.075	1/28.50	0.827	0.878	0.977	0.979	1.066	0.761
WF2.5x1.8	2.5	2.00	0.099	0.100	1/17.50	0.865	0.934	1.049	1.053	1.122	0.666
WF4x4.76	4.0	4.00	0.148	0.125	1/28.25	0.655	0.728	0.831	0.831	0.958	0.937
WF5x6.49	5.0	5.00	0.166	0.125	1/34.00	0.584	0.658	0.734	0.733	0.869	1.083
WF6x7.85	6.0	5.93	0.180	0.100	1/39.00	0.531	0.584	0.635	0.635	0.765	1.269
WF6x8.30	6.0	6.00	0.180	0.125	1/39.00	0.527	0.601	0.657	0.657	0.788	1.225
WF6x9.18	6.0	6.13	0.180	0.175	1/39.00	0.520	0.619	0.697	0.696	0.842	1.142
WF8x11.2	8.0	7.94	0.183	0.125	1/47.25	0.402	0.474	0.513	0.512	0.636	1.601
WF8x11.8	8.0	8.00	0.183	0.150	1/47.25	0.400	0.499	0.538	0.537	0.665	1.542
WF8x13.0	8.0	8.13	0.183	0.200	1/47.25	0.396	0.526	0.584	0.582	0.699	1.441
I3x1.96	3.0	2.33	0.103	0.068	1/15.00	0.780	0.838	0.965	0.968	1.036	0.807
I3x2.25	3.0	2.41	0.103	0.100	1/15.00	0.764	0.846	1.007	1.010	1.070	0.759
I3x2.59	3.0	2.51	0.103	0.140	1/15.00	0.744	0.852	1.029	1.034	1.086	0.721
I4x2.64	4.0	2.66	0.116	0.076	1/15.00	0.767	0.836	0.950	0.954	1.025	0.830
I4x3.28	4.0	2.80	0.116	0.130	1/15.00	0.743	0.852	1.022	1.026	1.075	0.756
I5x3.43	5.0	3.00	0.129	0.084	1/15.00	0.760	0.823	0.937	0.941	1.018	0.848
I5x4.23	5.0	3.14	0.129	0.139	1/15.00	0.739	0.854	1.011	1.016	1.068	0.773
I5x5.10	5.0	3.28	0.129	0.198	1/15.00	0.719	0.870	1.060	1.066	1.104	0.730
I6x4.30	6.0	3.33	0.142	0.092	1/15.00	0.752	0.810	0.924	0.928	1.004	0.865
I6x5.10	6.0	4.44	0.142	0.137	1/15.00	0.566	0.688	0.875	0.877	0.941	0.975
I6x5.96	6.0	3.57	0.142	0.186	1/15.00	0.720	0.866	1.043	1.048	1.088	0.754
I7x5.27	7.0	3.66	0.156	0.100	1/15.00	0.750	0.801	0.914	0.918	0.987	0.878
I7x6.05	7.0	3.76	0.156	0.138	1/15.00	0.737	0.851	0.967	0.971	1.038	0.825
I7x6.92	7.0	3.86	0.156	0.180	1/15.00	0.725	0.865	1.017	1.022	1.075	0.774
I8x6.35	8.0	4.00	0.168	0.108	1/15.00	0.742	0.788	0.903	0.907	0.988	0.895
I8x7.96	8.0	4.17	0.168	0.176	1/15.00	0.723	0.860	0.992	0.997	1.059	0.801
I8x8.81	8.0	4.26	0.168	0.213	1/15.00	0.714	0.871	1.031	1.036	1.088	0.768
I9x7.51	9.0	4.33	0.181	0.116	1/15.00	0.738	0.778	0.893	0.898	0.975	0.910
I10x8.76	10	4.66	0.195	0.124	1/15.00	0.737	0.772	0.886	0.891	0.965	0.921
I10x10.4	10	4.80	0.195	0.179	1/15.00	0.723	0.840	0.956	0.961	1.032	0.843
I10x12.1	10	4.94	0.195	0.238	1/15.00	0.711	0.873	1.018	1.023	1.080	0.780
I12x11.0	12	5.00	0.215	0.140	1/15.00	0.760	0.783	0.882	0.887	0.963	0.935
I12x12.1	12	5.08	0.215	0.171	1/15.00	0.752	0.822	0.922	0.928	1.007	0.881
I12x14.1	12	5.25	0.261	0.184	1/15.00	0.862	0.915	0.975	0.981	1.063	0.786
I12x15.6	12	5.36	0.261	0.226	1/15.00	0.856	0.952	1.013	1.019	1.102	0.743
I12x17.3	12	5.48	0.261	0.275	1/15.00	0.850	0.968	1.052	1.058	1.140	0.700

Note: 1. The designations given here are from AA (2000b). However, the thickness of all component elements of Series 2 sections is reduced by 60% from the original ones.

2. All dimensions are in inches

Table 6.23 I-sections with tapered thickness for Figure 4.15b (Figure 6.4b)

(a) Series 1

Desig-nation	h	w	t_f (mean)	t_w	$\dfrac{(t_2-t_1)}{b_0}$	$\dfrac{M_{NSA-U-WASA2}}{M_y}$	$\dfrac{M_{NSA-U-TMCA}}{M_y}$	$\dfrac{M_{FEM}}{M_y}$	$\lambda = \sqrt{\dfrac{F_y}{F_{cr}}}$
WF2x1.43	2.0	2.00	0.232	0.188	1/11.4	1.280	1.289	1.286	0.293
WF2.5x1.8	2.5	2.00	0.247	0.250	1/7.00	1.282	1.296	1.323	0.259
WF4x4.76	4.0	4.00	0.370	0.313	1/11.3	1.249	1.258	1.249	0.364
WF5x6.49	5.0	5.00	0.415	0.313	1/13.6	1.226	1.234	1.217	0.422
WF6x7.85	6.0	5.93	0.451	0.250	1/15.6	1.174	1.180	1.176	0.496
WF6x8.30	6.0	6.00	0.451	0.313	1/15.6	1.190	1.197	1.184	0.478
WF6x9.18	6.0	6.13	0.451	0.438	1/15.6	1.219	1.228	1.208	0.446
WF8x11.2	8.0	7.94	0.458	0.313	1/18.9	1.087	1.092	1.121	0.629
WF8x11.8	8.0	8.00	0.458	0.375	1/18.9	1.104	1.110	1.131	0.606
WF8x13.0	8.0	8.13	0.458	0.500	1/18.9	1.134	1.143	1.143	0.567
I3x1.96	3.0	2.33	0.257	0.170	1/18.9	1.245	1.254	1.268	0.315
I3x2.25	3.0	2.41	0.257	0.251	1/6.00	1.265	1.277	1.303	0.297
I3x2.59	3.0	2.51	0.257	0.349	1/6.00	1.284	1.301	1.333	0.284
I4x2.64	4.0	2.66	0.289	0.190	1/6.00	1.235	1.245	1.271	0.325
I4x3.28	4.0	2.80	0.289	0.326	1/6.00	1.266	1.282	1.322	0.298
I5x3.43	5.0	3.00	0.323	0.210	1/6.00	1.231	1.240	1.250	0.333
I5x4.23	5.0	3.14	0.323	0.347	1/6.00	1.261	1.277	1.314	0.305
I5x5.10	5.0	3.28	0.323	0.494	1/6.00	1.287	1.308	1.344	0.290
I6x4.30	6.0	3.33	0.355	0.230	1/6.00	1.229	1.238	1.243	0.339
I6x5.10	6.0	4.44	0.355	0.343	1/6.00	1.231	1.243	1.250	0.386
I6x5.96	6.0	3.57	0.355	0.465	1/6.00	1.276	1.294	1.331	0.299
I7x5.27	7.0	3.66	0.389	0.250	1/6.00	1.227	1.237	1.235	0.344
I7x6.05	7.0	3.76	0.389	0.345	1/6.00	1.248	1.261	1.289	0.325
I7x6.92	7.0	3.86	0.389	0.450	1/6.00	1.267	1.284	1.332	0.306
I8x6.35	8.0	4.00	0.421	0.270	1/6.00	1.226	1.236	1.235	0.351
I8x7.96	8.0	4.17	0.421	0.441	1/6.00	1.260	1.275	1.326	0.316
I8x8.81	8.0	4.26	0.421	0.532	1/6.00	1.275	1.293	1.328	0.305
I9x7.51	9.0	4.33	0.453	0.290	1/6.00	1.224	1.234	1.211	0.356
I10x8.76	10	4.66	0.487	0.310	1/6.00	1.224	1.234	1.228	0.360
I10x10.4	10	4.80	0.487	0.447	1/6.00	1.251	1.265	1.293	0.332
I10x12.1	10	4.94	0.487	0.594	1/6.00	1.274	1.292	1.328	0.309
I12x11.0	12	5.00	0.538	0.350	1/6.00	1.227	1.238	1.217	0.364
I12x12.1	12	5.08	0.538	0.428	1/6.00	1.245	1.258	1.236	0.345
I12x14.1	12	5.25	0.653	0.460	1/6.00	1.244	1.256	1.243	0.306
I12x15.6	12	5.36	0.653	0.565	1/6.00	1.259	1.273	1.301	0.291
I12x17.3	12	5.48	0.653	0.687	1/6.00	1.274	1.291	1.349	0.275

Note: 1. The designations given here represent the original ones in AA (2000b).

2. All dimensions are in inches.

Table 6.23 (Continued)
(b) Series 2 (60% thickness reduction)

Desig-nation	h	w	t_f (mean)	t_w	$\frac{(t_2-t_1)}{b_0}$	$\frac{M_{NSA-U-WASA2}}{M_y}$	$\frac{M_{NSA-U-TMCA}}{M_y}$	$\frac{M_{FEM}}{M_y}$	$\lambda = \sqrt{\frac{F_y}{F_{cr}}}$
WF2x1.43	2.0	2.00	0.093	0.075	1/28.50	1.007	1.012	1.066	0.761
WF2.5x1.8	2.5	2.00	0.099	0.100	1/17.50	1.065	1.073	1.122	0.666
WF4x4.76	4.0	4.00	0.148	0.125	1/28.25	0.903	0.907	0.958	0.937
WF5x6.49	5.0	5.00	0.166	0.125	1/34.00	0.791	0.794	0.869	1.083
WF6x7.85	6.0	5.93	0.180	0.100	1/39.00	0.671	0.673	0.765	1.269
WF6x8.30	6.0	6.00	0.180	0.125	1/39.00	0.697	0.699	0.788	1.225
WF6x9.18	6.0	6.13	0.180	0.175	1/39.00	0.750	0.753	0.842	1.142
WF8x11.2	8.0	7.94	0.183	0.125	1/47.25	0.529	0.531	0.636	1.601
WF8x11.8	8.0	8.00	0.183	0.150	1/47.25	0.550	0.552	0.665	1.542
WF8x13.0	8.0	8.13	0.183	0.200	1/47.25	0.590	0.593	0.699	1.441
I3x1.96	3.0	2.33	0.103	0.068	1/15.00	0.972	0.977	1.036	0.807
I3x2.25	3.0	2.41	0.103	0.100	1/15.00	1.006	1.013	1.070	0.759
I3x2.59	3.0	2.51	0.103	0.140	1/15.00	1.037	1.047	1.086	0.721
I4x2.64	4.0	2.66	0.116	0.076	1/15.00	0.957	0.962	1.025	0.830
I4x3.28	4.0	2.80	0.116	0.130	1/15.00	1.011	1.019	1.075	0.756
I5x3.43	5.0	3.00	0.129	0.084	1/15.00	0.945	0.950	1.018	0.848
I5x4.23	5.0	3.14	0.129	0.139	1/15.00	1.000	1.007	1.068	0.773
I5x5.10	5.0	3.28	0.129	0.198	1/15.00	1.037	1.047	1.104	0.730
I6x4.30	6.0	3.33	0.142	0.092	1/15.00	0.935	0.940	1.004	0.865
I6x5.10	6.0	4.44	0.142	0.137	1/15.00	0.876	0.882	0.941	0.975
I6x5.96	6.0	3.57	0.142	0.186	1/15.00	1.018	1.027	1.088	0.754
I7x5.27	7.0	3.66	0.156	0.100	1/15.00	0.927	0.932	0.987	0.878
I7x6.05	7.0	3.76	0.156	0.138	1/15.00	0.965	0.971	1.038	0.825
I7x6.92	7.0	3.86	0.156	0.180	1/15.00	1.002	1.010	1.075	0.774
I8x6.35	8.0	4.00	0.168	0.108	1/15.00	0.917	0.922	0.988	0.895
I8x7.96	8.0	4.17	0.168	0.176	1/15.00	0.983	0.991	1.059	0.801
I8x8.81	8.0	4.26	0.168	0.213	1/15.00	1.009	1.018	1.088	0.768
I9x7.51	9.0	4.33	0.181	0.116	1/15.00	0.909	0.914	0.975	0.910
I10x8.76	10	4.66	0.195	0.124	1/15.00	0.903	0.907	0.965	0.921
I10x10.4	10	4.80	0.195	0.179	1/15.00	0.955	0.962	1.032	0.843
I10x12.1	10	4.94	0.195	0.238	1/15.00	1.002	1.010	1.080	0.780
I12x11.0	12	5.00	0.215	0.140	1/15.00	0.895	0.900	0.963	0.935
I12x12.1	12	5.08	0.215	0.171	1/15.00	0.930	0.936	1.007	0.881
I12x14.1	12	5.25	0.261	0.184	1/15.00	0.986	0.992	1.063	0.786
I12x15.6	12	5.36	0.261	0.226	1/15.00	1.017	1.024	1.102	0.743
I12x17.3	12	5.48	0.261	0.275	1/15.00	1.051	1.059	1.140	0.700

Note: 1. The designations given here are from AA (2000b). However, the thickness of all component elements of Series 2 sections is reduced by 60% from the original ones.

2. All dimensions are in inches

Table 6.24 Edge-stiffened Z-sections for Figure 4.15c (Figure 6.4c)

t_f	t_w	t_s	d_s	$\dfrac{M_{AA\text{-}Y\text{-}MMCA}}{M_y}$	$\dfrac{M_{AA\text{-}Y\text{-}WASA}}{M_y}$	$\dfrac{M_{NSA\text{-}U\text{-}WASA2}}{M_y}$	$\dfrac{M_{NSA\text{-}U\text{-}TMCA}}{M_y}$	$\dfrac{M_{FEM}}{M_y}$	$\lambda = \sqrt{\dfrac{F_y}{F_{cr}}}$
0.164	0.164	0.164	0.122	0.906	0.995	1.036	1.033	1.020	0.745
0.164	0.164	0.164	0.247	0.964	1.038	1.064	1.061	1.030	0.695
0.164	0.164	0.164	0.368	1.000	1.061	1.097	1.094	1.050	0.636
0.164	0.164	0.164	0.552	1.000	1.057	1.134	1.132	1.060	0.568
0.082	0.082	0.082	0.271	0.607	0.791	0.765	0.765	0.828	1.118
0.082	0.082	0.082	0.551	0.811	0.940	0.942	0.942	0.941	0.860
0.082	0.082	0.082	0.822	0.869	0.946	1.001	1.004	0.973	0.751
0.082	0.082	0.082	1.234	0.588	0.702	1.020	1.026	0.904	0.711
0.491	0.491	0.491	0.247	1.000	1.055	1.333	1.311	1.281	0.274
0.491	0.491	0.491	0.368	1.000	1.053	1.329	1.308	1.286	0.273
0.491	0.491	0.491	0.552	1.000	1.050	1.323	1.306	1.295	0.265
0.245	0.245	0.245	0.271	1.000	1.061	1.207	1.200	1.158	0.495
0.245	0.245	0.245	0.551	1.000	1.055	1.235	1.230	1.180	0.435
0.245	0.245	0.245	0.822	1.000	1.051	1.236	1.234	1.186	0.396
0.245	0.245	0.245	1.234	1.000	1.045	1.231	1.236	1.197	0.373
0.123	0.123	0.123	0.175	0.743	0.878	0.915	0.913	0.980	0.928
0.123	0.123	0.123	0.355	0.862	0.967	0.999	0.998	1.026	0.783
0.123	0.123	0.123	0.529	0.976	1.043	1.053	1.052	1.044	0.688
0.123	0.123	0.123	0.794	1.000	1.054	1.097	1.099	1.067	0.605
0.164	0.164	0.327	0.165	0.951	1.026	1.058	1.054	1.010	0.704
0.164	0.164	0.327	0.246	0.991	1.052	1.078	1.075	1.030	0.665
0.164	0.164	0.327	0.369	1.000	1.054	1.105	1.104	1.040	0.611
0.082	0.082	0.164	0.208	0.574	0.774	0.740	0.740	0.757	1.155
0.082	0.082	0.164	0.422	0.734	0.898	0.895	0.896	0.877	0.937
0.082	0.082	0.164	0.630	0.890	0.990	0.951	0.953	0.946	0.833
0.082	0.082	0.164	0.944	1.000	1.041	0.991	0.996	0.876	0.754
0.491	0.491	0.982	0.327	1.000	1.048	1.320	1.302	1.276	0.268
0.491	0.491	0.982	0.410	1.000	1.046	1.316	1.299	1.278	0.266
0.491	0.491	0.982	0.492	1.000	1.044	1.312	1.298	1.278	0.262
0.491	0.491	0.982	0.615	1.000	1.041	1.307	1.295	1.278	0.256
0.245	0.245	0.491	0.331	1.000	1.053	1.217	1.211	1.161	0.464
0.245	0.245	0.491	0.545	1.000	1.047	1.226	1.223	1.173	0.422
0.245	0.245	0.491	0.752	1.000	1.042	1.223	1.224	1.184	0.395
0.245	0.245	0.491	1.067	1.000	1.036	1.217	1.225	1.187	0.373
0.123	0.123	0.245	0.199	0.785	0.911	0.951	0.950	0.973	0.864
0.123	0.123	0.245	0.342	0.880	0.980	1.007	1.006	1.014	0.762
0.123	0.123	0.245	0.480	0.973	1.035	1.043	1.043	1.035	0.695
0.123	0.123	0.245	0.689	1.000	1.046	1.073	1.076	1.063	0.632

Note: All dimensions are in inches.

Table 6.25 Edge-stiffened unsymmetric sections for Figure 4.15d
(a) (Figure 6.4d)

w_t	y_{NA}	y_{EP}	y_{RO}	$\dfrac{M_{AA\text{-}Y\text{-}MMCA}}{M_y}$	$\dfrac{M_{NSA\text{-}U\text{-}TMCA}}{M_y}$	$\dfrac{M_{NSA\text{-}U\text{-}TMCA2}}{M_y}$	$\dfrac{M_{NSA\text{-}U\text{-}EPMC}}{M_y}$	$\dfrac{M_{NSA\text{-}U\text{-}ROMC}}{M_y}$	$\dfrac{M_{FEM}}{M_y}$	$\lambda = \sqrt{\dfrac{F_y}{F_{cr}}}$
17	-0.02	1.00	-0.07	1.007	1.155	1.194	1.189	1.277	1.264	0.299
16	0.10	1.50	0.32	1.000	1.152	1.211	1.200	1.291	1.286	0.293
15	0.23	2.00	0.70	1.000	1.157	1.238	1.220	1.313	1.317	0.285
14	0.36	2.50	1.07	1.000	1.163	1.267	1.238	1.336	1.347	0.277
13	0.50	2.78	1.43	1.000	1.169	1.297	1.255	1.360	1.382	0.269
12	0.65	2.97	1.78	1.000	1.176	1.330	1.272	1.385	1.411	0.261
11	0.80	3.13	2.10	1.000	1.184	1.365	1.291	1.410	1.454	0.252
10	0.96	3.26	2.41	1.000	1.193	1.403	1.312	1.438	1.489	0.243
9	1.13	3.38	2.70	1.000	1.203	1.444	1.336	1.468	1.501	0.234
8	1.31	3.50	2.96	1.000	1.215	1.489	1.365	1.502	1.544	0.224
7	1.50	3.60	3.20	1.000	1.229	1.540	1.398	1.541	1.592	0.214
6	1.70	3.70	3.42	1.000	1.247	1.598	1.438	1.588	1.648	0.203
5	1.91	3.80	3.62	1.000	1.269	1.664	1.488	1.645	1.696	0.192
4	2.14	3.90	3.79	1.000	1.297	1.744	1.550	1.718	1.756	0.180
3	2.38	4.00	3.95	1.000	1.336	1.842	1.632	1.815	1.846	0.167

(b) (Figure 6.4e)

w_t	y_{NA}	y_{EP}	y_{RO}	$\dfrac{M_{AA\text{-}Y\text{-}MMCA}}{M_y}$	$\dfrac{M_{NSA\text{-}U\text{-}TMCA}}{M_y}$	$\dfrac{M_{NSA\text{-}U\text{-}TMCA2}}{M_y}$	$\dfrac{M_{NSA\text{-}U\text{-}EPMC}}{M_y}$	$\dfrac{M_{NSA\text{-}U\text{-}ROMC}}{M_y}$	$\dfrac{M_{FEM}}{M_y}$	$\lambda = \sqrt{\dfrac{F_y}{F_{cr}}}$
16	0.09	0.17	0.25	1.000	1.069	1.044	1.027	1.055	1.078	0.668
15	0.21	0.63	0.61	1.000	1.120	1.081	1.058	1.095	1.109	0.651
14	0.34	1.07	0.98	1.000	1.131	1.121	1.087	1.135	1.139	0.634
13	0.48	2.78	1.35	1.000	1.145	1.165	1.188	1.174	1.168	0.615
12	0.62	2.97	1.80	1.000	1.161	1.214	1.206	1.215	1.200	0.598
11	0.78	3.13	2.28	1.000	1.175	1.263	1.224	1.258	1.230	0.578
10	0.93	3.26	2.66	1.000	1.183	1.308	1.245	1.299	1.262	0.559
9	1.10	3.38	2.95	1.000	1.193	1.357	1.269	1.341	1.296	0.539
8	1.27	3.50	3.19	1.000	1.204	1.411	1.296	1.386	1.334	0.518
7	1.46	3.60	3.16	1.000	1.218	1.471	1.328	1.420	1.376	0.496
6	1.65	3.70	3.38	1.000	1.234	1.536	1.366	1.459	1.424	0.472
5	1.86	3.80	3.57	1.000	1.253	1.596	1.412	1.507	1.483	0.447
4	2.08	3.90	3.75	1.000	1.279	1.667	1.469	1.566	1.550	0.420
3	2.31	4.00	3.91	1.000	1.312	1.754	1.543	1.643	1.614	0.391
2	2.56	4.10	4.04	1.000	1.358	1.864	1.643	1.749	1.713	0.359
1	2.82	4.20	4.16	1.000	1.426	2.013	1.787	1.903	1.848	0.325

Note: 1. y_{NA} = distance from neutral axis based on linear-elastic stress distribution to mid-depth.
y_{EP} = distance from neutral axis based on elasto-plastic stress distribution to mid-depth.
y_{RO} = distance from neutral axis based on Ramberg-Osgood stress distribution to mid-depth.
2. All dimensions are in inches.

Table 6.26 Dome-strut sections for Figure 4.15e and Figure 4.16 (Figure 6.4f)

(a) Series 1

$t_f = t_s$	t_w	t_{w2}	d_w	$\dfrac{M_{AA\text{-}Y\text{-}MMCA}}{M_y}$	$\dfrac{M_{NSA\text{-}Y\text{-}TMCA}}{M_y}$	$\dfrac{M_{NSA\text{-}U\text{-}TMCA}}{M_y}$	$\dfrac{M_{NSA\text{-}U\text{-}TMCA2}}{M_y}$	$\dfrac{M_{FEM}}{M_y}$	$\lambda = \sqrt{\dfrac{F_y}{F_{cr}}}$
0.500	0.313	0.313	0.000	1.000	1.035	1.142	1.357	1.417	0.326
0.333	0.208	0.208	0.000	1.000	1.032	1.134	1.325	1.346	0.465
0.250	0.156	0.156	0.000	1.000	1.031	1.129	1.243	1.280	0.607
0.200	0.125	0.125	0.000	0.961	1.030	1.112	1.167	1.210	0.746
0.167	0.104	0.104	0.000	0.791	1.029	1.095	1.105	1.124	0.882
0.143	0.089	0.089	0.000	0.672	1.018	1.079	1.038	1.054	1.015
0.125	0.078	0.078	0.000	0.585	0.971	0.971	0.957	1.015	1.144
0.111	0.069	0.069	0.000	0.517	0.872	0.872	0.871	0.983	1.270
0.100	0.063	0.063	0.000	0.464	0.793	0.793	0.793	0.956	1.393
0.091	0.057	0.057	0.000	0.420	0.728	0.728	0.728	0.929	1.512

(b) Series 2

$t_f = t_s$	t_w	t_{w2}	d_w	$\dfrac{M_{AA\text{-}Y\text{-}MMCA}}{M_y}$	$\dfrac{M_{NSA\text{-}Y\text{-}TMCA}}{M_y}$	$\dfrac{M_{NSA\text{-}U\text{-}TMCA}}{M_y}$	$\dfrac{M_{NSA\text{-}U\text{-}TMCA2}}{M_y}$	$\dfrac{M_{FEM}}{M_y}$	$\lambda = \sqrt{\dfrac{F_y}{F_{cr}}}$
0.500	0.313	0.938	0.375	1.000	1.059	1.171	1.382	1.481	0.282
0.333	0.208	0.625	0.458	1.000	1.058	1.165	1.356	1.382	0.402
0.250	0.156	0.469	0.500	1.000	1.057	1.161	1.311	1.321	0.524
0.200	0.125	0.375	0.525	0.990	1.056	1.146	1.240	1.261	0.645
0.167	0.104	0.313	0.542	0.808	1.055	1.120	1.171	1.194	0.763
0.143	0.089	0.268	0.554	0.682	1.054	1.094	1.111	1.123	0.879
0.125	0.078	0.234	0.563	0.590	1.033	1.069	1.051	1.061	0.991
0.111	0.069	0.208	0.569	0.520	0.991	0.991	0.975	1.020	1.100
0.100	0.063	0.188	0.575	0.464	0.900	0.900	0.899	0.992	1.207
0.091	0.057	0.171	0.580	0.420	0.827	0.827	0.827	0.967	1.311

Note: All dimensions are in inches.

6.5 Uniaxial Tensile Coupon Test Results

Table 6.27 Uniaxial tensile coupon test results (a), (b) uniform I-sections (c) tapered I-section (d) mullion section

(a)

specimen name	F_y (ksi)	ε_y	F_u (ksi)	ε_u (ksi)	E (ksi)
1t1 (top flange)	29.91	0.00497	34.24	0.06250	10068
1t2 (top flange)	N.A.	N.A.	N.A.	N.A.	N.A.
1w1 (web)	29.82	0.00514	33.78	0.05400	9509
1w2 (web)	29.92	0.00506	33.89	0.06580	9775
1b1 (bottom flange)	28.84	0.00508	33.41	0.06270	9359
1b2 (bottom flange)	29.57	0.00598	33.98	0.06700	7430
average	29.61	0.00525	33.86	0.06240	9228
c.o.v.	0.015	0.079	0.009	0.081	0.113
6063-T6 (average in AA, 2000c)	31.00	0.00510	35.00	N.A.	10000
6063-T6 (minimum in AA, 2000c)	25.00	0.00448	30.00	N.A.	10100

(b)

specimen name	F_y (ksi)	ε_y	F_u (ksi)	ε_u (ksi)	E (ksi)
2t1 (top flange)	30.26	0.00519	35.09	0.06294	9498
2t2 (top flange)	30.38	0.00527	35.12	0.06407	9289
2w1 (web)	30.72	0.00523	35.38	0.06810	9526
2w2 (web)	31.02	0.00538	35.52	0.06690	9189
2b1 (bottom flange)	30.68	0.00520	35.50	0.06400	9596
2b2 (bottom flange)	30.25	0.00509	35.10	0.06750	9786
average	30.55	0.00522	35.29	0.06559	9481
c.o.v.	0.010	0.019	0.006	0.033	0.023
6063-T6 (average in AA, 2000c)	31.00	0.00510	35.00	N.A.	10000
6063-T6 (minimum in AA, 2000c)	25.00	0.00448	30.00	N.A.	10100

Table 6.27 (Continued)

(c)

specimen name	F_y (ksi)	ε_y	F_u (ksi)	ε_u (ksi)	E (ksi)
t2t1 (top flange)	41.00	0.006140	43.52	0.06830	9902
t2t2 (top flange)	40.81	0.006048	43.16	0.06783	10081
t2w1 (web)	40.58	0.006047	43.11	0.07187	10028
t2w2 (web)	40.15	0.005961	42.95	0.08132	10136
t2b1 (bottom flange)	41.45	0.006072	43.85	0.06134	10179
t2b2 (bottom flange)	41.46	0.006003	43.82	0.06960	10355
average	40.91	0.006045	43.40	0.07004	10113
c.o.v.	0.012	0.010	0.009	0.094	0.015
6061-T6 (average in AA, 2000c)	40.00	0.00600	45.00	N.A.	10000
6061-T6 (minimum in AA, 2000c)	35.00	0.00547	38.00	N.A.	10100

(d)

specimen name	F_y (ksi)	ε_y	F_u (ksi)	ε_u (ksi)	E (ksi)
m2t1 (top flange)	22.66	0.004412	25.73	0.048649	9394
m2t3 (top flange)	22.62	0.004217	26.34	0.043504	10203
m2b1 (bottom flange)	21.68	0.004300	25.46	0.054104	9426
m2b2 (bottom flange)	22.25	0.004292	25.81	0.047961	9709
m2w1 (web)	23.68	0.004403	27.42	0.053167	9853
m2w2 (web)	23.27	0.004362	26.98	0.043095	9853
m2w3 (web)	23.53	0.004422	27.24	0.048226	9714
average	22.81	0.004344	26.43	0.048387	9736
c.o.v	0.032	0.018	0.030	0.088	0.028
6063-T5 (average in AA, 2000c)	21.00	0.00410	27.00	N.A.	10000
6063-T5 (minimum in AA, 2000c)	16.00	0.00358	22.00	N.A.	10100

Note: a. Gage length used in these tests is one inch.
    b. ε_y = strain at the yield stress = $\sigma_y /E + 0.002$. ε_u = strain at the ultimate stress.
    c. Results from test specimens of 1t1, 1t2, 1w2, and 1b2 are based on extensometer measurements only. All others are based on both extensometer and strain gage measurements

6.6 *Local Geometric Initial Imperfection Measurements*

Before the tests have been conducted, initial geometric imperfections were measured on the flanges and webs of the specimens. On the flanges, the measured imperfection data are rotated along the web-flange junctions so that the average geometric line at the junction lies on the zero imperfection plane. On the web, the measured data are rotated along the mid-depth. The processed imperfection data are shown in Figure 6.5 and Figure 6.6. The maximum imperfection, which is expressed by a larger solid circle with a corresponding value in each figure, is less than the standard flatness tolerance by AA (2000c), except at the flange of the mullion section.

(a)

(b)
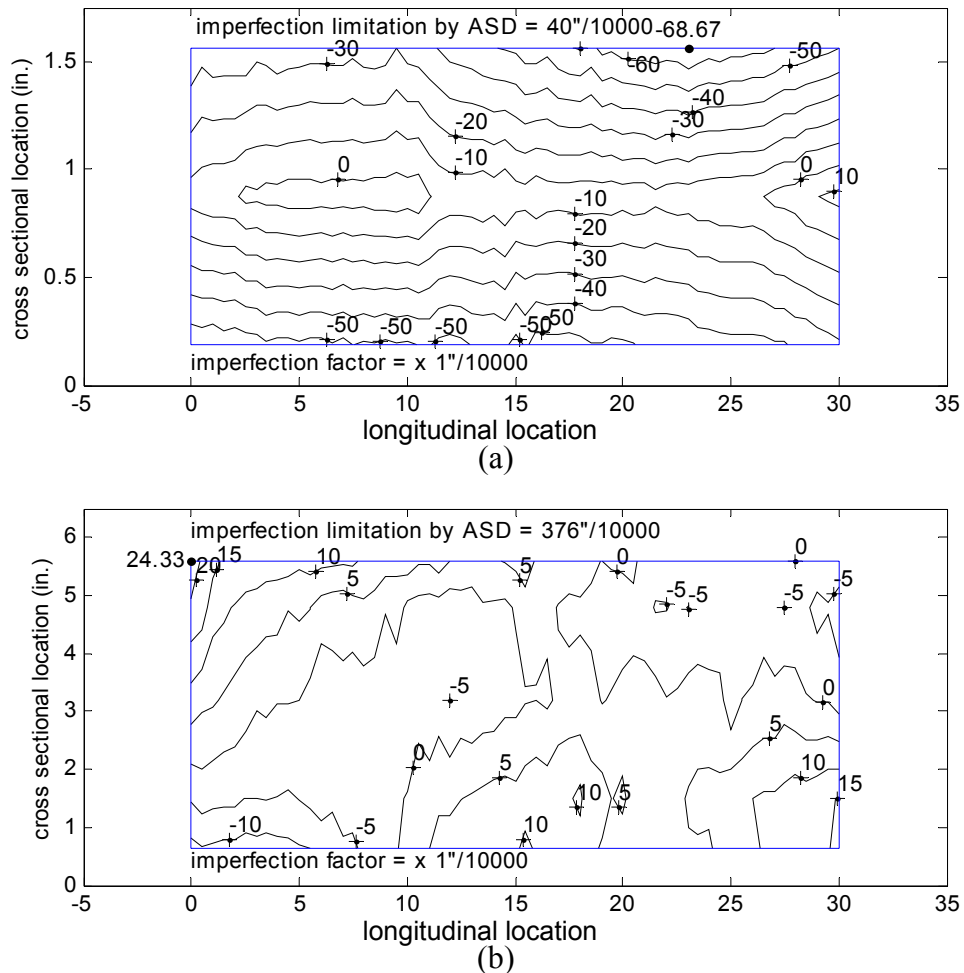
Note: All dimensions are in inches.

Figure 6.5 Imperfection measurements of a mullion section (a) top flange (b) web
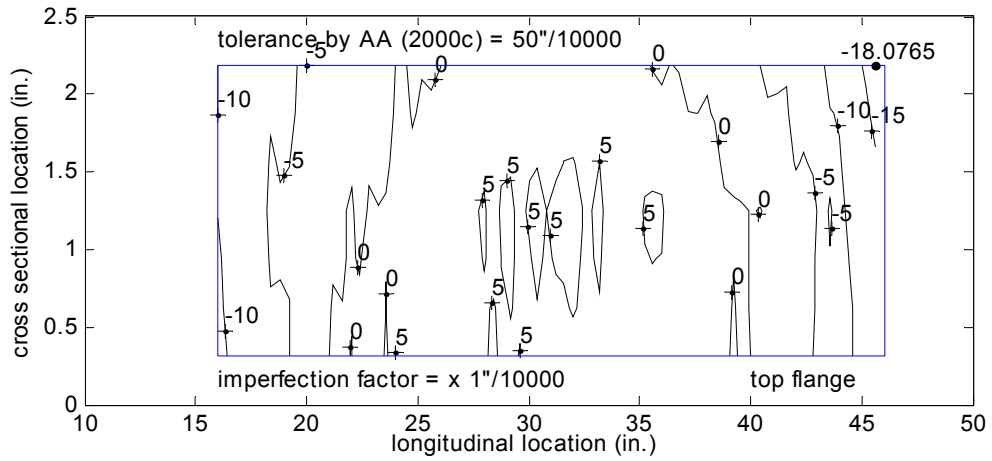
(a)
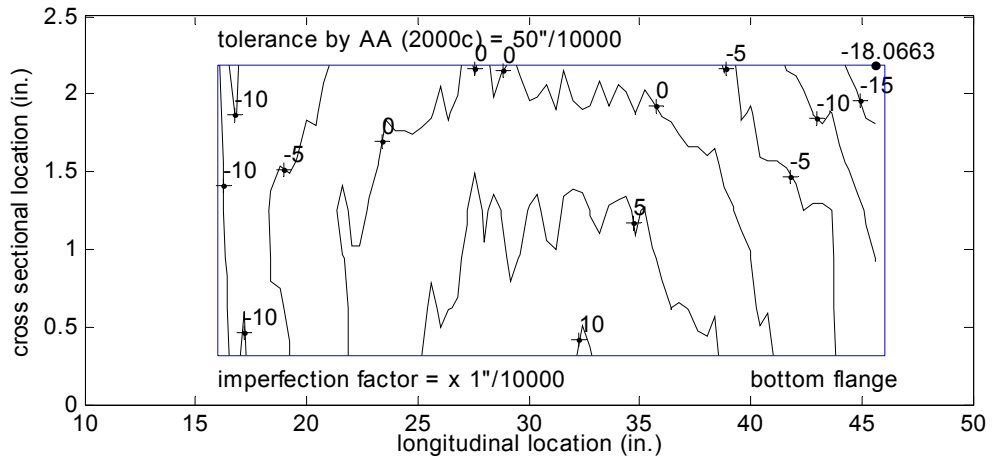
(b)
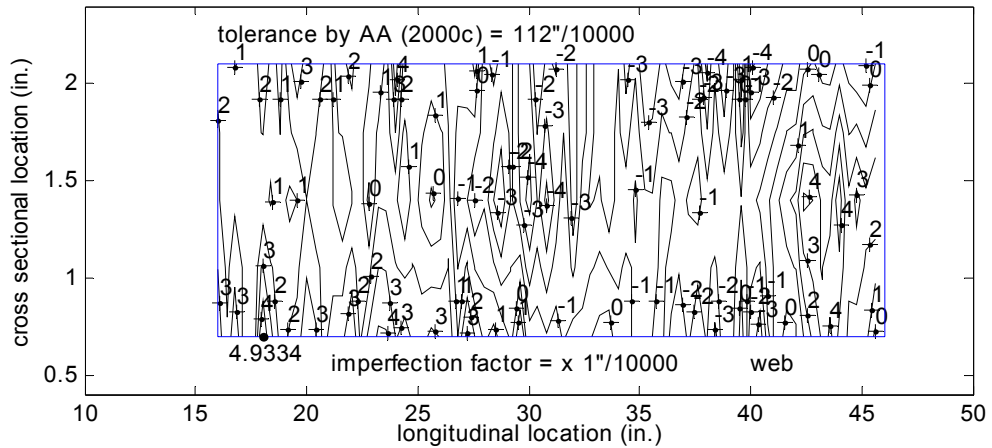
(c)

Note: All dimensions are in inches.

Figure 6.6 Imperfection measurements of an I-3x1.64 section (a) top flange (b) bottom flange (c) web

BIBLIOGRAPHY

The Aluminum Association, AA (2000a). The Specification for Aluminum Structures. *The Aluminum Association*.

The Aluminum Association, AA (2000b). The Aluminum Design Manual. *The Aluminum Association*.

The Aluminum Association, AA (2000c). Aluminum Standards and Data. *The Aluminum Association*.

Aluminum Company of America, Alcoa (1958). Alcoa Structural Handbook, A Design Manual for Aluminum. *Aluminum Company of America*.

American Institute of Steel Construction, AISC (1998). Manual of Steel Construction Load and Resistance Factor Design. *American Institute of Steel Construction*.

American Iron and Steel Institute, AISI (1996). Cold-Formed Steel Design Manual. *American Iron and Steel Institute*.

Anderson, R.A., Anderson M.S. (1956). "Correlation of Crippling Strength of Plate Structures with Material Properties". *NACA Technical note 3600*, Langley Memorial Aeronautical Laboratory.

Bleich, F. (1952). *Buckling Strength of Metal Structures*, McGraw-Hill.

Chehil, D.S. and Dua, S.S. (1973). "Bucking of rectangular plates with general variation in thickness." *Journal of Applied Mechanics Transaction, ASME*, 40(3), 745-751.

Cheung, Y.K., (1976). *Finite strip method in structural analysis.* Pergamon Press, New York

Clark, J.W., Rolf, R.L. (1966). "Buckling of Aluminum Columns, Plates, and Beams." *Journal of the Structural Division, ASCE*, Vol. 92, Proc. Paper 4838.

De Matteis, G., Moen, L.A., Langseth, M., Landolfo, R., Hopperstad, O.S., and Mazzolani, F.M. (2001). "Cross-Sectional Classification for Aluminum Beams-Parametric Study." *Journal of the Structural Engineering, ASCE*, Vol. 127, No. 3, Paper No. 22238.

Department of Defense, the United States of America, DOD (1994). Military Handbook Volume 1 and 2; Metallic Materials and Elements for Aerospace Vehicle Structures. *Department of Defense, the United States of America*.

Eberwien, U., Valtinat, G. (2001). "The fullness method: A direct procedure for calculation of the bending moment of a symmetrical aluminum cross section." *The 8th International Conference in Aluminum (INALCO)*, Munich, Germany, March.

European Committee for Standardization. Eurocode 9: *Design of Aluminium Structures*. Editorial Panel Version 2 (1996), European Committee for Standardization, December.

Faella, C., Mazzolani, F.M., Piluso, V., and Rizzano, G. (2000). "Local Buckling of Aluminum Members: Testing and Classification." *Journal of the Structural Engineering, ASCE*, Vol. 126, No. 3, Paper No. 20270.

Gaylord, Jr., E.H., Gaylord, C.N. (1979). *Structural Engineering Handbook*. McGraw-Hill.

Gerard, G. and Becker, H. (1957). "Handbook of Structural Stability. Part I- Buckling of Flat Plates." *NACA Technical Note* 3781. National Advisory Committee for Aeronautics.

Hibbitt, Karlsson & Sorensen, Inc. (1998). *ABAQUS Version 5.8,* Hibbitt, Karlsson & Sorensen, Inc.

Hill, H.N., Clark J.W. (1955). "Straight-line Column Formulas for Aluminum Alloys". *Alcoa Technical Paper No.12*, Pittsburgh, Pennsylvania.

Huebner, K.H., Thornton, E.A., Byrom, T.G. (1995). *The Finite Element Method for Engineers*. 3rd Ed, John Wiley & Sons, Inc.

Jombock, J.R., Clark, J.W. (1968). "Bending Strength of Aluminum Formed Sheet Members." *Journal of the Structural Division, ASCE*, Vol. 94, No. ST2, Proc. Paper 5816.

Kim, Y. (2000), "Behavior and Design of Laterally Supported Doubly Symmetric I-Shaped Extruded Aluminum Sections." M.S. Thesis, Cornell University, Ithaca, New York.

Kissell, J.R., Ferry, R.L. (1995). *Aluminum Structures*, John Wiley & Sons, Inc.

Kobayashi, H., Sonoda, K., (1990) "Buckling of rectangular plates with tapered thickness." *Journal of Structural Engineering*, *ASCE*, 116(5), 1278-1289.

Mazzolani, F.M. (1985). *Aluminum Alloy Structures*. 1st Ed., Pitman Publishing Inc.

Mazzolani, F.M. (1995). *Aluminum Alloy Structures*. 2nd Ed., E & FN Spon.

Mazzolani, F.M. and Piluso, V. (1997). "Prediction of the Rotational Capacity of Aluminum Alloy Beams." *Thin-Walled Structures*, Vol. 27, No.1, pp.103-116.

McGuire, W., Gallagher, R.H., Ziemian, R.D. (2000). *Matrix Structural Analysis*. 2nd Ed. John Wiley and Sons, Inc.

Mennink, J. (2002). "Cross-Sectional Stability of Aluminum Extrusions." Ph.D. Thesis. Eindhoven University of Technology, The Netherlands.

Mizusawa, T., (1993), "Buckling of rectangular Mindlin plates with tapered thickness by the spline strip method". *International Journal of Solids Structures*, 30(12), 1663-1677.

Ohga, M., Shigematsu, T., Kawaguchi, K., (1995) "Buckling analysis of thin-walled members with variable thickness". *Journal of Structural Engineering, ASCE*, 121(6), 919-924.

Pines, S., and Gerard, G. (1947). "Instability analysis and design of an efficiently tapered plate under compressive loading." *Journal of the Aeronautical Sciences*, 14(10), 594-599.

Plecher, R. (2000). "Aluminum for Bridges, Evaluation of Existing Structures in North America." Ph.D. Thesis. Technical University of Munich, Munich, Germany.

Ramberg, W., Osgood, W.R. (1943) "Description of Stress-Strain Curves by Three Parameters". *NACA Technical Note* 902, National Bureau of Standards.

Reck, P., Peköz, T., and Winter, G. (1975). "Inelastic strength of cold-formed steel beams", *Journal of Structural Division, ASCE*, 101 (ST11), Nov. 1975.

Schafer, B.W. (1997). "Cold-formed Steel Behavior and Design: Analytical and Numerical Modeling of Elements and Members with Longitudinal Stiffeners." Ph.D. Thesis, Cornell University, Ithaca, New York.

Schafer, B.W. and Peköz, T. (1998). "Direct Strength Prediction of Cold-Formed Steel Members Using Numerical Elastic Buckling Solutions." *Fourteenth International Specialty Conference on Cold-Formed Steel Structures*, St. Louis, Missouri. October.

Sharp, M. L. (1966). "Longitudinal Stiffeners for Compression Members." *Journal of the Structural Division, ASCE*, Vol. 92, No. ST5, Proc. Paper No. 4948.

Sharp, M.L. (1993). *Behavior and Design of Aluminum Structures*, McGraw-Hill.

Sooi, T. K. and Peköz, T. (1993). "Behavior of Component Elements of Aluminum Members." *Research Report No.93-1*, School of Civil and Environmental Engineering, Cornell University, Ithaca, New York.

Stowell E.Z. (1948). "A Unified Theory of Plastic Buckling of Columns and Plates". *NACA Technical Note* 1556, Langley Memorial Aeronautical Laboratory.

Stowell E.Z. (1950). "Compressive Strength of Flanges". *NACA Technical Note 2020*, Langley Memorial Aeronautical Laboratory.

Templin R.L., Sturm R.G., Hartmann E.C., Holt M. (1938). "Column Strength of Various Aluminum Alloys". *Alcoa Technical Paper No.1*, Pittsburgh, Pennsylvania.

Wittrick, W.H., and Ellen, C.H. (1962). "Buckling of tapered rectangular plates in compression." *The Aeronautics Quarterly*, 13(4), 308-326.